

Using gravitational waves to see the first second of the Universe

Rishav Roshan and Graham White

School of Physics and Astronomy, University of Southampton,

Southampton SO17 1BJ, United Kingdom

(Dated: January 10, 2024)

Gravitational waves are a unique probe of the early Universe, as the Universe is transparent to gravitational radiation right back to the beginning. In this article, we summarise detection prospects and the wide scope of primordial events that could lead to a detectable stochastic gravitational wave background. Any such background would shed light on what (if anything) lies beyond the Standard Model, sometimes at remarkably high scales. We overview the range of strategies for detecting a stochastic gravitational wave background before delving deep into three major primordial events that can source such a background. Finally, we summarize the landscape of other sources of primordial backgrounds.

CONTENTS

I. Introduction	4
II. Detection of GW backgrounds	6
A. GW Detectors	9
1. Pulsar Timing arrays	9
2. Astrometry	12
3. Interferometers	14
B. Cosmological detectors	18
C. High frequency proposals	19
III. Gravitational waves from cosmic phase transitions	20
A. Nucleation of bubbles	20
B. Effective potential and action at finite temperature	24
C. Possible sources	26
D. Narrative of a phase transition and modeling of the spectrum	30
1. Acoustic source	31
2. Collision source	33
3. Velocity of ultrarelativistic walls	34
4. Turbulence	35
E. Theoretical issues with thermal field theory	36
F. Simulations	40
IV. Gravitational waves from topological defects	43
A. Categorization by homotopy group	43
B. Gravitational waves from Domain walls	44
C. Gravitational waves from Cosmic Strings	49
1. Cosmic strings from global $U(1)$ symmetry breaking	54
2. Cosmic strings from gauged $U(1)$ symmetry breaking	57
D. Gravitational waves from Monopoles and Textures	58
E. Hybrid defects	60
F. Applications of gravitational waves from topological defects	75

V. Scalar induced gravitational waves	84
A. Enhanced scalar power spectrum during inflation	85
B. Models of scalar induced gravitational waves	86
C. Sudden changes in the equation of state	87
D. Gauge invariance	90
E. Applications of scalar induced gravitational waves	92
VI. Other significant sources	94
A. Inflation	94
B. (p)reheating	95
C. Graviton production as a big bang thermometer	97
VII. Conclusions	100
References	102

I. INTRODUCTION

Gravitational waves (GW) are one of the most striking predictions of Einstein’s theory of general relativity [1, 2]. Remarkably, the concept of gravitational waves predates Einstein, as physicists at the turn of the 19th century wondered if there was a gravitational analog of electromagnetic waves [3]. Moreover, Einstein famously published an incorrect proof that gravitational waves do not exist [4].¹ Even still, the recent discovery of gravitational waves by aLIGO [7] is widely seen as one of his greatest triumphs.

Decades before it became possible to observe the Universe via gravitational waves, another consequence of Einstein’s theory was being explored - that the Universe expanded from a hot dense point in a theory later coined the “big bang theory” [8]. The Big Bang theory predicts that the Universe should expand and cool until the point at which free protons and electrons combine into the first hydrogen atoms, after which the mean free path of photons rapidly grows to the point where its light is visible today in a black body spectrum. This cosmic microwave background radiation (CMB), was later seen in 1964, falsifying the steady state theory and verifying the Big Bang theory of cosmology [9]. Since then we have entered the era of precision measurements of nature’s first light, which allows us to probe features of the primordial fireball [10]. In particular, we can measure the expansion of the Universe and the asymmetry between matter and anti-matter [11–19] at the time when the CMB forms. We have an alternative measurement of these two observables. About a second after the moment of creation, the first nucleons were synthesized and we can cross-check the primordial abundances of hydrogen, helium, and deuterium with our predictions, the latter of which are sensitive to the precise value of the baryon asymmetry and the expansion rate of the Universe [20]. In other words, we can calculate the expansion rate and baryon asymmetry during Big Bang nucleosynthesis (BBN) by measuring the primordial abundances. Remarkably, in a triumph of modern cosmology, we find concordance between the cosmic microwave background and Big Bang nucleosynthesis [10, 21].

Despite the success of our current model of cosmology (up to some recent tensions with data [22]), physicists face a huge “gap problem” where we know nothing about the period between inflation and BBN. Measured in SI units, the problem does not seem alarming -

¹ This was in a paper that was originally rejected by physical review, with the referee later vindicated that Einstein made the mistake of making a pathological coordinate transformation [5]. Eventually, Einstein published a corrected version that argued for the existence of cylindrical gravitational waves [6].

we are in the dark by a mere second of our history. Measured in terms of temperature demotes cosmology to being a field in its infancy. The history of the Universe potentially spans twenty-two of magnitude in temperature between the end of inflation and the onset of BBN [23, 24]. Being ignorant of this period renders us incapable of understanding why there is more matter than antimatter [11–19], what dark matter is and how it came to be [25–33], how hot the Universe was and how did it become so hot after inflation [34, 35], was this period always dominated by radiation or were there early periods of matter domination [36], was it always in thermal equilibrium or did the Universe come to boil [37–42]?

Gravitational wave cosmology is the unrivaled method to make progress on the gap problem - the Universe is transparent to gravitational waves right up to the instant of its birth. Any violent event in that first second will leave a trace in the stochastic gravitational wave background (SGWB) which we can hope to detect today. The next generation promises to birth a new dawn of gravitational wave detection, with ground and space-based interferometers pledging to search for primordial spectra in the μHz to kHz range [43–54] whereas astrometry [55–67] and pulsar timing arrays [68–75] promise to be sensitive to low-frequency gravitational waves down to the nHz range. Moreover, there are even a rich set of ideas percolating to probe high-frequency gravitational wave sources which, if successful, would allow us to be even more ambitious with how close we can get to probing the instant after inflation [76].

In this review, we review how the scientific community pulled off the immense task of detecting gravitational waves and what efforts exist on the horizon to detect the SGWB in section II. We then review three types of events that can lead to a SGWB - cosmic first-order phase transitions, topological defects, and scalar-induced gravitational waves, whether from a period of ultra-slow roll or a sudden change in the equation of the state of the Universe. In all three sections III, IV and V respectively, we review applications of such sources to some of the deeper, outstanding questions in the field. Finally, we give a brief overview of other sources of gravitational waves in section VI before concluding.

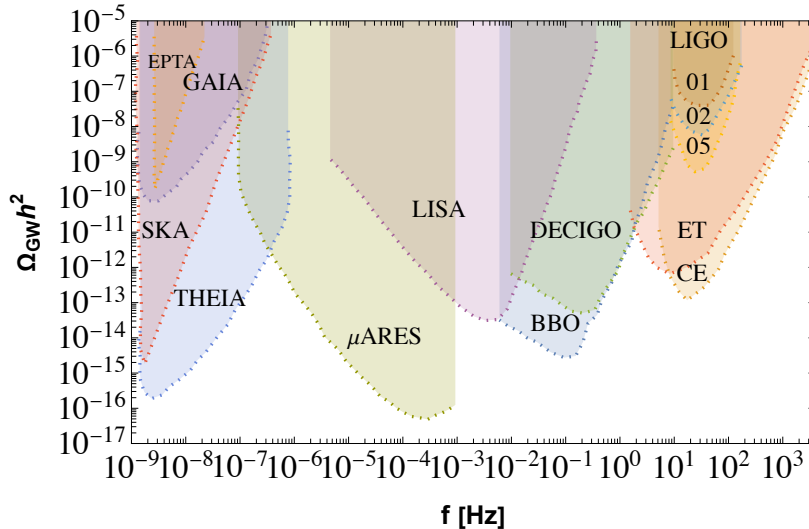


FIG. 1. Incomplete menu of current and future gravitational wave detectors. These include future pulsar timing arrays including the NANOGrav [69] (16 years), the EPTA [68] (5 years), IPTA [77] and SKA [71] (10 years), astrometry proposal like Gaia [56, 59] (5 years) and Theia [57, 62] (20 years), space-based interferometers including μ -Ares [53] (10 years), LISA [52] (4 years) and DECIGO [78] (3 years) and ground-based interferometers including LIGO [43] (20 years), cosmic explorer [51] (20 to 50 years) and the Einstein telescope [79] (3 years). In the () we mention the tentative mission lifetime of each detector.

II. DETECTION OF GW BACKGROUNDS

It was many decades after gravitational waves were first proposed that they were finally discovered, which speaks to the difficulty of the task. All experimental designs experience noise which dwarfs the amplitude of gravitational waves of any known signal. The ambitious effort to bring about an era of gravitational wave cosmology has therefore required remarkable ingenuity on both the theoretical and experimental fronts. In this section, we explain how to model gravitational waves and the main strategies the community has come up with to detect them.²

Let us begin by showing the large payoff to accurately modeling predicted gravitational wave spectra. We will begin by explaining how to extract transient sources from the noisy background to introduce key concepts of filtering before moving on to the more relevant

² For a very informative review, we highly recommend the seminal textbook by Maggiore [80] together with some review articles [76, 81–83]

stochastic gravitational wave backgrounds.

A gravitational wave detector can be thought of as a *linear system* whose output $s(t)$ is considered as a combination of a Gravitational wave signal ($h(t)$) and noise ($n(t)$),

$$s(t) = h(t) + n(t). \quad (1)$$

Assuming the noise to be stationary, one can define a noise spectral density or noise power spectrum ($S_n(f)$) as

$$\langle \tilde{n}^*(f)\tilde{n}(f') \rangle = \delta(f - f') \frac{1}{2} S_n(f), \quad (2)$$

where $\langle \dots \rangle$ represents the ensemble average which is obtained by repeating the process of measuring the noise over a given time interval and $\tilde{n}(f)$ denotes the Fourier component of noise. Next, one can define the *spectral strain sensitivity*, $\sqrt{S_n(f)}$, that characterizes the noise of the detector. As mentioned above, with the present sensitivity of all gravitational wave detectors on the horizon, it is always true that $|h(t)| \ll |n(t)|$. In such a situation, digging out the GW signal from a much larger noise becomes important. It is possible to detect a GW signal whose amplitude is much smaller than the noise if we have some knowledge of its form. Assuming we know the form of the signal, we can define a filter function, $K(T)$,

$$\hat{s} = \int_{-\infty}^{\infty} dt s(t) K(t). \quad (3)$$

that maximizes the signal-to-noise ratio for such a signal. *Match filtering* is a technique where a filter function is chosen to match the signal that we are looking for. We are also aided in our search for gravitational waves by the fact that the average noise vanishes. That is, $\langle n(t) \rangle = 0$. Under such a condition, the signal is

$$S = \int_{-\infty}^{\infty} dt \langle s(t) \rangle K(t) = \int_{-\infty}^{\infty} dt h(t) K(t) = \int_{-\infty}^{\infty} df \tilde{h}(f) \tilde{K}^*(f). \quad (4)$$

whereas the noise is by fiat defined in the absence of a signal, $\langle \hat{s}(t) \rangle = 0$, so we have

$$N^2 = [\langle \hat{s}^2(t) \rangle]_{h=0} = \int_{-\infty}^{\infty} dt dt' \langle n(t)n(t') \rangle K(t) K(t'). \quad (5)$$

Following Eq. (2), one can rewrite the above equation as,

$$N^2 = \int_{-\infty}^{\infty} df \frac{1}{2} S_n(f) |\tilde{K}(f)|^2, \quad (6)$$

and so the signal-to-noise ratio is then

$$\frac{S}{N} = \frac{\int_{-\infty}^{\infty} dt \tilde{h}(f) \tilde{K}^*(f)}{[\int_{-\infty}^{\infty} df \frac{1}{2} S_n(f) |\tilde{K}(f)|^2]^{1/2}}. \quad (7)$$

If we know the signal we are looking for, we can choose a filter function that optimizes the signal-to-noise ratio

$$\tilde{K}(f) = \text{const.} \frac{\tilde{h}(f)}{S_n(f)}. \quad (8)$$

Using this, one can write the optimal value of S/N [80],

$$\left(\frac{S}{N}\right)^2 \leq 4 \int_0^\infty df \frac{|\tilde{h}(f)|^2}{S_n(f)}. \quad (9)$$

However, one can only achieve this bound if we can accurately predict the signal. Primordial sources are particularly difficult to model - the formidable challenges in doing so we discuss in later sections. For now, we just make note of the big payoff in developing the theoretical technology to predict gravitational waves.

Primordial gravitational wave sources will be stochastic backgrounds which will have additional challenges compared to transient sources. To see why, let us assume that these stochastic gravitational wave backgrounds (SGWB)s are stationary, Gaussian, isotropic, and unpolarized and hence can be characterized by a spectral density of stochastic background $S_h(f)$ (defined analogously to the noise spectral density) as in Eq. 2

$$\langle \tilde{h}_A^*(f, \hat{\mathbf{n}}) \tilde{h}_{A'}^*(f', \hat{\mathbf{n}}') \rangle = \delta(f - f') \frac{\delta^2(\hat{\mathbf{n}}, \hat{\mathbf{n}}')}{4\pi} \delta_{AA'} \frac{1}{2} S_h(f), \quad (10)$$

where $\tilde{h}_A(f, \hat{\mathbf{n}})$ are the amplitudes of the stochastic GW with polarization A , coming from all possible propagation directions $\hat{\mathbf{n}}$. The dependence of $\langle \tilde{h}_A^*(f, \hat{\mathbf{n}}) \tilde{h}_{A'}^*(f', \hat{\mathbf{n}}') \rangle$ on $\delta^2(\hat{\mathbf{n}}, \hat{\mathbf{n}}')$ and $\delta_{AA'}$ is a result of uncorrelated and unpolarized nature of these waves.

Looking at Eqns. (2) and (10), it is clear that a detector sees a SGWB as an additional source of the noise, so the distinction of a SGWB signal from noise becomes a big challenge! This suggests that one needs to set a relatively higher threshold on SNR while detecting a SGWB signal. The next goal is to determine the minimum value of the energy density of the GW that can be measured at a given S/N. While this energy density is defined using a quantity $\Omega_{\text{GW}}(f)$

$$\Omega_{\text{GW}}(f) = \frac{4\pi^2}{3H_0} f^3 S_h(f). \quad (11)$$

The minimum detectable value of Ω_{GW} for a single detector is given by

$$\Omega_{\text{GW}}(f)|_{\min} = \frac{4\pi^2}{3H_0} f^3 [S_h(f)]_{\min}, \quad (12)$$

with

$$[S_h(f)]_{\min} = S_n(f) \frac{(S/N)^2}{F}. \quad (13)$$

Here F denotes the angular efficiency factor [80] whose value varies depending on the choice of detector. The presence of f^3 in the above expression plays a nontrivial role. High-frequency signals from a primordial source will have a very similar peak value of Ω_{GW} as low-frequency signals. However, detectors are sensitive to S_h , so it becomes progressively more difficult to resolve a gravitational wave source as the frequency gets higher.

Due to the unpredictable nature of the SGWB signal, the match-filtering technique is not easy for a single detector. The advantage of using two or more detectors over a single detector is that one can use a modified form of match-filtering where the output of one detector can be matched with the output of another. Analogous to Eq. (7), for a set of two detectors, one can follow the procedure for a single source and assume we know the signal shape we are looking for, and therefore the optimal filter function, to derive the optimal signal to noise ratio

$$\left(\frac{S}{N}\right)^2 = 2T \int_0^\infty df \Gamma^2(f) \frac{S_h^2(f)}{S_n^2(f)}. \quad (14)$$

Here $\Gamma(f)$ [80] is the overlap reduction function that takes into account the fact that two detectors can see different gravitational wave signals, either because they are at a different location or because they have different angular sensitivity.

Finally, one can also think of a situation where the number of identical detectors is more than two, *i.e.* $N > 2$. In such a case, with these N detectors we can form $N(N - 1)/2$ independent two-point correlators. It is interesting to point out that, for a stationary background, a scenario with N detectors running for time T is identical to a situation in which a pair of detectors run for a total time: $T \times N(N - 1)/2$. Hence, one can simply obtain the S/N with N identical detectors just by replacing,

$$T \rightarrow \frac{N(N - 1)}{2} T \quad (15)$$

in Eq. (14). This boost in the signal-to-noise ratio from correlating more than two detectors gets used in, for example, the μAres proposal [53] which we will discuss in section II A 3.

A. GW Detectors

1. Pulsar Timing arrays

Pulsar timing arrays (PTA) [72–74] are a promising method of detecting an ultra-low frequency ($10^{-9}\text{Hz} - 10^{-6}\text{Hz}$) GW. They can measure a tiny variation induced by a GW,

passing in between the Earth and a pulsar, in the time of arrival of the pulses emitted by the milliseconds pulsar by exploiting the telescope used for radio astronomy [75].

To understand how PTAs can detect SGWB we need to have information about the time interval (Δt) of two successive pulses reaching the Earth, the distance (d_a) between the Earth and the pulsar that emits the photons, the direction of propagation ($\hat{\mathbf{n}}_a$) of the GW and the timing residual denoted by R_a that describes the observed variation in the time of arrival of the pulses as a result of passing by GW. Now, working in a TT gauge and choosing a reference frame such that the Earth is at the origin of the coordinate system, one can model how the time interval, (Δt), between two successive pulses reaching the Earth from a pulsar depends upon passing through the gravitational wave background. To do that one can write,

$$\Delta t = T_a + \Delta T_a \quad (16)$$

where T_a denotes the rotational period of the pulsar which is typically of the order of a few milliseconds and ΔT_a represents the delay introduced as a result of a passing GW,

$$\frac{\Delta T_a}{T_a} = \frac{n_a^i n_a^j}{2} \int_{t_{em}}^{t_{em}+d_a} dt' \left[\frac{\partial}{\partial t'} h_{ij}^{\text{TT}}(t', \mathbf{x}) \right]_{\mathbf{x}=\mathbf{x}_0(t')}, \quad (17)$$

$$\mathbf{x}_0(t') = (t_{em} + d_a - t') \hat{\mathbf{n}}_a, \quad (18)$$

where t_{em} is the time of emission of the photons emitted from the pulsar. Assuming a monochromatic GW propagating along the $\hat{\mathbf{n}}$ direction, we can write

$$h_{ij}^{\text{TT}}(t, \mathbf{x}) = \mathcal{A}_{ij}(\hat{\mathbf{n}}) \cos[\omega_{\text{gw}}(t - \hat{\mathbf{n}} \cdot \mathbf{x})], \quad (19)$$

where $n^i \mathcal{A}_{ij}(\hat{\mathbf{n}}) = 0$. Let us also define a quantity

$$z_a(t) \equiv \left(\frac{\nu_0 - \nu(t)}{\nu_0} \right)_a, \quad (20)$$

such that $z_a(t) = -(\Delta \nu_a / \nu_a)(t) = (\Delta T_a / T_a)$ where $\nu_a = 1/T_a$ and substitute our form of the gravitational wave into Eq. 17 as,

$$z_a(t) = \frac{n_a^i n_a^j}{2(1 + \hat{\mathbf{n}} \cdot \hat{\mathbf{n}}_a)} [h_{ij}^{\text{TT}}(t, \mathbf{x} = 0) - h_{ij}^{\text{TT}}(t - \tau_a, \mathbf{x}_a)]. \quad (21)$$

Here, t_{ob} is simply replaced by t , and $\mathbf{x} = 0$ represents the observer's position. Finally, one can define the timing residuals R_a of the a^{th} pulsar as

$$R_a(t) = \int_0^t dt' z_a(t'). \quad (22)$$

With this, we can model the detection of SGWB using PTAs. Following Eq. 10 and Eq. 21, we can calculate ensemble average $\langle z_a(t)z_b(t) \rangle$ of the pulse redshift of a pair of millisecond pulsars,

$$\langle z_a(t)z_b(t) \rangle = \frac{1}{2} \int_{-\infty}^{\infty} df S_h(f) \int \frac{d^2 \hat{\mathbf{n}}}{4\pi} \sum_{A=+,x} F_a^A(\hat{\mathbf{n}}) F_b^A(\hat{\mathbf{n}}), \quad (23)$$

where $F_a^A(\hat{\mathbf{n}}) = \frac{n_a^i n_a^j e_{ij}^A}{2(1+\hat{\mathbf{n}} \cdot \hat{\mathbf{n}}_a)}$ represents the pattern function with e_{ij}^A bein the polarization tensor (see [80] for detail). We can now write the angular part of the integral as

$$C(\theta_{ab}) \equiv \int \frac{d^2 \hat{\mathbf{n}}}{4\pi} \sum_{A=+,x} F_a^A(\hat{\mathbf{n}}) F_b^A(\hat{\mathbf{n}}). \quad (24)$$

Here $C(\theta_{ab})$ is known as the Hellings and Downs function [84]. Substituting Eq. 24 in Eq. 23 we get

$$\langle z_a(t)z_b(t) \rangle = C(\theta_{ab}) \int_0^{\infty} df S_h(f). \quad (25)$$

Finally, it is useful to write the results in terms of the timing residual as they are directly related to the time of arrival of the pulses. The ensemble average between the timing residuals of a pair of millisecond pulsars can be determined as

$$\langle r_a(t)r_b(t) \rangle = 2C(\theta_{ab}) \int_0^{\infty} df \frac{S_h(f)}{(2\pi f)^2} 2[1 - \cos(2\pi ft)]. \quad (26)$$

Next, we would also like to comment briefly on the different kinds of noises that can affect the detection of GW signals by PTA and how they can be reduced. PTAs are subjected to the noises that can be generated due to the intrinsic timing irregularities in the spindown of the different pulsars or can be instrumental in origin like radiometer noise *etc.* Monitoring a large number of pulsar pairs provides us with the possibility of enhancing the GW signal concerning the noise.

The main international collaborations working on the detection of GW using PTAs are the European Pulsar Timing Array (EPTA) [68], the North American Nanohertz Observatory for Gravitational Waves (NANOGrav) [69], the Indian Pulsar Timing Array (InPTA) [85] and the Parkes Pulsar Timing Array (PPTA) [70]. All these collaborations work together as the International Pulsar Timing Array (IPTA). The EPTA uses five 100 m class telescopes across Europe and monitors 41 pulsars at several frequencies. Using these five telescopes as a single telescope gives the highest overall sampling rate of pulsars among the existing PTAs. NANOGrav is a combined effort of US and Canada which uses single-dish telescopes

that are among the world’s largest single-dish telescopes. NANOGrav currently monitors 49 pulsars. InPTA is an Indo-Japanese collaboration that makes use of the unique capabilities of the upgraded Giant Meterwave Radio Telescope (uGMRT) for monitoring a sample of nearby millisecond pulsars. PPTA uses the Parkes Observatory in Australia and can access pulsars in the Southern Hemisphere. It currently monitors 25 pulsars. Finally, the square kilometer array (SKA) [71] is an international radio telescope project that is being built in Australia (low-frequency) and South Africa (mid-frequency). It is expected to begin in 2028–29. Once ready, the SKA telescopes will be, by far, the most powerful instrument in the field of radio astronomy. Sensitivities for current and projected experiments we show in Fig. 1

2. Astrometry

Light passing through a scalar perturbation undergoes a random walk. By contrast, light through a gravitational wave background undergoes a correlated kick independent of the distance between the light source and the observer [55]. This remarkable fact allows us to search for correlated shifts in the angular velocity of many stars in order to reconstruct a gravitational wave background. The sensitivity of this approach grows linearly with time rather than the usual $1/\sqrt{T}$ convergence as the precision in measuring angular velocity kicks grows with time.

In this section, we will briefly explain these two facts before mentioning the reach of current and future astrometry experiments. For a more in-depth look, the reader is directed to refs. [55, 59, 64–67]. Let us begin with demonstrating the independence of the kicks with the distance from Earth. We begin with the geodesic equation in a gravitational wave background,

$$\ddot{d}(z) = \dot{H}(z) \quad (27)$$

where under the assumption of isotropy, we have

$$H(z) \sim \int k^2 dk h_a(k) T_a(k) e^{i(1-\mu)kz} + c.c. \quad (28)$$

and

$$T_+ = -\frac{1}{2}(1-\mu)\sqrt{1-\mu^2}(\cos\phi, \sin\phi), \quad T_x = -\frac{1}{2}\sqrt{1-\mu^2}(\sin\phi, \cos\phi). \quad (29)$$

We can then write a power spectrum of velocity kicks stars will have due to the gravitational wave background, as perceived by an observer on Earth,

$$P_{\dot{d}}(k) \sim \langle H(0) \cdot H(z) \rangle \quad (30)$$

$$\sim \int dz e^{ikz} \int q^2 dq P(q) (T_+^2 + T_x^2) e^{i(1-\mu)kz} \quad (31)$$

$$\sim k \int dp P(p) (1 - \dots) . \quad (32)$$

Here, $P(p)$ is the power spectrum for tensor perturbations

$$\langle h_a(k) h_b^*(p) \rangle = (2\pi)^3 \delta(k - p) \delta_{ab} P(k). \quad (33)$$

The power spectrum of displacements will be related to the spectrum for kicks by $P_d \sim P_{\dot{d}}/k^2$ and we get the scaling

$$P_d \sim \frac{1}{k} \frac{\langle h^2 \rangle}{k_h^2} . \quad (34)$$

The mean squared deviation averaged over a distance D scales as

$$\langle d^2 \rangle \sim (k P_d)|_{k=1/D} \sim D^0 . \quad (35)$$

In other words, the size of the kick is independent of the distance between the source and the observer. We should therefore see a kick of the same size from a stochastic gravitational wave background which grows with the size of the strain. Looking at a large number of stars and searching for such correlated kicks therefore becomes an efficient method for finding a SGWB.

As for the impressive scaling of astrometry, to reconstruct the background, we need to track N sources, for a time T , resolving angles with a precision of $\Delta\Theta$ and therefore the angular velocity to a precision $\Delta\Theta/(T\sqrt{N})$ [58]. Our precision with the gravitational wave background then scales (remembering that $\Omega \sim h^2$)

$$\Omega_{\text{GW}} \lesssim \frac{\Delta\Theta^2}{NT^2 H_0^2} . \quad (36)$$

Thus we see the powerful potential of using astrometry for gravitational wave detection - the sensitivity to a background scales much more efficiently with the lifetime of the experiment than other detectors.

Launched in 2013 by the European Space Agency, Gaia is a global space astrometry mission that maps more than a billion objects in the Milky Way. Detectors like Gaia [56]

use astrometric measurement to look for the low-frequency gravitational wave background [58–62]. Recently, it was also shown that Gaia can be an important tool for probing GW with frequencies in range $\sim [10^{-9} - 10^{-7}]$ Hz where the upper-frequency cut is set by the cadence and the lower frequency by the inverse lifetime of the experiment [59–62]. Gaia is expected to observe a billion stars at an angular velocity resolution of about $100\mu\text{as}$ resulting in a strain sensitivity of

$$h_{\text{GW}} \sim 10^{-14} \left(\frac{5\text{years}}{T_M} \right), \quad (37)$$

with T_M the mission lifetime. This makes it currently competitive with pulsar timing array measurements. There is a proposed upgrade to Gaia called Theia [57] which is expected to observe significantly more stars at a much higher angular resolution, which results in a strain sensitivity of

$$h_{\text{GW}} \sim 10^{-14} \left(\frac{5\text{years}}{T_M} \right) \left(\frac{\Delta\Theta_{\text{Theia}}}{\Delta\Theta_{\text{Gaia}}} \right) \sqrt{\left(\frac{N_{\text{stars, Gaia}}}{N_{\text{stars, Theia}}} \right)}, \quad (38)$$

where $(\Delta\Theta_x, N_x)$ are the angular resolution and number of stars observed in experiment x . Exactly how much Theia will improve from Gaia is not yet clear, and recent estimates range from a factor of 100 – 600 improvement in the strain sensitivity [62, 64]. A more exotic proposal aims to look for correlated kicks in asteroids in asteroid belt [63] which is projected to achieve an impressive strain sensitivity of 10^{-19} at frequencies of $10\mu\text{Hz}$. The sensitivity of Gaia as well as an approximate projection for Theia is given in Fig. 1

3. Interferometers

In 1887, Michelson-Morley for the first time used an interferometer to demonstrate the non-existence of ether in the Universe [86]. As interferometers are very sensitive to even tiny changes in a path difference, they are very useful in measuring small fluctuations in spacetime. In Fig. 2, we show a simple schematic of a Michelson-type interferometer.

In order to understand how the presence of GW affects the propagation of light in the interferometer [79, 81, 82], we first start with an assumption that GW has only a plus polarization and it arrives from the z direction, so we have,

$$h_+(t) = h_0 \cos \omega_{\text{GW}} t. \quad (39)$$

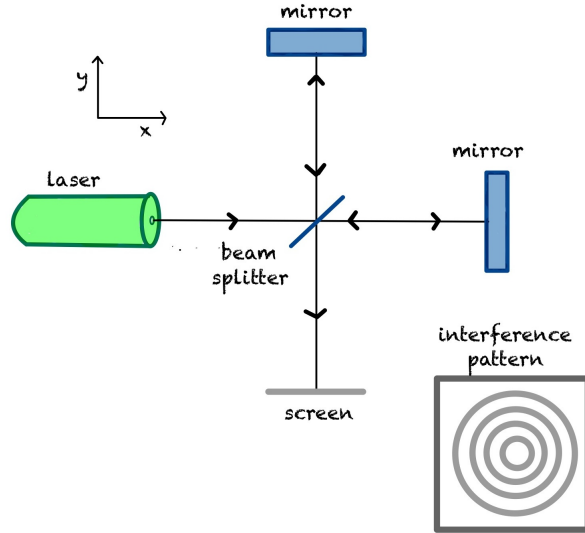


FIG. 2. Schematic representation of a Michelson-type interferometer.

Since the photons travel along a null geodesic *i.e.* $ds = 0$ this allows us to solve the change in the path length along a single direction in TT frame ³

$$dx = \pm c dt \left(1 - \frac{1}{2} h_+(t)\right) \quad (40)$$

reflection and transmissions at the beam splitter give an overall phase shift of a $1/2$. Let us consider a Michelson interferometer with arm length L where the beam splitter is at the origin at time t_0 with a phase $e^{-i\omega_L t_0}$. The phase shift from the gravitational wave due to the field going through the x and y arms are

$$\Delta\phi_x = -\Delta\phi_y = h_0 \frac{\omega_L L}{c} \text{sinc}(\omega_{\text{GW}} L/c) \cos[\omega_{\text{GW}}(t - L/c)] . \quad (41)$$

The total power at the detector is related to a phase, ϕ_0 , set by the experimenter

$$P = \frac{P_0}{2} \{1 - \cos[2\phi_0 + \Delta\phi_{\text{Mich}}(t)]\} . \quad (42)$$

For a given signal that peaks at a frequency $f_p = \omega_{\text{GW}}/2\pi$, the boost in power is maximal when

$$L = 750\text{km} \left(\frac{100\text{Hz}}{f_p}\right) \quad (43)$$

³ A similar calculation can also be performed in the proper frame. The computation of higher-order corrections becomes much more involved in the proper frame of the detector and hence for simplicity, we stick to the TT frame.

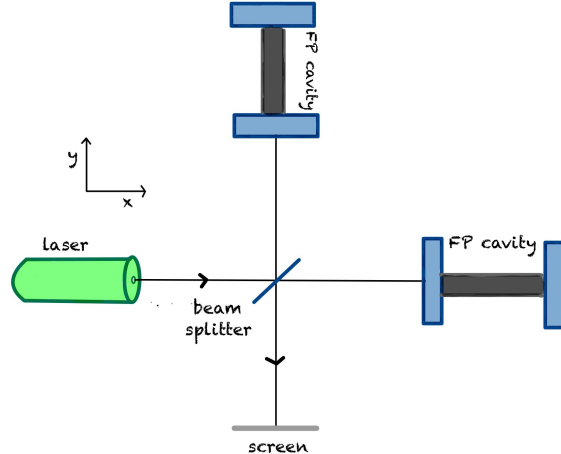


FIG. 3. Schematic representation of an interferometer with Fabry-Perot cavities .

Ground-based detectors don't achieve an arm length 100s of kilometers long, Ligo and Virgo has arms of 4 and 3km respectively [43–48]. However, to achieve a larger *effective* path length they use a Fabry-Perot cavity [43, 44]. Such a cavity traps light within it for a long time. If a Fabry-Perot cavity is a few kilometers long and has light trapped within it for around 100 trips between the edges of the cavity, then the gravitational wave detector can be sensitive to frequencies as low as 1 – 100 Hz. The phase shift in the Fabry-Perot cavity in the presence of the GW along the x and y axis is given by

$$\Delta\phi_x = -\Delta\phi_y \simeq h_0 2 \frac{\omega_L L \mathcal{F}}{c \pi} \frac{1}{[1 + (4\pi f_p \tau_s)^2]^{1/2}}, \quad (44)$$

where \mathcal{F} is known as the finesse of the cavity which is defined as the ratio of free spectral range ($\Delta\omega_L$) to the full-width half maximum and τ_s is the storage time of the cavity, *i.e.* the average time spent by a photon in the cavity. Comparing Eq. (44) with Eq. (41) we find that in a Fabry-Perot, the sensitivity of a phase shift is enhanced by a factor of $(2/\pi)\mathcal{F}$ in comparison to what is obtained in a Michelson interferometer.

These interferometers are also subjected to various types of noises that can affect the detection of GW signals, for example, optical read-out noises which are a combination of the shot noises of a laser (that results from the discretization of photons) and radiation pressure (generated from pressure exerted by the laser beam on the mirrors), displacement noises which are generated by the movement of a test mass and are not induced by the GWs. Other noises that can influence the detection of GW signals are Seismic and Newtonian noise that results from local movements like traffic, trains, or surface waves that shake

the suspension mechanism of the interferometer, thermal noises that are induced by the vibrations in mirrors and suspensions or the fluctuations in the test masses, etc. Apart from these sources, there exist several other sources of noise that can affect the detection of GW by an interferometer. Irrespective of the kind of noises, all of them can be characterized using their NSR which is further used to calculate the signal-to-noise ratios. For a detailed discussion, we refer the readers to [80].

With the first observation of the GW signals in 2015 by LIGO collaborations, the role and significance of interferometers in GW detection have increased manifold. At present, there exist several earth-based interferometers that are currently running and are aiming to detect more signals. Among them, the most popular ones are at Hanford and Livingston both located in the US with 4 km arms which are run by LIGO collaborations [43–46], and the VIRGO interferometer [47, 48] with arms of 3 km located near Pisa, Italy. KAGRA [49, 50] is another recently built underground laser interferometer with 3 km arm lengths located in Japan. Other smaller detectors like GEO600 (arms with 600 m) and TAMA (arms with 600 m) are situated in Hannover, Germany, and Tokyo, Japan respectively. Due to the longer arm lengths, better sensitivity can be achieved by detectors like LIGO, VIRGO, and KAGRA.

Apart from these existing detectors, there have been proposals to build next-generation detectors with better sensitivity. Cosmic Explorer [51] is one of them which features two *L-shaped* detectors one with arm lengths of 40 km and another with 20 km arm lengths. The Einstein Telescope [79] is another proposed underground interferometer with arms of 10 km in length and it is expected to start its observations in 2035. Other than these ground-based detectors, there are several proposals for space-based detectors like LISA (Laser Interferometer Space Antenna) [52], μ -ARES [53] and DECIGO (DECi-hertz Interferometer Gravitational wave Observatory) [54]. These space-based interferometers have a few advantages over ground-based detectors. For starters, larger arm lengths can be achieved in space which in turn can help in increasing the sensitivity, and various noises that provide a hindrance for the earth-based detectors can easily be avoided. Space-based detectors are the future of GW detection as they will help us further in unfolding the mysteries of the early Universe. For the sensitivity of a selection of these detectors see Fig. 1

B. Cosmological detectors

In the era of precision cosmology, state-of-the-art analysis of the cosmic microwave background (CMB) and the abundance of light elements shed light on the gravitational wave background. First, both the production of light elements and the CMB are highly sensitive to the expansion rate of the Universe during each epoch (around 1 second and 1 million years respectively). If there is a gravitational wave background, the total radiation density is slightly higher than it would be otherwise. Precision fits to data for both the CMB and the abundances of light elements put a limit on the extra radiation allowed that is usually written in terms of the effective number of extra relativistic freedom,

$$N_{\text{eff}} \leq \begin{cases} 2.88 \pm 0.54 & \text{(BBN) [87]} \\ 2.00 \pm 0.34 & \text{CMB (lensing+BAO) [10]} \\ 3.01 \pm 0.15 & \text{(Combined) [87]} \end{cases} \quad (45)$$

To make use of this bound, we need to convert the additional gravitational wave radiation from its stochastic background into an effective amount of relativistic degrees of freedom. After electron-positron annihilation at 0.5 MeV, the ratio of gravitational radiation to electromagnetic radiation becomes constant. This means for both BBN and CMB observables we can, to a good approximation, use

$$\Delta N_{\text{eff}} = \frac{8}{7} \left(\frac{11}{4} \right)^{\frac{4}{3}} \frac{\Omega_{\text{GW}}^0}{\Omega_{\gamma}^0} \quad (46)$$

where the 0's indicate the values of their abundances today. The total gravitational radiation is of course

$$\Omega_{\text{GW}}^0 = \int \frac{df}{f} \Omega_{\text{GW}}^0(f) . \quad (47)$$

The second cosmological observable is temperature-polarization B-modes in the CMB, which are induced by gravitational waves (for a review see [88]). The CMB is sensitive to very low frequencies, around 10^{-17} Hz [89]. The only known candidate to produce a source at such frequencies is inflation itself. We will cover higher frequency signals from gravitational waves due to a blue tilted spectrum in section VI

C. High frequency proposals

Many gravitational wave sources are strongly peaked at a frequency that approximately corresponds to the Hubble scale at the time the source was produced. We will get into specifics in later sections. For now, we wish to draw attention to the fact that the higher the frequency, the higher the energy scale a gravitational wave detector can probe. The maximum temperature the Universe can reach is at around the GUT scale, depending upon the details of preheating.⁴ This means that gravitational wave cosmology has an incredible scope to probe physics at scales we could only dream of on Earth. On the other hand, the challenge is enormous.

As mentioned in the previous subsection, gravitational waves act as a source of dark radiation in the early Universe, mildly changing the expansion rate during Big Bang nucleosynthesis and recombination. The degree to which this expansion rate can change is restricted by observation. To shed light on any cosmological events before Big Bang nucleosynthesis, a gravitational wave detector must be more sensitive than limits on extra dark radiation. Since the abundance of gravitational radiation is related to the strain by $\Omega_{\text{GW}} \sim h^2 f^2$, the target strain sensitivity needed to beat limits on dark radiation grows quadratically with the frequency. As such, no proposal currently exists that can unambiguously probe gravitational waves at higher than around 1 KHz and beat the bounds on dark radiation. Even still, the opportunities presented by high-frequency gravitational wave physics have led to some ingenious proposals which are summarized in a living review in ref. [76].

⁴ It depends upon the details of the model. If there is an instability scale, then finite temperature corrections can render the Universe unstable [24], alternatively, gravitational freezeout could clash with ΔN_{eff} bounds for a modestly higher temperature [90]

III. GRAVITATIONAL WAVES FROM COSMIC PHASE TRANSITIONS

Gravitational waves from first-order cosmic phase transitions is a scenario that has arguably attracted more attention than any other source of a primordial background [41]. The concepts involved are in some ways quite familiar, everyone encounters phase transitions in their daily lives. Yet theoretically handling such an out-of-equilibrium quantum field theory has challenged the field for decades. In this section, we first make use of classical phase transitions to build an intuition for the subject before outlining the narrative of a cosmic phase transition, and the range of motivations for considering them and we review our current best understanding of how to model them.

A. Nucleation of bubbles

It is instructive to start with classical nucleation theory. Consider a bubble of a low-temperature phase nucleating in the background of the high-temperature phase. The Energy of the bubble of radius R can be expressed in terms of a pressure term that prompts expansion and a surface tension term that attempts to collapse the bubble [91]

$$E = -\frac{4\pi}{3}R^3\Delta p + \sigma 4\pi R^2 . \quad (48)$$

Such a bubble has a maximum in energy when the radius is at a critical value where the pressure and surface tension cancel each other out at $R = 2\sigma/\Delta p$. Above this critical radius, the pressure begins to overwhelm the surface tension and the bubble expands. The nucleation rate is the exponential of the energy of a bubble with a critical radius divided by the temperature

$$\Gamma \sim e^{-\frac{16\pi\sigma^3}{3\Delta p^2 T}} \quad (49)$$

so we see that a large surface tension suppresses nucleation and is the main proxy for the strength of a transition. The pressure difference between the two phases will grow as the system cools, so the nucleation rate will increase at least as long as Δp grows faster than the square root of temperature. In practice, Δp can reach a maximum and it is possible for a phase transition to never complete. A cosmic phase transition has three additional ingredients to classical nucleation theory - a field-theoretic treatment, an expanding background, and quantum corrections. Let us begin by considering how field theory modifies the

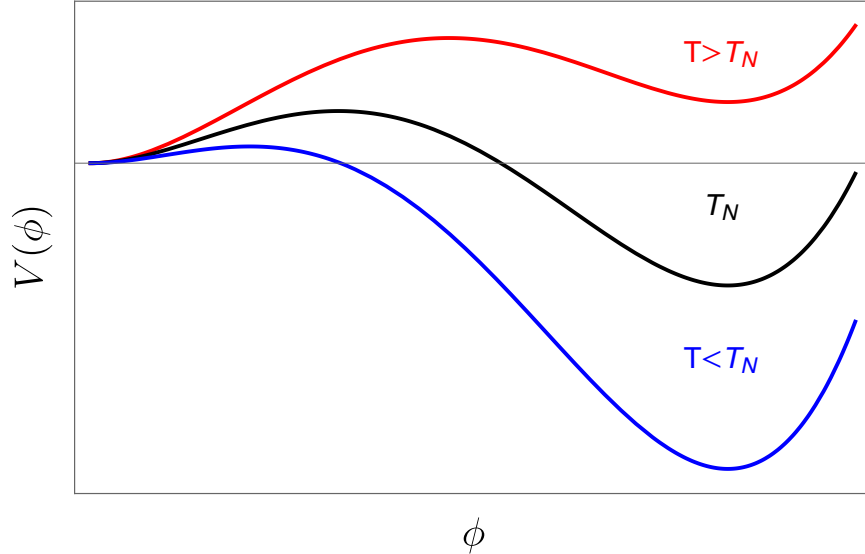


FIG. 4. Schematic of an effective potential for some scalar field, ϕ , evolving with temperature with a nucleation temperature denoted by T

classical nucleation prescription. It is most common to consider phase transitions driven by the thermal evolution of the effective potential, sketched in Fig. 4, for a scalar field which we will denote as ϕ . In such a case, we can derive the existence and behaviour of a bubble as a classical solution to the equations of motion. We simplify our lives by considering only spherical bubbles, and approximating $\int dt \rightarrow \frac{1}{T}$, in which case the equations of motion are

$$\frac{\partial^2 \phi}{\partial r^2} + \frac{2}{r} \frac{\partial \phi}{\partial r} = \frac{\partial V}{\partial \phi}. \quad (50)$$

A solution to this is of course that the field occupies an extremum where the gradient of the potential vanishes. However, imagine the above equation with the r coordinate replaced with time - it now describes the equations of motion of a ball on a hill of shape $-V$ with a strange time-dependent friction term. If we place the ball close to its maximum value, it will roll down towards the other local maximum. An initial condition that is too high will result in the ball rolling past the local maximum and continuing forever. If the initial condition is too low, the ball will roll around forever in the minimum connecting the two maxima. However, there is a Goldilocks solution where the ball starts in just the right place to land on the top of the local maximum.

Returning our imagination to the field theory case with radial rather than time derivatives, the solution we have found is of a spherically symmetric object that is in the true

vacuum at the center and becomes more like the false vacuum as we venture further out in radius. Or, in other words, it is a bubble of true vacuum nucleating in the medium of false vacuum [92].

So let us connect with what we learnt in nucleation theory. First, we can estimate the nucleation probability with the path integral formalism. We can take a saddle point approximation to then estimate the path integral as the exponential of the action [92–94],

$$\Gamma \sim e^{-S} \sim e^{-S_E/T} \quad (51)$$

where in the second line we have again used the approximation that $\int_0^\beta dt \rightarrow \beta$, leaving a Euclidean action that involves only a spatial integral. If we approximate the bubble profile as having a very thin wall, it is possible to make a direct analogue of classical nucleation theory,

$$S_E(\phi_{\text{bubble}}) = \frac{16\pi\sigma^3}{\Delta p^2} \quad (52)$$

where $\Delta p = \Delta V$ and

$$\sigma = \text{Re} \left[\int_{v_1}^{v_2} d\phi \sqrt{2V} \right]. \quad (53)$$

The thin wall approximation is only accurate very close to the critical temperature, however, we can nonetheless learn physical insight from the above. Recall that the strength of the transition is controlled by the surface tension. The surface tension grows with the height and width of the barrier separating the two phases. In the case of a scalar field theory, the surface tension will grow with the number of bosonic degrees of freedom that are made heavy by the change in phase as the change in mass of such Bosons. It is also possible in scalar field theories for there to be a large contribution to the surface tension from the tree-level shape of the potential if cubic terms are permitted by the symmetries of a theory. We thus expect these two paths to be the main avenues for producing a strong first-order phase transition - a large number of bosonic degrees of freedom gaining a large mass in the new phase and the symmetries of the theory allowing the potential to have a tree-level barrier.

Confining transitions are much more difficult to theoretically model than transitions involving the vacuum expectation value of a scalar field. However, the methods we do have seem to find similar wisdom where large changes in mass [95] of large degrees of freedom can lead to stronger transitions [62, 95–97].

The last pieces of the picture needed to mimic the situation of the early Universe are the quantum effects and the expanding background. A modest quantum effect arises from the

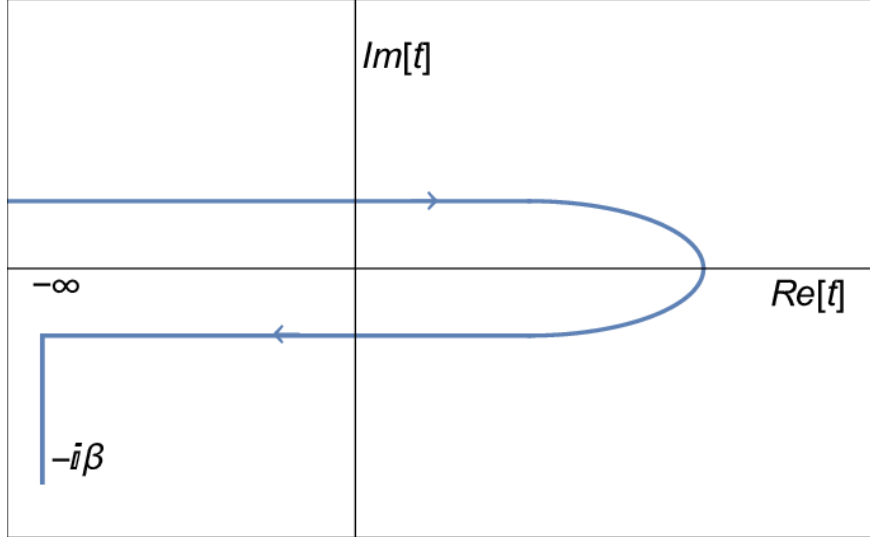


FIG. 5. The contour used in the real-time formalism is known as the closed-time path.

fluctuations around the bubble solution to the classical equations of motion. This results in a logarithmic correction to the effective action, and therefore a modification of the prefactor. A more dramatic effect is in the evolution of the effective potential - all thermal corrections are due to loops.⁵ The fact that these loop corrections need to be large enough to qualitatively change the features of the tree level effective potential signals that we should worry about the efficacy of perturbation theory! This issue we will return to shortly. Finally, the expansion of the Universe means that the phase transition does not begin the moment it becomes energetically favourable for there to be a change in the ground state. Instead, we should compare the nucleation rate to the expansion of the Universe. When the nucleation rate is large enough that there is at least one critical size bubble per Hubble volume per Hubble time, the phase transition can be thought to begin. However, if the nucleation rate does not further increase from this minimum rate, the phase transition could never be complete as the bubbles cannot catch up to the expanding volume around them. Because of this, the time scale of the phase transition, β^{-1} is controlled not by the nucleation rate, but its first (and occasionally second [98]) derivative,

$$\beta \sim \frac{1}{\Gamma} \frac{d\Gamma}{dt} \rightarrow \frac{\beta}{H} \sim T \frac{d(S_E/T)}{dT} . \quad (54)$$

⁵ We acknowledge that the precise demarcation between what is truly quantum and what isn't can be subtle. For this review, we use the term quantum to refer to things that would vanish if $\hbar \rightarrow 0$ which, perhaps counterintuitively, is the case for all finite temperature corrections to a quantum field as all finite temperature terms are loop-induced

B. Effective potential and action at finite temperature

There are in general two ways people tend to include temperature corrections to quantum field theory - the imaginary time formalism and the real time or closed time path formalism. The closed time path formalism assumes that the system was at once in equilibrium in the past. Starting with the finite temperature density matrix, one can then derive using the interaction picture of quantum mechanics that the expectation value of an operator is evaluated using the time contour shown in Fig. 5. A consequence of this unusual time contour is that there are no longer just time-ordered and time-anti-ordered propagators, there are also mixed two-point correlators that involve on field moving in opposite directions in time. The propagators in equilibrium are just a zero temperature contribution (which vanishes in the case of the mixed correlators) summed with a finite temperature piece. This means that when one writes the corrections to the effective potential by calculating the 1-particle-irreducible loop diagrams, the result is a sum of the loop corrections at zero temperature and the finite temperature corrections. The closed time path formalism has the potential to handle departures from equilibrium, though this review is not aware of any attempt to take advantage of this in gravitational wave calculations.

In equilibrium, an alternative formalism considers the propagators in imaginary time and in equilibrium. In this case, the k_0 contribution to the zero temperature propagators is replaced by Matsubara modes and the dk_0 integrals are replaced by a sum over these modes. The result is not obviously equivalent to the sum of zero and finite temperature pieces that one derives in the closed time path formalism. However, as long as one approximates the background plasma as being in equilibrium⁶, then after some massaging, the result of both approaches are the same

$$V_T = \sum_{i \in \text{bosons}} n_i \frac{T^4}{2\pi^2} J_B \left(\frac{m_i^2}{T^2} \right) - \sum_{i \in \text{fermions}} n_i \frac{T^4}{2\pi^2} J_F \left(\frac{m_i^2}{T^2} \right), \quad (55)$$

where the thermal functions have the form

$$J_B(z^2) = \int_0^\infty dx x^2 \log \left[1 + e^{-\sqrt{x^2+z^2}} \right] \sim \frac{z^2}{24} - \frac{z^3}{12\pi} + \dots \quad (56)$$

$$J_F = \int_0^\infty dx x^2 \log \left[1 + e^{-\sqrt{x^2+z^2}} \right] \sim -\frac{z^2}{48}. \quad (57)$$

⁶ calculating the effective potential in a non-equilibrium background was recently done at zero temperature [99], though we are not aware of an attempt to do the equivalent at finite temperature

In the above, the right-hand approximations are the high-temperature expansions when $z = m/T$ is small.

We can now sketch how a first-order phase transition is generated. Consider a Bosonic field whose mass scales as $m = g\phi$ where ϕ is the scalar field undergoing a change in its vacuum expectation value during the phase transition. In such a case, the thermal corrections to the potential due to this field in the high-temperature limit is

$$\Delta V_T = \frac{g^2 \phi^2 T^2}{24} - \frac{g^3 \phi^3 T}{12\pi} + \dots \quad (58)$$

The second term in the above equation produces a barrier as the full potential can have three consecutive terms with alternating signs. Let the tree-level potential be of the form

$$V = \mu^2 \phi^2 + \lambda \phi^4 . \quad (59)$$

After rescaling $V \rightarrow \Lambda^4 \tilde{V}$ and $\phi \rightarrow v\varphi$ where v is the vacuum expectation value, then absorbing a redundant parameter into the definition of Λ , one can rewrite the potential and mass as

$$\tilde{V} = \Lambda^4 \left(-\frac{1}{2} \left[\frac{\varphi}{v} \right]^2 + \frac{1}{4} \left[\frac{\varphi}{v} \right]^4 \right) \quad (60)$$

$$m_\phi = \sqrt{2} \frac{\Lambda^2}{v} \quad (61)$$

$$m_g = gv . \quad (62)$$

If we consider the temperature at which the potential is double-welled, that is the critical temperature, the surface tension scales as

$$\sigma \approx \frac{gm_g^5}{m_\phi^2} \quad (63)$$

as long as $3\pi^2 m_\phi^2 \gg g^2 m_g^2$. This limit is chosen to simplify our expression but is similar to the regime at which the high-temperature regime is valid. Regardless, we are only interested in a qualitative picture and indeed we see from the above that the strength of the phase transition grows with the ratio of the mass of the masses as we expected from our discussion in the previous section. Repeating the above for n copies of m_g finds that the strength of the transition grows with n . So we find a rule of thumb - *the strength of the transition grows with the number of bosonic degrees of freedom becoming nonrelativistic during the transition and the ratio of their masses to the mass of the dynamical scalar*. Remarkably this seems to be

true of chiral transitions as well [95]. From this rule of thumb, we can see why the Standard model is expected to have a crossover transition. The Higgs boson is in fact heavier than all gauge bosons that acquire a mass during electroweak symmetry breaking and the size of the gauge group, $SU(2) \times U(1)$, doesn't have enough gauge bosons to compensate for such a small ratio.⁷

C. Possible sources

If the reheating temperature reached at least the electroweak scale, then it is likely that our Universe experienced at least two changes in its ground state - an epoch of electroweak symmetry breaking at temperatures of around 100 GeV and an epoch where the quark-gluon plasma hadronizes at around 100 MeV. As mentioned above, both transitions are crossovers in the Standard Model at the low densities expected in the early Universe [100–106]. However, this picture can change if the physics beyond the Standard Model permits it, and these transitions could occur via the nucleation and percolation of bubbles of the low-temperature phase. Such a spectacular process of the early Universe boiling for an epoch naturally leads to a gravitational wave signal that could be visible today.

In the case of electroweak symmetry breaking, the most common ways to modify it to catalyze a strong first-order phase transition are

- 1 Introduce more bosonic degrees of freedom that couple to the Higgs. The canonical examples are the two Higgs doublet model [107–127] (including the inert doublet model [128–135]) and the light stop mechanism [136–153]. However, it is also possible with a scalar electroweak triplet [129, 154–157], and complex [158–163] or real scalar singlet(s) [164–183].
- 2 Introduce an effective tree-level barrier between the true and false vacuum. This means that the surface tension between the two phases may not vanish even at zero temperature. The two most common ways of achieving this are through an effective cubic coupling from a gauge singlet, $sH^\dagger H$, or having a heavy degree of freedom integrated out such that the effective potential of the Higgs has alternating signs of

⁷ Strictly speaking, there is no surface tension for a crossover transition. However, analysing the surface tension does give the correct wisdom about how to make the transition stronger

the form [184–191]

$$V = \mu^2 H^\dagger H - \lambda (H^\dagger H)^2 + \frac{1}{\Lambda^2} (H^\dagger H)^3 . \quad (64)$$

Unfortunately, the Standard Model requires such a dramatic change to its effective potential to catalyze a first-order transition, that there is only one UV complete model that can be accurately characterized by the above potential - the real scalar singlet extension of the Standard Model [192]. This renders an effective field theory approach to be of questionable utility.

A more exotic approach is to have a multi-step transition [154, 182, 193–205] where the direction the field goes during the phase transition is no longer from the origin. Turning to the case of the QCD transition, again we expect a crossover transition. The first hint of this was from Pisarski and Wilcheck who argued that one needs at least three light quark flavours in order to have a stable infrared fixed point [206]. The existence of such fixed points would put the QCD transition in the same Universality class as a first-order phase transition. All models of the QCD transition seem to suggest that at large baryon chemical potential, the QCD transition becomes strongly first order [207–215]. However, the lattice is yet to confirm the existence of a critical endpoint at which the baryon density is large enough to change the nature of the transition [216, 217]. Finally, the pure Yang Mills theory is easier to model due to the absence of fermions. We know that pure Yang Mills always yields a first-order phase transition. We therefore have three possible methods for inducing a strong QCD phase transition

- 1 Render the mass of the strange quark dynamical such that it is much lighter in the early Universe. This can be achieved through a flavon field which renders the effective coupling between the Higgs and strange quark to be proportional to the vacuum expectation value of the flavon field [218]. Another option is to have Higgs field supercool until the QCD era, at which the QCD transition catalyzes both electroweak and chiral symmetry breaking [219].
- 2 In principle one could use flavon fields to render all quarks heavy in the early Universe. In such a case one would have a strong first order glueball transition. This option has not been analyzed in the literature, though glueball transitions have [62, 220–226]. We include it for completeness.

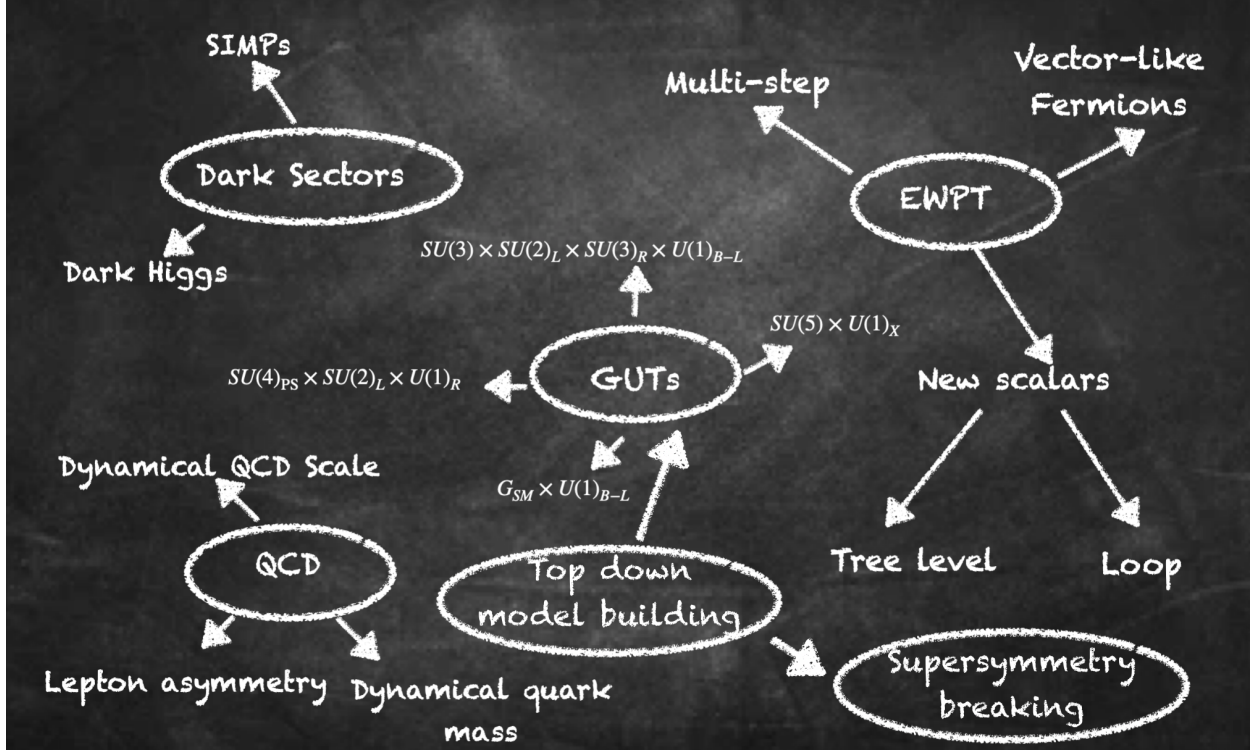


FIG. 6. Current landscape of possible sources of gravitational waves from a cosmic first order phase transition

- 3 A third option is to have a large baryon chemical potential. The only known way to do this is to have a large lepton asymmetry [227–229].

While the QCD and electroweak eras are arguably the most well-motivated epochs to search for (as we know that at least a change in ground state likely occurred) there are many more motivations for a strong first-order phase transition in the early Universe. A popular model to realize a scale-invariant potential as described in section III D 2 is B-L breaking [230–238] (or B/L breaking [239]). Additionally people have considered phase transitions in neutrino mass models [240–242], GUT symmetry breaking chains [243–247], flavour physics [248, 249], supersymmetry breaking [250–253], hidden sectors [62, 95, 220, 223, 225, 254–266] and axions [267–269]. The full landscape of ideas we show in Fig. 6.

Most of the above involve phase transitions involving scalar fields. However, it takes different technology to model a confining transition. The typical approach in the literature is to model some condensate as a scalar field and consider its effective potential [95, 264]. In the case of the linear Sigma model, one writes an effective potential for the quark condensate

where the parameters of the potential are free and the one-loop corrections are derived in exact analogue with a scalar field theory [95]

$$V(\Sigma) = -m_\Sigma^2 \text{Tr}(\Sigma \Sigma^\dagger) - (\mu_\Sigma \det \Sigma + h.c.) + \frac{\lambda}{2} [\text{Tr}(\Sigma \Sigma^\dagger)]^2 + \frac{\kappa}{2} \text{Tr}(\Sigma \Sigma^\dagger \Sigma \Sigma^\dagger) \quad (65)$$

where $\Sigma_{ij} \sim \langle \bar{\psi}_{Rj} \psi_{Li} \rangle$ is the quark condensate that is decomposed as

$$\Sigma_{ij} = \frac{\phi + i\eta'}{\sqrt{2N_F}} \delta_{ij} + X^a T_{ij}^a + i\pi^a T_{ij}^a \quad (66)$$

and ϕ is what acquires a vacuum expectation value. The determinant term in the effective potential above arises from instanton effects. In this model, it seems that the strength of the gravitational wave signal grows with the number of light flavours (at least going from 3 flavours to 4) and the hierarchy between the meson and the axion mass.

For the Nambu-Jona-Lasino model (NJL), again an effective potential is written for mesons but the mesons are non-propagating and the loop corrections are derived from considering quarks running in the loop [270–273]

$$V_0^{\text{NJL}}(\sigma) = \frac{3}{8G} \bar{\sigma}^2 - \frac{G_D}{16G^3} \sigma^3 \quad (67)$$

$$V_{\text{CW}}^{\text{NJL}}(\sigma) = -\frac{3n_c}{16\pi^2} \left[\Lambda^4 \log \left(1 + \frac{M^2}{\Lambda^2} \right) - M^4 \log \left(1 + \frac{\Lambda^2}{M^2} + \Lambda^2 M^2 \right) \right] \quad (68)$$

$$V_{\text{T}}^{\text{NJL}}(\sigma, T) = 6n_c \frac{T^4}{\pi^2} J_F(M^2/T^2) \quad (69)$$

$$M = \bar{\sigma} - \frac{G_D}{8G^2} \bar{\sigma}^2 \quad (70)$$

where G and G_D are free parameters. Unlike the linear sigma model. The latter model can be enhanced by adding the Polyakov loop resulting in a gluon potential [274]. If the model in question has three colours, lattice data can be used to model the gluon contribution to the potential,

$$\mathcal{L}_{\text{PNJL}}^{\text{MFA}} = \mathcal{L}_{\text{PNJL}}^{\text{MFA}} - V_{\text{Glue}}(L, T) \quad (71)$$

[89]

$$T^{-4} V_{\text{glue}}(L, T) = -\frac{1}{2} a(T) L \bar{L} + b(T) \log [1 - 6L\bar{L} - 3(L\bar{L})^2 + 4(L^3 + \bar{L}^3)] \quad (72)$$

$$a(T) = 3.51 - 2.47 \frac{T_{\text{glue}}}{T} + 15.2 \left(\frac{T_{\text{glue}}}{T} \right)^2 \quad (73)$$

$$b(T) = -1.75 \left(\frac{T_{\text{glue}}}{T} \right)^3 \quad (74)$$

In this case, the strength of the phase transition grows as G goes near a critical point that depends on G_D (or vice versa) where the nucleation rate becomes too slow compared to the expansion rate of the Universe. In the case of Yang-Mills the surface tension and latent heat have been calculated on the lattice for $N_C \lesssim 8$ [96, 97],

$$\sigma = (0.013N_C^2 - 0.104)T_C^3, \quad L = \left(0.549 + \frac{0.458}{N_C^2}\right)T_C^4 \quad (75)$$

which in principle allows one to use critical nucleation theory to estimate the properties of the phase transition using an extrapolation for the pressure difference using the above result for the latent heat as was done in ref. [62]. Alternatively, there exist attempts to model glueball transitions using lattice data to inform an ansatz for a potential for the Polyakov loop as was done in refs [220, 223, 225]. Most methods tend to find that the more colours, the stronger the transition and that one needs more than 3 colours to be seen by any next-generation gravitational wave detector.

D. Narrative of a phase transition and modeling of the spectrum

There are in principle three sources that lead to a gravitational wave signal that roughly correspond to the three sources of energy released when boiling a kettle. There is a source from the bubble nucleation itself [275, 276], the scalar shells expand and crash into each other. A second source is an acoustic contribution, where sound shells collide [277]. The third source is from an afterparty of turbulence [278], where large eddy currents break down into smaller eddy currents. It is customary for each stage of the narrative to be described separately, though simulations may suggest that there may be no demarcation between the acoustic and turbulence sources [279]. Usually, the acoustic source dominates, therefore so much of the theoretical modeling has been dedicated to understanding it. However, if the bubble walls become ultra-relativistic the collision term can dominate [237]. This has motivated a flurry of recent work focused on understanding this term as well as the kind of phase transition that can achieve such enormous Lorentz factors for the bubble walls. We will briefly cover the basic modeling techniques for each source before venturing into some of the current challenges in reproducing simulations.

1. Acoustic source

The acoustic source is widely believed to be the dominant source of gravitational waves and in the usual narrative is from the collision of sound shells before the onset of turbulence. In reality, it might be difficult to separate the turbulence and acoustic eras. The contribution to the stress-energy tensor from the acoustic source is controlled by the fluid velocity [277, 280, 281],

$$T^{\mu\nu} \supset (e + p)U^\mu U^\nu + g^{\mu\nu}p \quad (76)$$

where the 4-velocity of the fluid $U^\mu = \gamma(1, \vec{v})$ and the energy and momentum densities are given by

$$e = a_B^4 + V - T \frac{\partial V}{\partial T} \quad (77)$$

$$p = \frac{1}{3}a_B T^4 - V \quad (78)$$

with $a = g_*\pi^2/30$. One typically separates the field and fluid components of the stress-energy tensor by adding and subtracting a friction term to the equations of motion and then solving it. If the sound shell has enough time to expand before colliding, the initial size of the sound shell becomes irrelevant and the fluid velocity profile becomes self-similar, which is dependent only upon the ratio r/t . If one takes the RMS of the resulting velocity profile, one can derive a gravitational wave spectrum that has the form of a broken power law

$$h^2\Omega_{\text{GW}}(f) = 2.5 \times 10^{-6} \left(\frac{100}{g_*(T_p)} \right)^{1/3} \Gamma^2 U_f^4 \left[\frac{H_p}{\beta} \right] v_w S_{\text{sw}} \Gamma(y) \quad (79)$$

where the spectral shape has the form

$$S_{\text{sw}} = \left(\frac{f}{f_{\text{sw}}} \right)^3 \left[\frac{7}{4 + 3(f/f_{\text{sw}})^2} \right]^{7/2}. \quad (80)$$

In reality, the finite width of the velocity profile results in there being two peaks to the spectrum corresponding to the two scales - the mean bubble separation and the width of the sound shell. So calculating the RMS of the fluid velocity rather than using the full velocity profile turns out to be quite a crude approximation [284] (see fig. 7 for a comparison). In this case, the gravitational wave spectrum has the form [285]

$$\Omega_{\text{GW}} = F_{\text{GW},0} \Omega_p M(s, r_b, b) \quad (81)$$

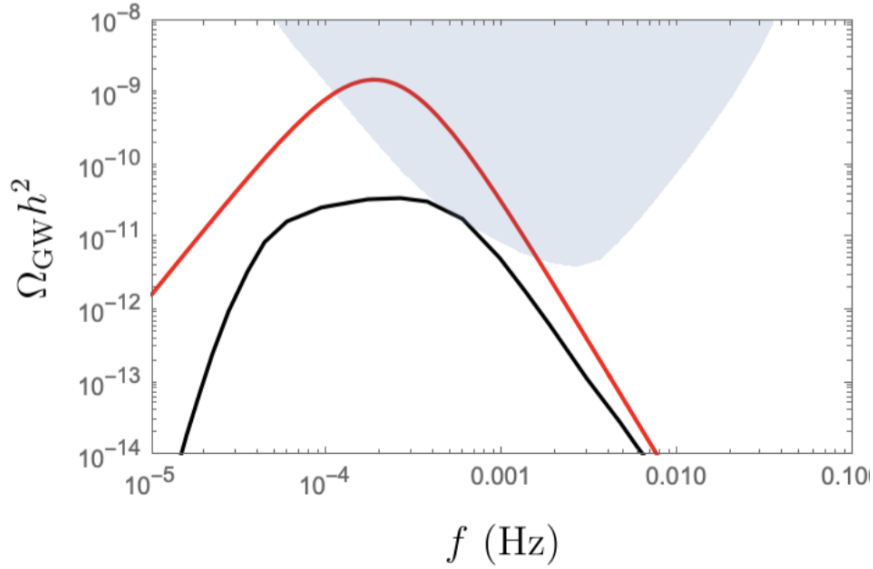


FIG. 7. An example of how poor the simplest calculations of the sound wave source can be. In the above, we compare the sound shell model using the RMS fluid velocity (red) with a numerical treatment that uses the whole velocity profile (blue). Note that the latter curve also the suppression factor from the energy lost to vorticity, likely due to the fact that some sound shells do not have enough time to reach a self-similar solution [282]. Figure taken from [283] and data taken from [284]

with a spectral shape now having two peaks

$$M(s, r_b, b) = s^9 \left(\frac{1 + r_b^4}{r_b^4 + s^4} \right)^{(9-b)/4} \left(\frac{b + 4}{b + 4 - m + ms^2} \right)^{(b+4)/2} \quad (82)$$

where $s = f/f_p$, r_b is the ratio between the peaks, b controls the slope and m is chosen so that the peak is located at $s = 1$, $M = 1$ for $r_b < 1$,

$$m = (9r_b^4 + b)/(r_b^4 + 1) . \quad (83)$$

The parameters (r_b, b) need to be obtained numerically from the numerical calculation of the gravitational wave spectrum. Numerical simulations demonstrate that the sound shell model overestimates the gravitational wave spectrum as some sound shells do not have enough time to reach a self-similar solution before colliding [282]. This suppression becomes large when the trace anomaly is large and the wall velocity is small. Other recent improvements come

from allowing the speed of sound to vary from its equilibrium value [286, 287] and considering how the nucleation rate is affected by the reheating of the plasma [288].

2. Collision source

This source captures the collision of the scalar shells and was the original focus of early research into gravitational waves from phase transitions [275, 276]. It arises from the field component of the stress-energy tensor,

$$T_{\mu\nu} \left(\frac{\partial \mathcal{L}}{\partial \partial^\mu \phi} \partial_\nu \phi + c.c. \right) + \dots . \quad (84)$$

The fraction of energy that becomes dumped into the collision term is severely suppressed due to friction terms that are related to the Lorentz boost factor [289]. The exact dependence is a matter of ongoing debate [290, 291], which we will return to shortly. For a linear dependence on the boost factor, the pressure difference between the two phases has to be an incredible trillion times larger than the radiation energy density for this source to dominate [237]. Surprisingly, this does not necessarily require fine-tuning. One option is to have a classical conformal symmetry such that the mass terms in the tree-level potential vanishes. In the case of scalar electrodynamics charged under a U(1) symmetry, the one-loop corrections have the approximate form under the high-temperature expansion [292–300]

$$V \sim \frac{g^2}{2} T^2 \phi^2 + \frac{3g^4 \phi^4}{4\pi^2} \left(\log \left[\frac{\phi^2}{v^2} \right] - \frac{1}{2} \right) . \quad (85)$$

In reality, such use of a high-temperature expansion is a little scandalous if we are considering supercooling so severe that the collision term dominates. In fact, it is not clear how to accurately calculate the dynamics of the phase transition. We will later discuss methods of resummation to tame finite temperature field theory. The most successful method, dimensional reduction [301–308], requires a hierarchy between the Matsubara modes and other masses of the theory [309]. Another method using gap equations is expected to be most useful precisely when the high-temperature expansion breaks down [309–315], however, the high-temperature expansion is breaking down so badly that the momentum dependence would need to be taken into account. This is not insurmountable, but whether gap equation methods are reliable in such an extreme regime is yet to be tried let alone tested. Regardless, taking the above potential at face value one finds that for modestly small values of the gauge

coupling, $g \lesssim 0.4$, one can achieve a large enough amount of supercooling that the collision term dominates [299].

3. Velocity of ultrarelativistic walls

Let us briefly digress to discuss the current status of an ongoing debate on how one achieves an enormous Lorentz factor needed for the collision term to dominate. It was originally argued that a heuristic check of whether a bubble wall runs away was all that was needed [316]. Bodecker and Moore considered the $1 \rightarrow 1$ interactions with the bubble wall. For $\gamma \gg 1$, if the pressure on the bubble wall from $1 \rightarrow 1$ processes is $V_{0-T} + V_T$ (mean field). If this pressure is less than zero, the bubble wall will run away and the Lorentz factor will diverge. In a follow-up work [289], they found that $1 \rightarrow 2$ interactions with the bubble wall scale linearly with γ . If the scalar field undergoing a change in vacuum expectation value has any gauge charges, such a process will exist and the bubble will reach a terminal velocity [289]. Recent work painted a more pessimistic picture, where interactions with the bubble wall involving multiple gauge bosons were shown to yield a pressure contribution quadratic in the Lorentz factor, $P\gamma^2 T^4$ [290]. By contrast, ref. [291] argued that such a severe scaling no longer appears when one includes a non-homogeneous temperature background. In fact, taking into account the finite width of the wall, one finds that the dependence on the boost is logarithmic which presents a far rosier picture of the ability to achieve runaway transitions where the collision term dominates [317]. No doubt this debate is still in flux and a resolution is needed. A simple estimate of the gravitational wave spectrum arising from the collision term can be calculated using the envelope approximation [318–321]. Here, it is assumed that the bubble walls are infinitesimally thin, and just after the nucleation, the energy-momentum tensor not only vanishes everywhere in the space except on these walls but also in the sections of the wall that are contained inside other bubbles after the overlap. This leaves only the envelope surrounding the region of true vacuum.

A spherically symmetric system does not change the gravitational field and hence can never act as a source of GWs. This suggests that a spherically symmetric expanding bubble can only generate GW after its collision with other bubbles which results in the breaking of spherical symmetry on the highly energetic walls of the bubble. Assuming that the bubble nucleation takes place exponentially and the thin-wall and envelope approximation remains

valid, the GW spectrum that should be seen today can be written as [321]

$$\Omega_{\text{co}}(f)h^2 = 1.67 \times 10^{-5} \left(\frac{g_\star}{100}\right)^{-1/3} \left(\frac{\kappa_{\text{co}}\alpha}{1+\alpha}\right)^2 \left(\frac{\beta}{H_\star}\right)^{-2} S_{\text{co}}(f)\Delta, \quad (86)$$

where the spectral form is given by

$$S_{\text{co}}(f) = \left[0.064\left(\frac{f}{f_{\text{co}}}\right)^{-3} + 0.456\left(\frac{f}{f_{\text{co}}}\right)^{-1} + 0.48\left(\frac{f}{f_{\text{co}}}\right)\right]^{-1} \quad (87)$$

with the peak frequency

$$f_{\text{co}} = 1.65 \times 10^{-5} \text{Hz} \left(\frac{g_\star}{100}\right)^{1/6} \left(\frac{T_\star}{100 \text{ GeV}}\right) \left(\frac{f_\star}{\beta}\right) \left(\frac{\beta}{H_\star}\right). \quad (88)$$

Here, f_\star/β denotes the peak frequency at creation in the Hubble units and may depend on the bubble wall velocity v_w whereas H_\star/β represents the nucleation rate relative to the Hubble rate. A more careful analysis was performed recently in ref [299] that included the contributions to the stress-energy tensor after the collision. In this case, the resulting spectrum still follows a broken power law. The envelope predicts an infrared spectrum scaling as f^3 and a UV spectrum scaling as f^{-1} whereas this analysis found the power law of the infrared and UV spectrum could vary in an approximate range of $(f^{[1-3]}, f^{[2-2.5]})$ respectively.

4. Turbulence

The aftershock or the turbulence developed in the plasma following the bubble collisions also leads to the generation of the GWs. It is interesting to point out that while the turbulent motion can generate the GWs on its own, it can also impact the GWs sourced from sound waves even if the GWs from turbulence are negligible. This is because turbulence transfers energy from bulk motion on large scales to small scales. The turbulence can be characterized by irregular eddy motions and is typically modeled by Kolmogorov's theory [322–324]. The expansion and the collision of bubbles tend to stir the background plasma resulting in eddies that can be of the order of the bubble radius. Now, in order to develop a stationary, homogeneous, and isotropic turbulence, the plasma needs to be stirred continuously which is only possible if the stirring time is larger than the circulating time of the largest eddies. Early work on turbulence was able to obtain an analytic handle on the non-stationary case and consider a finite source [324]. Beyond this, it is an enormous challenge to get an analytic

handle on turbulence and so far we must rely largely on simulations, which we summarize in section III F. Here we briefly summarize the gravitational wave spectrum from Kologorov turbulence with a finite time source as outlined in ref [324].

The spectrum is given by,

$$\Omega_{\text{tur}}(f)h^2 = 3.35 \times 10^{-4} \left(\frac{g_\star}{100}\right)^{-1/3} \left(\frac{\kappa_{\text{tur}}\alpha}{1+\alpha}\right)^{3/2} \left(\frac{\beta}{H_\star}\right)^{-1} S_{\text{tur}}(f)v_w, \quad (89)$$

where κ_{tur} denotes the efficiency of conversion of latent heat into the turbulent flows and the spectral shape of the turbulent contribution is given by,

$$S_{\text{tur}}(f) = \left(\frac{f}{f_{\text{tur}}}\right)^3 \left(\frac{1}{[1 + (f/f_{\text{tur}})]^{11/3}(1 + 8\pi f/h_\star)}\right)^{7/2}, \quad (90)$$

with h_\star being the Hubble rate at T_\star ,

$$h_\star = 16.5 \times 10^{-6} \text{Hz} \left(\frac{g_\star}{100}\right)^{1/6} \left(\frac{T_\star}{100 \text{ GeV}}\right), \quad (91)$$

and f_{tur} being the peak frequency and is almost three times larger than the one obtained from the sound wave,

$$f_{\text{tur}} = 27 \times 10^{-6} \text{Hz} \frac{1}{v_w} \left(\frac{g_\star}{100}\right)^{1/6} \left(\frac{T_\star}{100 \text{ GeV}}\right) \left(\frac{\beta}{H_\star}\right). \quad (92)$$

E. Theoretical issues with thermal field theory

Achieving a phase transition requires that the thermal loop corrections to the tree level potential modify it drastically enough to substantially alter its shape and qualitative features. Having loop corrections being dominant is cause for alarm if we are to use perturbation theory. A second issue is that perturbation theory might actually diverge [325]. Consider the expansion parameter in the loop expansion for bosonic virtual states at zero temperature compared to its finite temperature counterpart

$$\frac{g}{\pi^2} \rightarrow \frac{g}{\pi^2} f \sim \frac{g}{\pi^2} \frac{T}{m}. \quad (93)$$

Here f is the bosonic distribution function and we have used the high-temperature expansion. Note that for some bosons the mass scales with the field value, $m \propto \phi$. However, if we are describing corrections to the potential we need to consider corrections when $\phi \rightarrow 0$ and

T/m diverge. A partial fix to this issue is to resume our theory to modify the masses of all particles running in loops by their loop correction,

$$\frac{g}{\pi^2} \frac{T}{m} \rightarrow \frac{g}{\pi^2} \frac{T}{\sqrt{m^2 + \Pi}} \quad (94)$$

where Π is the thermal correction to the mass. The downside of this is that the mass of the dynamical scalar field is usually tachyonic at the origin. It is in principle possible for the thermal mass to cancel the tachyonic mass, again resulting in an infrared divergence. Indeed this is what occurs in a second-order transition which is why even sophisticated uses of perturbation theory badly estimate the critical mass at which the electroweak phase transition changes from crossover to weakly first order [103, 326]. Fortunately, this does not appear to be an issue for phase transitions strong enough to detect [327]. While Linde's infrared problem presents a catastrophic failure of perturbation theory at high orders, one can still use perturbation theory to understand the behaviour of strong first-order transitions (and recent work that Linde's infrared problem may not be as numerically important as previously thought [328]). However, we still have an issue of loop corrections needing to dominate to ensure that temperature corrections qualitatively modify the nature of the effective potential. This calls for a reorganization of perturbation theory so that instead of a loop expansion, we ought to organize the theory in order of the size of each contribution. Consider the most simple scalar field theory with a potential

$$V = \frac{m^2}{2} \phi^2 + \frac{g^2}{4!} \phi^4 \quad (95)$$

The loop corrections, assuming the validity of the finite temperature expansion, are

$$V_{0-T} = \frac{(m^2 + \frac{g^2}{2} \phi^2)^2}{64\pi^2} \left(\log \left[\frac{(m^2 + \frac{g^2}{2} \phi^2)}{\mu^2} - \frac{3}{2} \right] \right) \quad (96)$$

$$V_{1-T} = \frac{g^2}{24} \phi^2 T^2 - \frac{1}{12\pi} (m^2 + \frac{g^2}{2} \phi^2)^{3/2} T, \quad (97)$$

where μ is the renormalization scale in the \overline{MS} scheme. A method of testing the size of higher-order corrections is to measure the scale dependence. If perturbation theory is working well, the implicit scale dependence from RG running should approximately cancel the explicit scale dependence in the loop correction, with any residual scale dependence indicating the approximate size of the neglected higher-order terms. The renormalization

group equations for this minimal theory is

$$\mu \frac{\partial m^2}{\partial \mu} = \frac{g^2 m^2}{16\pi^2} \quad (98)$$

$$\mu \frac{\partial g^2}{\partial \mu} = 3 \frac{g^4}{16\pi^2} \quad (99)$$

from which we can derive the scale dependence of each contribution to the potential to $O(g^4)$

$$\mu \frac{\partial V}{\partial \mu} = \frac{m^2 g^2}{32\pi^2} \phi^2 + \frac{g^4}{128\pi^2} \phi^4 \quad (100)$$

$$\mu \frac{\partial V_{0-T}}{\partial \mu} = -\frac{m^4}{32\pi^2} - \frac{m^2 g^2}{32\pi^2} \phi^2 - \frac{g^4}{128\pi^2} \phi^4 \quad (101)$$

$$\mu \frac{\partial V_{1-T}}{\partial \mu} = \frac{g^4}{256\pi^2} T^2 \phi^2. \quad (102)$$

Apart from the running of the cosmological constant, the scale dependence from the temperature-independent pieces cancels to this order. On the other hand, there is nothing to cancel the temperature-dependent piece indicating that perturbation theory is not giving us the correct hierarchy of terms (from largest to smallest). Including the thermal mass correction in the loop partially solves our issue by yielding an additional piece

$$V_{0-T} = \frac{(m^2 + \frac{g^2}{2}\phi^2 + \Pi)^2}{64\pi^2} \left(\log \left[\frac{(m^2 + \frac{g^2}{2}\phi^2) + \Pi}{\mu^2} - \frac{3}{2} \right] \right) \rightarrow \mu \frac{\partial V_{0-T}}{\partial \mu} \text{ sup} = -\frac{g^4}{48 \times 16\pi^2} T^2 \phi^2. \quad (103)$$

So we partially solve our issue by resumming the mass. However, there is a 2-loop sunset diagram that has a term of the same order and completes the cancellation of the scale dependence of the thermal quadratic contribution to the effective potential

$$V_{\text{sun}} = -\frac{1}{12} g^4 \phi^2 \frac{3T^2}{32\pi^4} \left(\log \left[\frac{\mu^2}{m^2 + \frac{g^2}{2}\phi^2} \right] + 2 \right) \left(\frac{\pi^2}{6} - \frac{\pi M}{2T} \right). \quad (104)$$

Taking the derivative on the logarithm will yield a term $\sim -g^4 T^2 \phi^2 / \pi^2$ which is precisely what we require to cancel the scale dependence. If only we were done. If we fish around in thermal field theory for all terms $O(g^4)$ we find more terms. Even in this unrealistically simple theory, it is quite cumbersome to collect all the terms needed to define the theory to accuracy g^n . Unlike zero temperature perturbation theory, a naive finite temperature loop expansions does not naturally organize perturbation theory into a series in terms of a small parameter $(g/\pi)^n$. Fortunately, there is a method to naturally organize perturbation theory. In imaginary time, the time domain is compact of size $1/T$. Thus the theory looks

like a three-dimensional theory with a compactified extra dimension with the tower of heavy Kaluza Klein modes known as Matsubara modes. These modes are at the scale πT so they can be integrated out as long as the high-temperature expansion is valid resulting in an effective three-dimensional theory [301–308]. Integrating out these heavy modes results in the mass terms being shifted by their thermal masses. The temporal modes of vector bosons in the effective theory have masses of the scale $O(gT)$ due to the Debye masses, which usually is large compared to the masses of the dynamical scalar as the Debye mass partially cancels against the tachyonic mass. This means that it might be appropriate to make an additional step in integrating the temporal modes of vector bosons. Further corrections to the dimensionally reduced theory arise from the matching relations between the 4-dimensional and 3-dimensional theories, which for the general field has the form

$$\phi_{3D}^2 = \frac{1}{T}(1 + \Pi'_{\phi\phi})\phi_{4D}^2, \quad (105)$$

where $\Pi' = \frac{d}{dk^2}\Pi$ is the derivative of the self-energy evaluated at zero momentum. These self-energies can be reabsorbed into the definition of all parameters in the theory. Unlike a loop expansion, dimensional reduction naturally organizes the theory into powers of the coupling g_2 . For instance, in the standard model, we have

$$V_3 \supset \frac{1}{2}\mu_{h,3}^2 h_3^2 + \frac{1}{4}\lambda_3 h_3^4 + \dots \quad (106)$$

$$\mu_{h,3}^2 = \mu_h^2(\Pi_{hh}) - (\mu_h^2 - \Pi_{hh})\Pi'_{hh} \quad (107)$$

$$\lambda_3 = T(\lambda - \frac{1}{2}\Gamma_{hhhh} - 2\lambda\Pi'_{hh}) \quad (108)$$

where Γ_{hhhh} is the four-point function calculated in the full, four-dimensional theory. In the above, the self energies are themselves dependent on gauge couplings whose definitions have themselves been redefined by the matching relations. One can then use either one or two loop matching relations in order to write the theory to the desired order in g_2 . Of course, even the Standard Model has many more parameters than g_2 , so it is customary to consider each parameter as approximately equal to some power of g_2 when deciding which terms are small enough to leave out. The process of dimensional reduction for the case of the Standard Model is shown in table I. The process is admittedly complicated. However, as shown in Fig. 8 the theoretical uncertainties of ordinary perturbation theory is multiple orders of magnitude [329, 330], even for simple extensions of the Standard Model. This can often be tamed if one calculates the dimensionally reduced theory at next to the leading

Start: $(d + 1)$ -dimensional SM

Scale	Validity	Dimension	Lagrangian	Fields	Parameters
<i>Hard</i>	πT	$d + 1$	\mathcal{L}_{SM}	$A_\mu, B_\mu, C_\mu, \phi, \psi_i$	$m_h^2, \lambda, g_1, g_2, g_s, y_t$
			↓ <i>Integrate out $n \neq 0$ modes and fermions</i>		
<i>Soft</i>	gT	d	\mathcal{L}_{3d}	$A_r, B_r, C_r,$ A_0, B_0, C_0, ϕ	$\mu_{h,3}^2, \lambda_3, g_3, m_D,$ $g_{1,3}, m'_D, g_{s,3}, m''_D$
			↓ <i>Integrate out temporal adjoint scalars A_0, B_0, C_0</i>		
<i>Ultrasoft</i>	$g^2 T / \pi$	d	$\bar{\mathcal{L}}_{3d}$	A_r, B_r, C_r, ϕ	$\bar{\mu}_{h,3}^2, \bar{\lambda}_3, \bar{g}_{23}, \bar{g}_{13}, \bar{g}_{s,3}$

End: d -dimensional Pure Gauge

TABLE I. Dimensional reduction of $(d + 1)$ -dimensional SM into effective d -dimensional theories based on the scale hierarchy at high temperatures. The effective couplings are functions of the couplings of their parent theories and temperature and are determined by a matching procedure. The first step integrates out all hard non-zero modes. The second step integrates out the temporal adjoint scalars A_0, B_0, C_0 with soft Debye masses m_D, m'_D, m''_D . At the ultrasoft scale, only ultrasoft spatial gauge fields A_r, B_r, C_r (with corresponding field-strength tensors G_{rs}, F_{rs}, H_{rs}) remain along with a light Higgs that undergoes the phase transition. Table adapted from ref. [329]

order, as shown in Fig. 8. However, Dimensional reduction assumes a hierarchy of scales so that we can integrate out the Matsubara modes. However, for sufficiently strong phase transitions, this hierarchy disappears. For stronger phase transitions, it is plausible that techniques that work in QCD could be repurposed. In particular, numerically solving the Dyson Schwinger equations is a technique that has borne fruit in solving strongly coupled theories [331]. Such a technique has been recently developed for thermal field theory, so far ignoring the momentum dependence of the gap equations [309, 315]. A schematic of the current situation is shown in Fig 9 and, as we will see in the next section, simulations do seem to reproduce the above heuristic arguments.

F. Simulations

Cosmic phase transitions are such complicated systems, far from equilibrium, that it is necessary to check our analytic methods against simulations. Current numeric results seem

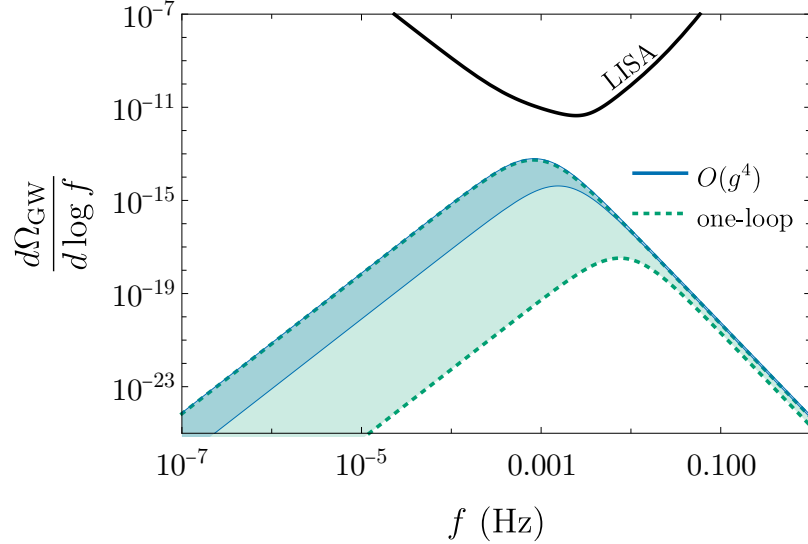


FIG. 8. Theoretical uncertainties for a singlet extension to the Standard model are multiple orders of magnitude, with the more common one loop band not even capturing the range of values predicted at next to leading order. Figure taken from ref. [330].

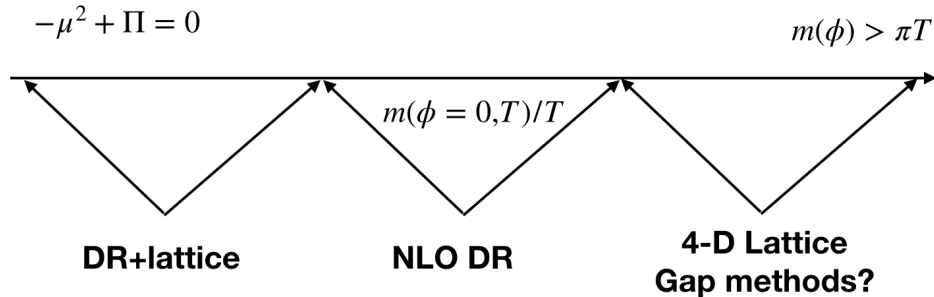


FIG. 9. Perturbation theory is expected to only be valid in a narrow window where the masses are small enough that the high-temperature regime is valid but large enough to avoid infrared divergences near the critical temperature. For lighter masses, dimensional reduction allows the numerical simulation to be more tractable. For larger masses a large 4-dimensional simulation, although perhaps gap equation techniques show some early promise.

to indicate that the theory community has a long way to go in both steps, understanding finite temperature perturbation theory and modeling the gravitational wave spectrum. Recent Monte-Carlo analysis treatments of thermal field theory demonstrated that, in line with expectations, there is indeed a Golilocks zone where perturbation theory yields correct answers when the phase transition is strong enough that infrared catastrophes aren't

numerically important near the critical temperature, yet not so strong that expansions in the coupling constant have slow convergence. However, they found convergence only when expanding in g^2/λ rather than the traditional expansion in g^2 , where g is the SU(2) gauge coupling constant and λ is the Higgs quartic [327].

Recent simulations of the sound shell model indicate that the sound shell model overestimates the gravitational wave spectrum due to energy lost to vorticity modes [282]. Generally, this is a small suppression unless the velocity is small and the trace anomaly large. As for the shape, numerical treatment of the soundshell model does appear to agree fairly well with simulations [280, 332].

The gravitational wave spectrum from scalar shell collisions differs quite dramatically in shape, size, and peak frequency when one compares the predictions of lattice and the envelope approximation [333–335]. A significant issue is probably that the contribution to the stress-energy tensor from the bubble wall is ignored after the collision. There has been recent work to try and model this effect and it remains to be seen how much this closes the gap between simulations and theory [299, 336–339].

Of all sources of gravitational waves during a phase transition, our understanding of turbulence is perhaps the most remedial. Recent work considered the gravitational wave background produced a period of freely decay vortical turbulence [279]. They were able to analytically fit the predicted gravitational wave spectrum, however this eventually needs to be matched with a sufficient understanding of how first-order phase transitions source turbulence.

IV. GRAVITATIONAL WAVES FROM TOPOLOGICAL DEFECTS

Cosmic phase transitions are not the only source of gravitational waves that can be produced during an event of cosmological symmetry breaking. One possibility is that the vacuum manifold is sufficiently interesting to allow massive configurations of fields that are at least metastable, known as topological defects [340–342]. What makes topological defects a particularly compelling source of gravitational waves is that one does not need to live in a corner of the parameter space to produce such defects. This is in contrast to gravitational waves from phase transitions, which require a strong first-order phase transition. Second, and also in contrast to cosmic phase transitions, a gravitational wave signal from such defects can become easier to detect if the scale of physics involved is higher. This is assured directly in the case of cosmic strings as the waveform is relatively flat over many decades of frequency with an amplitude that grows with the symmetry-breaking scale. In the case of domain walls, there is an interplay between the symmetry-breaking scale which determines the power of the gravitational waves emitted, and the lifetime of the wall. In this section, we will give a brief introduction to how to use topology to characterize topological defects, what we know about the gravitational wave signals in the case of each defect as well as hybrids before giving an overview of some recent applications.

A. Categorization by homotopy group

During an epoch of cosmological spontaneous symmetry breaking, if the topology of the vacuum manifold is non-trivial, the transition leaves traces known as topological defects. Depending on the nature of the symmetry under consideration, these defects can be global or local and the phenomenology differs in each case. The full set of possible global or local defects includes domain walls (DW), cosmic strings (CS), monopoles, and textures. To describe the topology of the vacuum manifold, let us use the notation $\mathcal{M} = \mathcal{G}/\mathcal{H}$, where \mathcal{G} and \mathcal{H} are, respectively, the symmetry groups before and after the symmetry breaking. The topological properties of the manifold, \mathcal{M} , can be diagnosed using homotopy theory. The n^{th} homotopy group $\Pi_n(\mathcal{M})$ classifies qualitatively distinct mapping from the n -dimensional sphere S^n into the manifold \mathcal{M} . Below we classify different topological defects based on their vacuum manifold properties and homotopy group,

1. Domain Walls: They are formed when the vacuum manifolds are disconnected, *i.e.* $\Pi_0(\mathcal{M}) \neq \mathcal{I}$, where \mathcal{I} denotes a trivial homotopy group. In other words $\Pi_0(\mathcal{M})$ is a homotopy group that counts disconnected components. For example, let us consider a discrete symmetry Z_2 spontaneously broken to an \mathcal{I} . In this case, the vacuum manifold is given by $\mathcal{M} = Z_2/\mathcal{I}$ and $\Pi_0(\mathcal{M}) = Z_2 \neq \mathcal{I}$.
2. Cosmic strings: CS are formed when the vacuum manifolds are not simply connected, *i.e.* $\Pi_1(\mathcal{M}) \neq \mathcal{I}$. Considering a $U(1)$ symmetry that is spontaneously broken to \mathcal{I} , the vacuum manifold can then be written as $\mathcal{M} = U(1)/\mathcal{I}$ and $\Pi_1(\mathcal{M}) = U(1) \neq \mathcal{I}$.
3. Monopoles: These point like defects are formed when $\Pi_2(\mathcal{M}) \neq \mathcal{I}$ *i.e.* when the manifold of degenerate vacua contains non-contractible two-surfaces
4. Textures: Textures appear in the scenarios where the vacuum manifold has a non-trivial third homotopy group, $\Pi_3(\mathcal{M}) \neq \mathcal{I}$. For example, if a $O(4)$ is spontaneously broken to $O(3)$, the vacuum manifold is given by $\mathcal{M} = O(4)/O(3)$ and $\Pi_3(\mathcal{M}) = O(4)/O(3) \neq \mathcal{I}$.

B. Gravitational waves from Domain walls

A stochastic GW background can be sourced from different topological defects. As a first example, let us consider domain walls [340, 341, 343]. These are sheet-like topological defects that form if a discrete symmetry is spontaneously broken in the early Universe. Once created, their energy density scales inversely with the scale factor. Therefore, they can soon dominate the total energy density of the Universe and later alter the products of BBN as well as the Cosmic microwave background (CMB).

Several solutions exist to overcome domain wall domination [341]. For example, if the formation of DW takes place before the inflation, the walls can be inflated away far beyond the present Hubble radius. On the other hand, wall domination can also be avoided in a model where a discrete symmetry that is broken at a very scale is restored at a lower temperature. In this scenario, wall tension (discussed later) is temperature dependent and walls are always over-damped ($\rho_{\text{DW}}/\rho \ll 1$), hence they never dominate the Universe. Another way out is if the DWs are unstable [341]. If domain walls arise from the spontaneous breaking of a global discrete symmetry, one can introduce a small bias to the scalar potential

from an explicit symmetry-breaking term that allows the walls to annihilate. Finally, a wall-dominated universe can be avoided if the discrete symmetry responsible for the generation is embedded in a continuous symmetry group and a prior step in the symmetry-breaking chain admits cosmic strings. In such a case, the walls can be bounded by strings and these hybrid defects [341, 344] can decay before they dominate the Universe.

We initiate our discussion by briefly describing the dynamics of DW followed by how it generates the SGWB that can be detected by the current and future GW detectors. To do that we consider a simplistic scenario of a real scalar field ϕ that remains invariant under a discrete Z_2 symmetry ($\phi \rightarrow -\phi$). The Z_2 symmetry is spontaneously broken, once the scalar obtain a non-zero vacuum expectation value (vev), *i.e.* $\langle\phi\rangle = \pm v$. A simple example of such a potential is,

$$V(\phi) = \frac{\lambda}{4}(\phi^2 - v^2)^2, \quad (109)$$

where λ is a quartic coupling. Notice, that the scalar has two degenerate minima at $\phi = \pm v$. As a result of this spontaneous symmetry breaking (SSB), two domains can appear and walls are produced at the boundary. The analytical solution to the equation of motion for this scalar is,

$$\phi(x) = v \tanh\left(\sqrt{\frac{\lambda}{2}}vx\right). \quad (110)$$

Here a local *kink* is observed at $x = 0$, that takes ϕ from $-v$ at $x = -\infty$ to $+v$ at $x = +\infty$. The surface tension, σ , is controlled by the symmetry breaking scale,

$$\sigma = \int_{-\infty}^{\infty} dx \left(\frac{1}{2} \left[\frac{\partial\phi(x)}{dx} \right]^2 + V(\phi(x)) \right) = \sqrt{\frac{8\lambda}{9}}v^3. \quad (111)$$

Once the DWs are formed they can eventually dominate the energy budget of the Universe as their energy density dilutes much slower than radiation. Their dynamics can be described by considering them as a system of isotropic gas [341] with an equation of state,

$$p_{\text{DW}} = \left(u^2 - \frac{2}{3}\right)\rho_{\text{DW}}, \quad (112)$$

where p_{DW} and ρ_{DW} denotes the pressure and energy density of the DWs while u represents the wall's velocity. While in the case of highly relativistic walls, $u \rightarrow 1$, a usual equation of state for a relativistic gas is obtained *i.e.* $p_{\text{DW}} = \frac{1}{3}\rho_{\text{DW}}$, the non-relativistic regime ($u \ll 1$) gives *i.e.* $p_{\text{DW}} = -\frac{2}{3}\rho_{\text{DW}}$. Shortly after forming, the domain walls are expected to have a large mass compared to the background temperature, implying that they will be non-relativistic.

Assuming the Universe to be homogeneous on a scale much greater than the wall separation, it can be approximately described by an FRW metric,

$$ds^2 = dt^2 - a^2(t)dx^2, \quad (113)$$

with the equation of state $p = w\rho$, the scale factor is then given by,

$$a(t) \propto t^{\frac{2}{3(w+1)}}. \quad (114)$$

The DW energy density can then be related to the scale factor as $\rho_{\text{DW}} \propto a^{-3(1+w)}$. For non-relativistic DWs while $a(t) \propto t^2$, the energy density is $\rho_{\text{DW}} \propto a^{-1}$. This slow dilution is what makes a stable domain wall network cosmologically dangerous and in conflict with observation. Even if their energy density is subdominant today, they may still produce excessive density perturbations observable in the CMB epoch if their surface energy density is above $\mathcal{O}(\text{MeV}^3)$, this bound is also known as the Zel'dovich-Kobzarev- Okun bound [345].

As we mentioned, one way to resolve this issue is to make the DWs unstable and allow the network to decay. Let us consider a scenario where the degeneracy of the vacuum is broken by introducing an energy bias in the scalar potential [346–348]. It is important to point out that, although an energy bias [349–352] is required to make the DWs unstable, a very large energy difference from the beginning will not allow the formation of DWs at the first place [347]. So there must be a hierarchy between the bias terms and the rest of the potential. If the discrete symmetry is approximate, a bias can be established by introducing an explicit symmetry-breaking (in this case Z_2) term [343],

$$\Delta v(\phi) = \epsilon v \phi \left(\frac{1}{3} \phi^2 - v^2 \right), \quad (115)$$

where ϵ is a dimensionless constant. Although this potential has a minima at $\pm v$, there also exists an energy difference between them,

$$V_{\text{bias}} = V(-v) - V(+v) = \frac{4}{3} \epsilon v^4. \quad (116)$$

As a result of this energy difference, the false vacuum tends to shrink *i.e.* there exists a volume pressure force acting on the walls whose magnitude can be estimated as $p_V \sim V_{\text{bias}}$. DW collapses when this pressure force becomes greater than the tension force $p_T \sim \sigma \frac{\mathcal{A}}{t}$ with $\mathcal{A} \simeq 0.8 \pm 0.1$ being the area parameter [353]. Their annihilation time can be estimated by comparing these two forces,

$$t_{\text{ann}} = C_{\text{ann}} \frac{\sigma \mathcal{A}}{V_{\text{bias}}}, \quad (117)$$

where C_{ann} is a coefficient of $\mathcal{O}(1)$. Assuming the annihilation occurs in the radiation-dominated era, the temperature at $t = t_{\text{ann}}$ becomes proportional to the inverse square root of Eq. 117,

$$T_{\text{ann}} = 3.41 \times 10^{-2} \text{ GeV } C_{\text{ann}}^{-1/2} \mathcal{A}^{-1/2} \left(\frac{g_*(T_{\text{ann}})}{10} \right)^{-1/4} \left(\frac{\sigma}{\text{TeV}^3} \right)^{-1/2} \left(\frac{V_{\text{bias}}}{\text{MeV}^4} \right)^{1/2}, \quad (118)$$

The annihilation of DWs may produce GWs, which are potentially observable today. The Gravitational wave spectrum produced by a DW at cosmic time t can be characterized by the ratio of the rate of change of GW energy density ρ_{GW} with respect to the frequency of the GW f to the critical energy density of the Universe ρ ,

$$\Omega_{\text{GW}}(t, f) = \frac{1}{\rho_c(t)} \frac{d\rho_{\text{GW}}(t)}{d \ln f} \quad (119)$$

where ρ_{GW} and f denote the energy density and the frequency of the GW respectively. The main feature of the GW spectrum from DW is that it follows a broken power law, where the breaking point has a frequency determined by the annihilation time and the peak amplitude is determined by the energy density in the domain walls (which in turn determines the gravitational power radiated). The peak amplitude is therefore dependent upon the fraction of energy radiated into gravitational waves, ϵ , the surface tension, σ , and the radius of the domain wall which is the Hubble radius at the collapse time. Finally, it will depend upon an $\mathcal{O}(1)$ factor \mathcal{A} that captures the precise details of a simulation. Assuming an instantaneous annihilation of the DWs at $t = t_{\text{ann}}$, the peak amplitude is then [343],

$$\Omega_{\text{GW}}(t_{\text{ann}})_{\text{peak}} = \frac{1}{\rho_c(t_{\text{ann}})} \left(\frac{d\rho_{\text{GW}}(t_{\text{ann}})}{d \ln f} \right)_{\text{peak}} = \frac{8\pi \tilde{\epsilon}_{\text{GW}} G^2 \mathcal{A}^2 \sigma^2}{3H^2(t_{\text{ann}})}, \quad (120)$$

where the parameter $\tilde{\epsilon}_{\text{GW}}$ is estimated to be $\tilde{\epsilon}_{\text{GW}} \simeq 0.7 \pm 0.4$ [354] and G is the Newton's gravitational constant. Once the DWs have entered the scaling regime [355], they decay, *i.e* when their energy density evolves according to the simple scaling law $\rho_{\text{DW}} \propto t^{-1}$, and their size is typically given by the Hubble radius $\sim t$ and hence the peak amplitude at present time t_0 is,

$$\Omega_{\text{GW}} h^2(t_0)_{\text{peak}} = 7.2 \times 10^{-18} \tilde{\epsilon}_{\text{GW}} \mathcal{A}^2 \left(\frac{\sigma}{\text{TeV}^3} \right)^2 \left(\frac{T_{\text{ann}}}{10^{-2} \text{ GeV}} \right)^{-4}. \quad (121)$$

The redshifted peak frequency can be determined by

$$f_{\text{peak}} \simeq \left(\frac{a(t_{\text{ann}})}{a(t_0)} \right) H(t_{\text{ann}}) \quad (122)$$

$$f_{\text{peak}} \simeq 1.1 \times 10^{-9} \text{ Hz} \left(\frac{T_{\text{ann}}}{10^{-2} \text{ GeV}} \right). \quad (123)$$

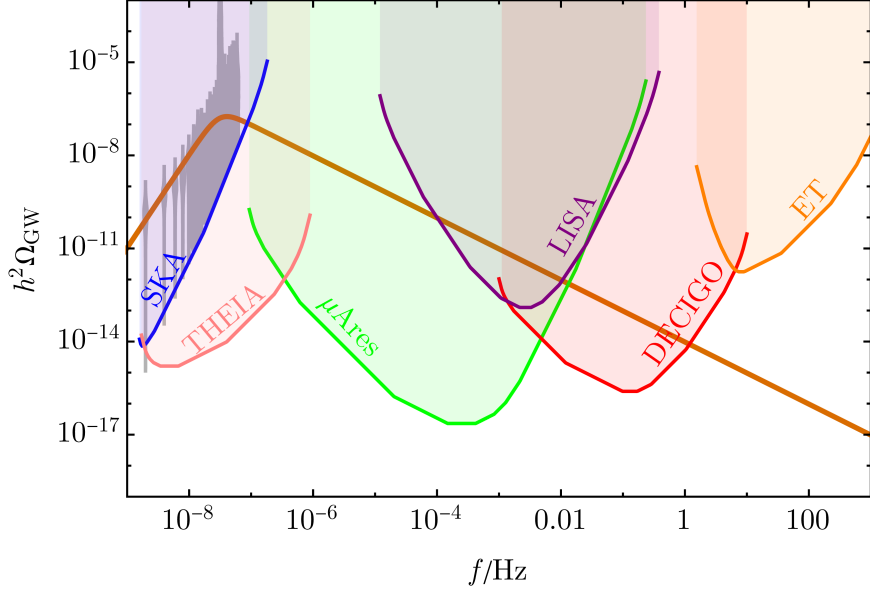


FIG. 10. Shape of gravitational wave spectra as a function frequency generated from DW annihilation. Figure taken from ref [352]

To depict the GW spectrum, the following parametrization for a broken power-law spectrum [356, 357] can be adopted

$$\Omega_{\text{GW}} h^2 = \Omega_{\text{GW}} h_{\text{peak}}^2 \frac{(a+b)^c}{(bx^{-a/c} + ax^{b/c})^c}, \quad (124)$$

where $x := f/f_p$, and a , b and c are real and positive parameters. Here the low-frequency slope $a = 3$ can be fixed by causality, while numerical simulations suggest $b \simeq c \simeq 1$ [353]. While these simulations agree with a scenario where the Z_2 symmetry is broken, the scenarios with larger discrete symmetries require careful treatment.

For the case where $N > 2$, the UV power law can be modified [354, 357, 358]. In this case, multiple degenerate vacua appear, hence leading to a domain wall network that is more complicated to the Z_2 case. Again, the degeneracy among the vacua can be broken by introducing a bias term in the scalar potential, and eventually, a domain with the lowest energy dominates over others, which causes the annihilation of the walls and the production of GW. It is interesting to point out that GW signals observed in these scenarios can deviate from what is observed in the case of Z_2 domain walls as also pointed out by a recent study [354], that suggests that b in Eq.124 decreases with the increasing value of N .

C. Gravitational waves from Cosmic Strings

Let us now turn our attention to cosmic strings (CS). CSs are one-dimensional defects that appear in many extensions of the SM, e.g., field theories with a spontaneously broken U(1) symmetry (gauge or global) [247, 341, 359–363], and the fundamental and/or composite strings in superstring theory [364–368]. On the other hand, more complicated strings, such as Z_N -strings, can also be encountered during the phase transitions followed by a remnant discrete symmetry. For example a Z_2 string can appear in a GUT model discussed in [369]

$$SO(10) \longrightarrow SU(5) \times Z_2 \quad (125)$$

In a situation where $N > 2$, Z_N -strings can form networks with vertices from which several strings can emerge.

Just like the DWs, once the strings are formed they can also eventually dominate the energy density of the Universe. The effective equation of state for the strings is then given by,

$$p_S = \left(\frac{2}{3}u^2 - \frac{1}{3} \right) \rho_S, \quad (126)$$

where p_S and ρ_S denotes the pressure and energy density of the strings while u represents the string's velocity. For a non-relativistic strings ($u \ll 1$) gives *i.e.* $p_S = -\frac{1}{3}\rho_S$. Following Eq. 114, the CS energy density can then be related to the scale factor as $\rho_S \propto a^{-3(1+w)}$. For non-relativistic string while $a(t) \propto t$, the energy density is $\rho_S \propto a^{-2}$. This suggests that strings can also act as a cosmological disaster. However, the evolution of the string network is much more complicated than this. One should include the two important effects

- The intercommutation of intersecting string segments leads to the formation of loops of different sizes.
- The decay of smaller loop by radiating GWs.

At the time of the CS formation, the Universe might have been filled with a surplus amount of strings per horizon. This results from the fact that the correlation length of the field associated with the strings is often much less than the horizon size. Their abundance is then reduced by their self-intersection. String friction with the background plasma, if

present, tends to freeze the string on the length scale which is larger than the friction length scale,

$$R_{\text{fric}} = v_{\text{drag}} \times t, \quad (127)$$

where v_{drag} is the drag speed of the string in the plasma due to friction. This friction retards the rate at which strings reach scaling. However, during this time, strings can still self-intersect and reduce their abundance slowly until typically one string exists per horizon, thereby reaching the scaling regime. At this stage, one string per horizon is maintained as the strings typically intersect whenever

$$t_{\text{intersect}} = L/v_{\text{string}} = \text{Hubble time} \quad (128)$$

is satisfied where L denotes the average inter-string separation scale. This is an attractor solution since the strings will not dilute less than one per horizon since if they dilute a bit more they become superhorizon, and they are stretched as $a(t) \sim t^{1/2}(t^{2/3})$ in the RD (MD) era which is slower than the horizon expansion of t . As a result of this, the horizon always “catches” up with the superhorizon strings as long as the scale factor grows slower than t .

There exist several studies in the literature that have calculated the SGWB from evolving cosmic string networks [370–374]. Nevertheless, there exists a technical challenge that persists for pure numerical simulation to track the network’s evolution over the entire relevant cosmic history. The issue with the CS network is that at the micro level, we use a field-theoretic treatment. Simulations of the field-theoretic treatment seem to suggest that very limited energy radiated into GW. Once the string is long enough we use a classical Nambu-Goto action string theory treatment. Here, most of the energy is dumped into GWs. It is hard to tell which treatment is right due to the enormous hierarchy of scales involved *i.e.* inverse string length vs symmetry-breaking scale. Therefore it is difficult to make predictions for observations today. The debate has been ongoing for quite some time, with new insights on both sides of the argument appearing in the last couple of years (see for instance [372–374]) leaving little confidence that the last word has been uttered.

For the purposes of this review we will proceed with the assumption that the Nambu-Goto treatment is valid. We will use the Velocity-dependent One-Scale (VOS) model [375, 376] that captures the essential physics, and use it to study and predict the evolution of the string network over a long range of time while calibrating the input model parameters with

data points for early time evolution that have been made available by simulations. Next, we briefly review the VOS model.

The GW spectrum produced by evolving CS can be quantified using Eq. 119. The idea here is to add up the GW emission from all the loops throughout the history of the Universe. Now, the first basic ingredient for calculating the GW spectrum from the CS is the GW power P_{GW} . The total power emitted in gravitational waves by strings loops can be estimated from the quadrupole formula, $P_{\text{GW}} \approx \frac{G}{45} \sum_{i,j} \langle \ddot{Q}_{ij} \ddot{Q}_{ij} \rangle \propto G\mu^2$. The power $P_{\text{gw}}(f, l)$ in units of $G\mu^2$ and l is

$$P_{\text{GW}}(f, l) = G\mu^2 l P(fl), \quad (129)$$

where the function $P(fl)$ takes a different form for each loop of length l , depending on its configuration. The first step in calculating $\Omega_{\text{GW}}(t_0, f)$ is to assume the presence of an averaged function, $P(fl)$, which is computed from a group of loops of length l obtained from simulations. Following this, the observed energy density of GW at a particular frequency f today is obtained by adding the amount of energy produced at each moment of cosmic evolution for loops of all sizes. Including the result of redshifting, the emission for the moment of emission to today is,

$$\frac{d\rho_{\text{GW}}}{df}(t_0, f) = G\mu^2 \int_0^{t_0} dt \left(\frac{a(t)}{a_0} \right)^3 \int_0^\infty dl l n(l, t) P\left(\frac{a_0}{a(t)} fl \right), \quad (130)$$

where $a(t)$ is the scale factor which takes the value a_0 today. At this stage, we would also like to point out that, more precise numerical computations and calibrations with simulations find the total power emitted as,

$$P_{\text{GW}} = \Gamma G\mu^2, \quad (131)$$

where GW emission efficiency, $\Gamma \sim 50$ [377–380] is determined by Nambu-Goto simulations and μ denotes the energy per unit length of a string or the string tension.

The second important ingredient for calculating the GW spectrum from the CS is the number density $n(l, t)$ of non-self-intersecting, sub-horizon, CS loops of invariant length l at cosmic time t . To do that one approach is to determine the loop production function $f(l, t)dl$ namely the number density of non-self-intersecting loops of lengths between l and $l + dl$ produced per unit time, per unit volume. The loop number density can be obtained

by integrating [381]

$$n(l, t) = \int_{t_i}^t dt' f(l', t') \left(\frac{a(t')}{a(t)} \right)^3, \quad (132)$$

where the effect of the expansion is explicitly seen through the dependence of the scale factor $a(t)$, and l' (which is given below) contains information on the evolution of the length of the loop due to its gravitational decay from the time of formation t' to the observation time t . Assuming that the production of loops is the dominant energy loss mechanism of the long string network, which is given by

$$\frac{d\rho_\infty}{dt} = -2H(1 + \bar{v}^2)\rho_\infty - \left. \frac{d\rho_\infty}{dt} \right|_{\text{loop}}, \quad (133)$$

where $\bar{v} = \sqrt{\langle v^2 \rangle}$ is the root-mean-squared (RMS) velocity of the long strings and ρ_∞ denotes the long string network energy density. The first term in this equation describes the dilution of the long string energy density in an expanding Universe, while the second, describes energy loss into loop formation. The energy loss in loop formation is proportional to the loop production function, loop length, and string tension,

$$\left. \frac{d\rho_\infty}{dt} \right|_{\text{loop}} \equiv \mu \int_0^\infty l f(l, t) dl. \quad (134)$$

Loop production is essential to achieve the linear scaling of long strings, see e.g. [341].

To determine $n(l, t)$, it is necessary to have a handle on the evolution of the long string energy density ρ_∞ and the root mean velocity \bar{v} of the long string as a first step. To do that one can use the VOS as it describes both the scaling evolution of the long string together with non-scaling evolution through the radiation-matter transition. The evolution can be obtained by solving the coupled differential equations (VOS equation of motion) involving the rate of change of RMS velocity of the long strings and the characteristic length between the strings,

$$\begin{aligned} \frac{d\bar{v}}{dt} &= (1 - \bar{v}^2) \left[\frac{k(\bar{v})}{L} - 2H\bar{v} \right], \\ \frac{dL}{dt} &= (1 + \bar{v}^2) HL + \frac{\tilde{c}}{2}\bar{v}, \end{aligned} \quad (135)$$

where $L \equiv (\mu/\rho_\infty)^{1/2}$ denotes the characteristic length that measures the average distance between long strings and \tilde{c} quantifies the efficiency of the loop-chopping mechanism. The function $k(\bar{v})$ accounts for the effects of small-scale structure (namely, multiple kinks) on

long strings [376],

$$k(\bar{v}) = \frac{2\sqrt{2}}{\pi} (1 - \bar{v}^2) \left(1 + 2\sqrt{2}\bar{v}^3\right) \frac{1 - 8\bar{v}^6}{1 + 8\bar{v}^6}, \quad (136)$$

This reproduces the expected asymptotic behavior of $k(\bar{v})$ both in the relativistic and non-relativistic limits. The linear scaling of the long string network in the radiation- and matter-dominated backgrounds follows directly from Eq. 135 since the particular solutions are

$$\frac{L}{t} = \sqrt{\frac{k(\bar{v})(k(\bar{v}) + \tilde{c})}{4\nu(1 - \nu)}} \equiv \xi_s \quad \text{with} \quad \bar{v} = \sqrt{\left(\frac{k(\bar{v})}{k(\bar{v}) + \tilde{c}}\right) \left(\frac{1 - \nu}{\nu}\right)} \equiv \bar{v}_s, \quad (137)$$

where the subscript s stands for ‘scaling’, are attractor solutions of these equations for $a \propto t^\nu$ and $0 < \nu < 1$. More generally, Eq. 135 can be solved throughout any cosmological era, including the radiation-to-matter and matter-to-dark-energy transitions, and hence one can trace the evolution of cosmic string networks in a realistic cosmological background [382].

The second step in determining $n(l, t)$ is to relate the loop production function and the long string network as described by the VOS model. Now defining two new variables $\xi \equiv \frac{L(t)}{t}$ which describes the length parameter and, $x \equiv \frac{l}{t}$ that describes the ratio of the size of the loop to roughly the horizon scale, it follows from Eq. (135) that the loop production function can be expressed in terms of \tilde{c}, \bar{v} and ξ ,

$$\int_0^\infty x f(x) dx = \frac{2}{\xi^2} [1 - \nu(1 + \bar{v}^2)] = \tilde{c} \frac{\bar{v}}{\xi^3} \equiv C_{\text{eff}}. \quad (138)$$

Now, one can make the following assumption⁸ *throughout cosmic history, all loops are assumed to be created with a length l that is a fixed fraction of the characteristic length of the long string network*, namely $l = \alpha_L L$, with $\alpha_L < 1$. Thus

$$f(x) = \left(\frac{\mathcal{F}}{f_r}\right) \tilde{C} \delta(x - \alpha_L \xi) \equiv A \delta(x - \alpha_L \xi), \quad (139)$$

where $f_r \sim \sqrt{2}$ denotes the reduction factor that accounts for the energy loss into redshifting of the peculiar velocities of loops, \mathcal{F} denotes the fraction of loops formed with size α_L and from Eq. (138)

$$\tilde{C} = \frac{\tilde{c} \bar{v}}{\alpha_L \xi^4} \quad (140)$$

⁸ There exist two other models to calculate the loop number density. In the first one [377, 381, 383] one can use loop production functions for non-self-intersecting loops directly from NG simulations of cosmic string and in the second one [381, 384, 385] the loop production function is not the quantity inferred from the simulation but the distribution of non-self-intersecting scaling loops is directly extracted from the simulation.

with \bar{v} and $\xi = L/t$ being the solutions of the VOS Eq. 135.

Finally, substituting Eq. 139 in Eq. 132 one can obtain loop number density for all times including during the radiation-to-matter and matter-to-dark-energy transitions but this requires solving the VOS equation of motion. During the *radiation era* ($\nu = 1/2$), the long string network is scaling and described by the VOS solutions (Eq. 137), namely $\xi_r = 0.271$ and $v_r = 0.662$, hence it follows that the loop distribution takes a simple form

$$n_r(x) = \frac{A_r (\alpha + \Gamma G\mu)^{3/2}}{\alpha (x + \Gamma G\mu)^{5/2}}, \quad (141)$$

with $A_r = 0.54$ (fixing $\mathcal{F} = 0.1$), and where $\alpha = \alpha_L \xi_r$. As noted above, this expression is only valid for $x \leq \alpha$. In a matter-only universe ($\nu = 2/3$), the VOS scaling solutions (Eq. 137) give $\xi_m = 0.625$ and $v_m = 0.583$ and the loop distribution is

$$n_m(x) = \frac{A_m \alpha_m + \Gamma G\mu}{\alpha_m (x + \Gamma G\mu)^2}, \quad (142)$$

where $\alpha_m = \alpha_L \xi_m$, $A_m = 0.039$ and $x \leq \alpha_m$.

We are now at a point where we must take divergent paths - the evolution of the string network is qualitatively different if the strings arise from a global or a local symmetry. We will refer to each case as a global and local string network respectively and separately describe their evolution including the above effects.

1. Cosmic strings from global $U(1)$ symmetry breaking

Let us first consider the case of global strings. Although we will introduce some key concepts that are common for both global as well as local strings. We will consider a simple setup with a global $U(1)$ symmetry that is spontaneously broken by a complex scalar ϕ . The model features global strings that result from this breaking. The setup can be described by the Lagrangian,

$$\mathcal{L} = \partial_\mu \phi^* \partial^\mu \phi - V(\phi), \quad (143)$$

$$V(\phi) = \frac{1}{2} \lambda (|\phi|^2 - \frac{1}{2} \eta^2)^2, \quad (144)$$

where η denotes the vacuum expectation value of ϕ . This spontaneous breaking of global $U(1)$ also leads to the formation of a massless Nambu-Goldstone boson. Depending on the magnitude of η , these global strings can either decay dominantly to the Goldstone bosons

or the GWs (see the discussion below Eq. 145). The GW spectrum produced by the global Strings in this situation is typically suppressed as it falls off with frequency. Although, this makes their detection a bit difficult, works like [386–388] suggest that they can still be detected by GW experiments like LISA, AEDGE, DECIGO, and BBO by considering the breaking scale η above 10^{14} GeV.

Once formed, the loop oscillates and emits its energy in the form of Goldstone (first term) and gravitational waves (second term) as shown in the equation below [389]

$$\frac{dE}{dt} = -\Gamma_a \eta^2 - \Gamma G \mu^2, . \quad (145)$$

The parameter $\Gamma_{(a)}$ depends only on the loop trajectory [341, 390], and hence we expect that the value of the Goldstone radiation constant Γ_a must be close to the value of the GW radiation constant $\Gamma \sim \Gamma_a$ [390]. The Goldstone radiation constant is found to be $\Gamma_a \sim 65$ [341, 390]. The absence of the gauge field in the breaking of the global $U(1)$ symmetry implies the presence of Goldstone (as discussed earlier) with logarithmically divergent gradient energy,

$$\mu(t) = 2\pi\eta^2 \log \frac{L(t)}{\delta}, \quad (146)$$

The string tension depends on the ratio of two scales, a macroscopic scale $L(t)$ (close to the Hubble scale), and a microscopic scale $\delta(t) \propto 1/\eta$ representing the width of the string core. It is interesting to point out that even though the $\Gamma_{(a)}$ are similar in size, the GW radiation has a relative suppression of η^2/M_p^2 . However, this suppression becomes less severe once the symmetry-breaking scale η gets closer to M_p . For this reason, next-generation gravitational wave detectors are only sensitive to global strings formed during symmetry breaking occurring near the GUT scale. Due to the emission of the Goldstones together with the GW, a loop of initial length $\ell_i = \alpha t_i$ at a later time reduces,

$$\ell(t) \simeq \alpha t_i - \Gamma G \mu (t - t_i) - \frac{\Gamma_a}{2\pi} \frac{t - t_i}{\log \frac{L(t)}{\delta}}, \quad (147)$$

where the second and third terms denote the decrease in loop size for gravitational wave emission and Goldstone emission, respectively.

A string loop emits the Goldstone and the GW from normal mode oscillations with frequencies [342, 391, 392],

$$\tilde{f}_k = 2k/\tilde{l}, \quad (148)$$

where $k = 1, 2, 3, \dots$, and $\tilde{l} \equiv l(\tilde{t})$ is the instantaneous size of a loop when it radiates at \tilde{t} . The distribution of power in the different harmonics is determined by the small-scale structure of the loops. It was shown [391, 392] that, in the large k limit, the power emitted in each mode scales as $k^{-4/3}$ if the loop contains points where the velocity is locally 1 known as cusps; as $k^{-5/3}$, if it has kinks (which are discontinuities in the tangential vector introduced by the intercommutation process); and k^{-2} when kink-kink collisions occur. In principle, when computing the SGWB generated by cosmic string loops, one should consider the contribution of all the harmonic modes of emission. The radiation parameters can be decomposed as $\Gamma = \sum_k \Gamma^{(k)}$ and $\Gamma_a = \sum_k \Gamma_a^{(k)}$, with

$$\Gamma^{(k)} = \frac{\Gamma k^{-n}}{\sum_{j=1}^{\infty} j^{-n}}, \quad \text{and} \quad \Gamma_a^{(k)} = \frac{\Gamma_a k^{-n}}{\sum_{j=1}^{\infty} j^{-n}}, \quad (149)$$

and the normalization factor is approximately $\sum_{j=1}^{\infty} j^{-4/3} \simeq 3.60$.

Taking into account the redshifted frequency $f_k = \frac{a(\tilde{t})}{a(t_0)} \tilde{f}_k$, with t_0 denoting the present time and $a(t_0) \equiv 1$ being scale factor today, the gravitational wave amplitude is summed over all normal modes

$$\Omega_{\text{GW}}(f) = \sum_k \Omega_{\text{GW}}^{(k)}(f) = \sum \frac{1}{\rho_c} \frac{d\rho_{\text{GW}}}{d \log f_k}. \quad (150)$$

Now, the contribution from an individual k mode can be obtained by taking an integral over the evolving number density,

$$\Omega_{\text{GW}}^{(k)}(f) = \frac{\mathcal{F}_\alpha F_a}{\alpha \rho_c} \frac{2k}{f} \int_{t_f}^{t_0} d\tilde{t} \frac{C_{\text{eff}}(t_i^{(k)})}{t_i^{(k)4}} \frac{\Gamma^{(k)} G \mu^2}{\alpha + \Gamma G \mu + \frac{\Gamma_a}{2\pi \frac{L(\tilde{t})}{\delta}}} \left[\frac{a(\tilde{t})}{a(t_0)} \right]^5 \left[\frac{a(t_i^{(k)})}{a(\tilde{t})} \right]^3 \theta(\tilde{\ell}) \theta(\tilde{t} - t_i), \quad (151)$$

while t_f denotes the time of network formation, the Heaviside theta functions guarantee causality and energy conservation. Following Eq. 147, one can easily find that a loop that emits GW at time \tilde{t} leading to an observed frequency f was formed at the time

$$t_i^{(k)} = \frac{\tilde{\ell}(\tilde{t}, f, k) + \left(\Gamma G \mu + \frac{\Gamma_a}{2\pi \frac{L(\tilde{t})}{\delta}} \right) \tilde{t}}{\alpha + \Gamma G \mu + \frac{\Gamma_a}{2\pi \frac{L(\tilde{t})}{\delta}}}, \quad (152)$$

where the loop size can be written as $\tilde{\ell} = 2ka(\tilde{t})/f$.

The GW spectrum can be divided into three regions. In the first region where the frequency is very high, $f_\eta < f$ [393], the signal falls off, and the exact shape depends on the

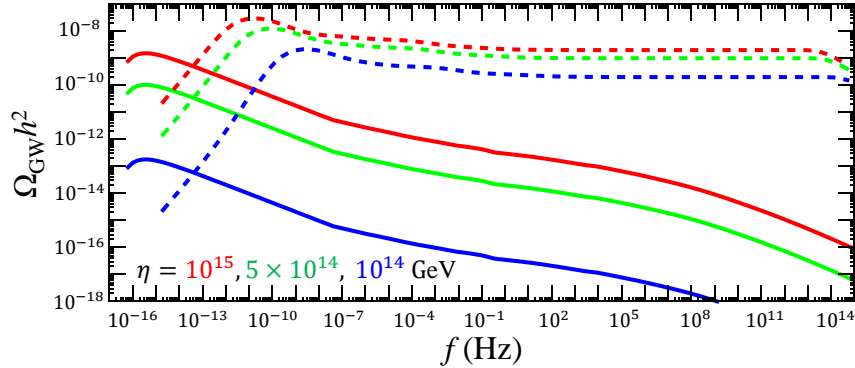


FIG. 11. Shape of gravitational wave spectra as a function frequency generated from global and local (NB) cosmic strings for different values of η . Figure taken from ref [387]

initial conditions and very early stages of the string network evolution not fully captured by the VOS model [375, 376, 394–397] discussed above. f_η is related to the time when the Goldstone radiation becomes significant. The radiation-dominated era that corresponds to the second region, $f_{\text{eq}} < f < f_\eta$, the spectrum fall as $\log^3(1/f)$. f_{eq} indicates the frequency corresponding to the emission around the time of matter-radiation equality. Finally, in the last region that corresponds to the matter-domination $f_0 < f < f_{\text{eq}}$, the spectrum falls as $f^{-1/3}$. f_{eq} is related to the time of matter-radiation equality, and f_0 is related to the emission at the present time. These characteristic frequencies are given by

$$f_\eta \sim \frac{2}{\alpha t_n} \frac{a(t_\eta)}{a(t_0)} \sim 10^{10} \text{ Hz}, \quad (153)$$

$$f_0 \sim \frac{2}{\alpha t_0} \sim 3.6 \times 10^{-16} \text{ Hz}, \quad (154)$$

$$f_{\text{eq}} \sim 1.8 \times 10^{-7} \text{ Hz}. \quad (155)$$

2. Cosmic strings from gauged $U(1)$ symmetry breaking

Unlike global strings, local strings or the Nambu-Goto strings are formed by gauging a $U(1)$ symmetry. In this scenario, the Goldstones are eaten by $U(1)$ vector bosons. Once formed, these Nambu-Goto strings radiate their energy primarily via loop generation and emission of GW which has a flat spectrum [398–402]. 10% of the loops formed are large and the remaining are highly boosted smaller loops [378, 385, 403–405]. The loop formation from the long strings can again be described using the VOS model. Contrary to the case of global strings where energy per unit length, μ has a logarithmic dependence (see Eq. 146),

the energy is radiated at a constant rate during the oscillation of the larger loops for Nambu-Goto strings as μ remains constant,

$$\frac{dE}{dt} = -\Gamma G\mu^2. \quad (156)$$

In general, for local strings $\mu \sim \mathcal{O}(\eta)$. Since there is no emission of Goldstone, Eq. 147 can now be written as,

$$l(t) \simeq \alpha t_i - \Gamma G\mu(t - t_i). \quad (157)$$

Integrating over the emission time, the gravitational wave amplitude of the k -th mode is given by

$$\Omega_{\text{GW}}^{(k)}(f) = \frac{1}{\rho_c} \frac{2k}{f} \frac{\mathcal{F}_\alpha \Gamma^{(k)} G\mu^2}{\alpha(\alpha + \Gamma G\mu)} \int_{t_F}^{t_0} d\tilde{t} \frac{C_{\text{eff}}(t_i^{(k)})}{t_i^{(k)4}} \left[\frac{a(\tilde{t})}{a(t_0)} \right]^5 \left[\frac{a(t_i^{(k)})}{a(\tilde{t})} \right]^3 \Theta(t_i^{(k)} - t_F), \quad (158)$$

where $\Gamma^{(k)}$ can be obtained from Eq. 149, $t_i^{(k)}$ is the formation time of loops contributing to the k -th mode and is given by

$$t_i^{(k)}(\tilde{t}, f) = \frac{1}{\alpha + \Gamma G\mu} \left[\frac{2k}{f} \frac{a(\tilde{t})}{a(t_0)} + \Gamma G\mu\tilde{t} \right]. \quad (159)$$

Summing over all modes, we get the total amplitude of the gravitational waves

$$\Omega_{\text{GW}}(f) = \sum_k \Omega_{\text{GW}}^{(k)}(f), \quad (160)$$

where the sum can be easily evaluated using

$$\Omega_{\text{GW}}^{(k)}(f) = \frac{\Gamma^{(k)}}{\Gamma^{(1)}} \Omega_{\text{GW}}^{(1)}(f/k) = k^{-4/3} \Omega_{\text{GW}}^{(1)}(f/k). \quad (161)$$

A typical shape of a GW signal generated by Nambu-Goto strings is a rising spectrum at a low frequency and thereafter a plateau is observed at higher frequencies. The height of the plateau is proportional to the symmetry-breaking scale η . This gentle dependence (linear) of Ω on η in Fig. 11 means next-generation detectors can probe a large range of symmetry-breaking scales.

D. Gravitational waves from Monopoles and Textures

Monopoles or localized defects are point-like defects that arise from the SSB of some larger spherical symmetry. The existence of a monopole solution was first discussed by 't

Hooft and Polyakov in a gauge $SO(3)$ model with a scalar triplet field. The setup can be described by the Lagrangian,

$$\mathcal{L} = \frac{1}{2} D^\mu \phi D_\mu \phi - \frac{1}{4} B_{\mu\nu} B^{\mu\nu} - \frac{\lambda}{4} (\phi^2 - v_\phi^2)^2 . \quad (162)$$

where ϕ is a scalar triplet. The 't Hooft-Polyakov monopole [406, 407] has the solution

$$\begin{aligned} \phi &= \hat{r} \frac{h(v_\phi e r)}{e r} \\ W_a^i &= \epsilon_{aij} \hat{x}^j \frac{1 - f(v_\phi e r)}{e r} \\ W_a^0 &= 0 , \end{aligned} \quad (163)$$

where, using the shorthand $\xi = v_\phi e r$ for the product of v_ϕ with the gauge coupling constant e and radial coordinate r , the functions f and h are solutions to the equations [406, 407].

$$\xi^2 \frac{d^2 f}{d\xi^2} = f(\xi) h(\xi)^2 + f(\xi) (f(\xi)^2 - 1) \quad (164)$$

$$\xi^2 \frac{d^2 h}{d\xi^2} = 2f(\xi)^2 h(\xi) + \frac{\lambda}{e^2} h(\xi) (h(\xi)^2 - \xi^2) . \quad (165)$$

The boundary conditions satisfy $\lim_{\xi \rightarrow 0} f(\xi) - 1 = \lim_{\xi \rightarrow 0} h(\xi) \sim \mathcal{O}(\xi)$ and $\lim_{\xi \rightarrow \infty} f(\xi) = 0$, $\lim_{\xi \rightarrow \infty} h(\xi) \sim \xi$. The monopole mass again comes from solving the equations of motion and then calculating the static Hamiltonian,

$$\begin{aligned} E = m &= \frac{4\pi v_\phi}{e} \int_0^\infty \frac{d\xi}{\xi^2} \left[\xi^2 \left(\frac{df}{d\xi} \right)^2 + \frac{1}{2} \left(\xi \frac{dh}{d\xi} - h \right)^2 \right. \\ &\quad \left. + \frac{1}{2} (f^2 - 1)^2 + f^2 h^2 + \frac{\lambda}{4e^2} (h^2 - \xi^2)^2 \right] . \end{aligned} \quad (166)$$

It has the form

$$m = \frac{4\pi v_\phi}{e} f(\lambda/e^2) . \quad (167)$$

The solution has been calculated numerically for multiple values, and one finds that for $0.1 < \lambda/e^2 < 10^1$, $f(\lambda/e^2)$ is slowly varying $\mathcal{O}(1)$ function [406].

It is well known that monopoles with an initial abundance of roughly one per horizon at formation as computed by Kibble [359], have no gravitational wave amplitude. Following the Kibble-Zurek mechanism [408], it was recently shown in [344] that a relativistic monopole-bounded string network can emit a pulse of GW before decaying assuming the friction is low. Such a scenario falls under the category of hybrid defects and is discussed in section [IV E](#).

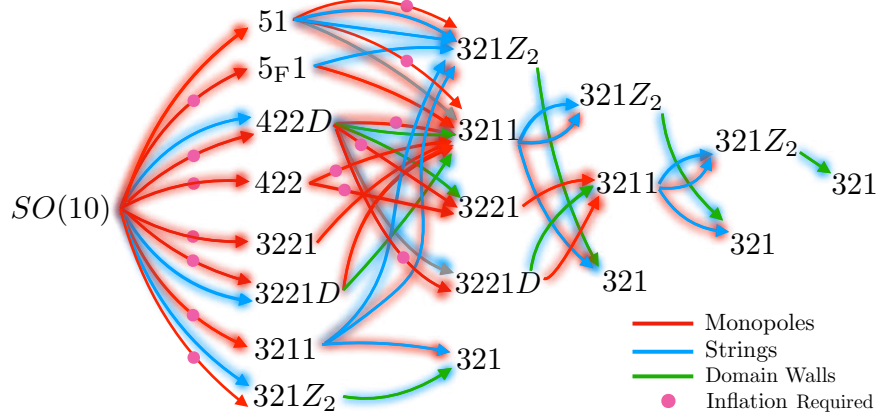


FIG. 12. A simple schematic of $SO(10)$ symmetry breaking chain to SM that produces hybrid defects. Arrows with different colors represent different topological defects. The figure is taken from [344]

Textures, on the other hand, are defects in three spatial directions [341]. Sometimes they are also referred to as non-singular soliton, as the scalar field is nowhere topologically constrained to rise from the minimum of the scalar potential. They can arise either from the breaking of a global symmetry or the breaking of a gauge symmetry. After their formation, the global texture releases their energy during their collapse in the form of Goldstone bosons and GWs. The produced gravitational wave spectrum is scale-invariant and its peak amplitude is controlled by the symmetry-breaking scale. It produces a flat spectrum that goes as $\Omega_{\text{GW}} h^2 \sim v^4$, where v is the breaking scale of global symmetry. On the other hand, gauged textures also can generate GW once produced from the breaking of local symmetry. The GW generated from the gauged texture is not scale invariant, this is because the gauge field configuration cancels the gradient of the scalar field on the large scale. In this case, there exists a cutoff on the spectrum $f_0 \sim 10^{11}$ Hz [409]. To test the GW generated from the gauged textures one requires future GW experiments that are sensitive to a very high frequency.

E. Hybrid defects

Hybrid defects [341, 344, 410–413] are generated due to a chain of symmetry breaking events, $\mathcal{G} \rightarrow \mathcal{H} \rightarrow \mathcal{K}$, where the defects of different dimensionalities get clubbed together. For example, a Hybrid effect can be generated where cosmic strings are attached to DWs

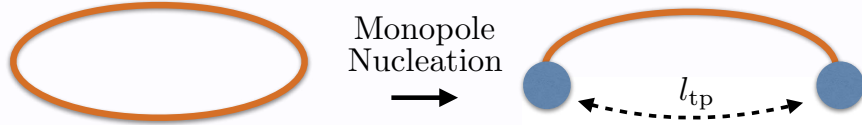


FIG. 13. A cartoon showing a monopole nucleation process where a string is eaten and replaced by a monopole-antimonopole pair. The figure is taken from [344]

or monopoles are attached to a string. Such hybrid defects are generally unstable with one defect eating the other via the conversion of its rest mass into the other's kinetic energy. The leftover defect decays further resulting in the production of GW. We now, briefly summarize some of these hybrid defects and the GW spectrum generated as a result of their collapse. It was proven in ref. [344] that if a defect involving an n dimensional object appears in the first symmetry breaking step, any defects from the next symmetry breaking step must have a dimension higher than n , so we can write the full list of possible hybrid defects as follows,

- **String-Monopole network:** The hybrid defects associated with the string-monopole system [344, 410–413] can be categorized be either monopoles nucleating and eating a string network or strings attaching to and eating a preexisting monopole network. In the first case, a vacuum manifold \mathcal{H}/\mathcal{K} is not simply connected to a full vacuum manifold \mathcal{G}/\mathcal{K} . Then $\pi_1(\mathcal{H}/\mathcal{K}) \neq I$ results in the formation of topologically unstable strings that manifest themselves by nucleation of magnetic monopole pairs that eat the strings. Such kinds of monopoles must always arise from the earlier phase transition \mathcal{G}/\mathcal{H} (generally before inflation) so that $\pi_2(\mathcal{G}/\mathcal{H}) \neq I$. Consider a scenario where in the first phase a spherical symmetry (non-abelian gauge group) is broken to a $U(1)$ leading to a formation of monopoles, and in the second phase when $U(1)$ is broken, strings are formed. If the $U(1)$ symmetry involved in the production of monopoles partially overlaps or coincides with the $U(1)$ symmetry responsible for the string formation, the strings become metastable as monopoles-antimonopole pairs nucleate along the strings (see Fig. 13) through Schwinger nucleation by quantum tunneling. Conversion of the string's rest mass into monopole's kinetic energy leads to relativistic oscillations of the monopoles before the system collapses via radiating GW and monopole annihilations [414–416].

The total power emitted in the form of GW by string loops before nucleation or by the relativistic monopoles post-nucleation can be calculated using the gravitational power as given in Eq. 131. The power emitted by the string loops or monopole-bounded strings should be comparable since the kinetic energy of the relativistic monopoles originates from the rest mass of the string. Here, $\Gamma \approx 50$ for string loops prior to nucleation and $\Gamma \approx 4 \ln \gamma_0^2$ for relativistic monopoles bounded to strings post-nucleation [415], whereas $\gamma_0 \approx 1 + \mu l / 2m$ is the monopole Lorentz factor arising from the conversion of string rest mass energy to monopole kinetic energy. The power emitted by gravitational waves reduces the string length (see Eq. 157) with a loop lifetime of order $\alpha t_k / \Gamma G \mu$. The string length (l) and harmonic number n is set by the emission frequency, $f' = n/T = 2n/l$, where $T = l/2$ is the period of any string loop [417, 418]. The redshifted frequency observed today is,

$$f = \frac{2n a(t_0)}{l a(t)}, \quad (168)$$

where t_0 is the present time.

The number density spectrum of string loops is as before but modified by a term that captures the rate of cutting strings by monopoles,

$$\begin{aligned} \mathcal{N}(l, t)_{\text{Schwinger}} &\equiv \frac{dn}{dt}(l, t) \approx \frac{dn}{dt_k} \frac{dt_k}{dt} e^{-\Gamma_m l(t-t_k)} \\ &= \frac{\mathcal{F}C_{\text{eff}}(t_k)}{t_k^4 \alpha(\alpha + \Gamma G \mu)} \left(\frac{a(t_k)}{a(t)} \right)^3 e^{-\Gamma_m l(t-t_k)}, \end{aligned} \quad (169)$$

where the tunneling rate per unit string length can be estimated from the bounce action formalism [419, 420] and is exponentially suppressed by powers of the ratio of the symmetry breaking scales [415]

$$\Gamma_m = \frac{\mu}{2\pi} \exp(-\pi \kappa_m), \quad (170)$$

with $\kappa_m = m^2/\mu$. Typically, $m \sim v_m$ and $\mu \sim v_\mu^2$ where v_μ (v_m) is the breaking scale that leads to the formation of CS (monopole). To get a GW signal in this situation, one needs to have $v_m \sim v_\mu$ so that κ_m is not extremely large otherwise the GW spectrum remains identical to the standard stochastic string spectrum as the string remains stable for a larger value of κ_m . Going back to Eq. 169, the exponential factor on the right side of Eq. 169 is the monopole nucleation probability. The probability of

nucleation is initially negligible and the string network evolves like a standard, stable string network when $\Gamma_m l(t - t_k) \ll 1$.

Note that this cutoff is time-dependent,

$$\Gamma_m l(t - t_k) = \Gamma_m \frac{2n}{f} \frac{a(t)}{a(t_0)} (t - t_k). \quad (171)$$

Following Eq. 169 one finds that even though the number density of string loops decreases when nucleation occurs (exponential suppression), the number density of string-bounded monopoles still increases. A loop that nucleates monopoles will continue to nucleate and fragment into many monopole-bounded strings for $l_{\max} \gg l_{\text{tp}}$, with size of order $l \sim l_{\text{tp}} \ll l_{\max}$. In this situation, the net energy density eventually deposited into gravitational waves is much less even if the the total energy density in these pieces is comparable to the original energy density of the parent string loop. This can be understood in the following manner, the lifetime of the string-bounded monopoles $\sim \mu l_{\text{tp}} / \Gamma G \mu^2$ is much smaller than the parent loop because their power emitted in gravitational waves is similar to pure loops while their mass is much smaller. The net energy density that is transferred into gravitational waves is, to a good approximation, the energy density of the defect at the time of decay. Since these pieces decay quickly and do not redshift $\propto a^3$ for as long as pure string loops, their relative energy density compared to the background at their time of decay is much less than for pure string loops. As a result, the net energy density that goes into gravitational radiation by monopole-bounded string pieces compared to string loops is small, and hence their contribution to the spectrum can be neglected.

The gravitational wave energy density spectrum generated from a network of metastable cosmic strings, including dilution and redshifting due to the expansion history of the Universe can be obtained using Eq. 130 and replacing,

$$\frac{dn}{dl}(l, t') = \mathcal{N}(l, t')_{\text{Schwinger}}, \quad \text{and} \quad \frac{dP(l, t')}{df'} = \Gamma G \mu^2 l g \left(f \frac{a(t)}{a(t')} l \right), \quad (172)$$

with t' being the emission time, $f' = a(t)/a(t')f$ being the emission frequency, and f is the redshifted frequency observed at time t . The normalized power spectrum for a discrete spectrum is [418, 421]

$$g(x) = \sum_n \mathcal{P}_n \delta(x - 2n) \quad (173)$$

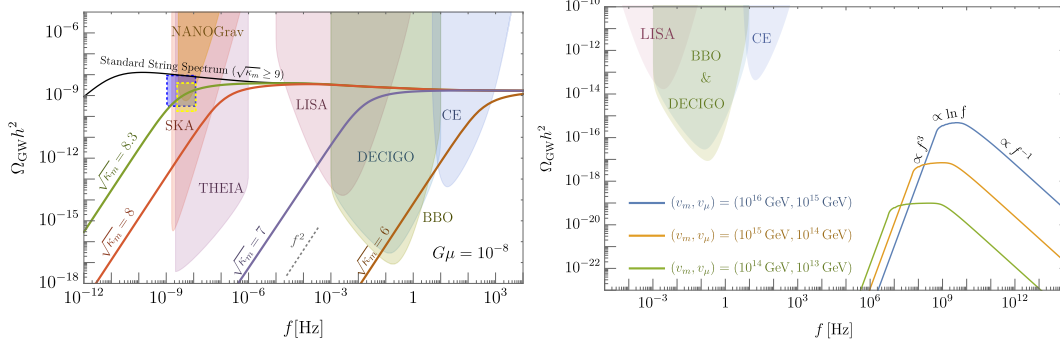


FIG. 14. Left panel: GW spectrum emitted by strings that are eaten up by the nucleation of monopoles for a fixed $G\mu = 10^{-8}$ and different values of κ_m . Right Panel: GW spectrum emitted by monopoles that are eaten up by the string. The figures are taken from [344]

which ensures the emission frequency is $f' = 2n/l$. $\mathcal{P}_n = n^{-q}/\zeta(q)$ is the fractional power radiated by the n th mode of an oscillating string loop where the power spectral index, q , is found to be $4/3$ for string loops containing cusps [381, 422]. The GW spectrum from a metastable can be obtained by including the Schwinger production term, $\mathcal{N}_{\text{Schwinger}}$ in EQ. 150,

$$\Omega_{\text{GW}}(f) = \frac{8\pi}{3H_0} (G\mu)^2 \sum_{n=1}^{\infty} \frac{2n}{f} \int_{t_{\text{form}}}^{t_0} dt \left(\frac{a(t)}{a(t_0)} \right)^5 \times \mathcal{N}_{\text{Schwinger}} \left(l = \frac{2n}{f} \frac{a(t)}{a(t_0)}, t \right) \mathcal{P}_n. \quad (174)$$

The left panel of Fig. 14 shows the GW spectra emitted by the strings eaten up by the monopole nucleation for different values of κ_m and a fixed value of $G\mu = 10^{-8}$. One notices that by increasing the value of κ_m , the nucleation rate decreases, which corresponds to a cosmologically stable CS. Larger loops, corresponding to lower frequencies and later times of formation, vanish because of Schwinger production of monopole-antimonopole pairs and hence the gravitational wave spectrum is suppressed at low frequencies, scaling as an f^2 power law in the infrared. The slope is therefore easily distinguishable from the one obtained from strings without monopole pair. production

In the second case, one can consider a similar breaking chain but with a subtle difference, here the inflation occurs before the formation of monopole and string. The magnetic field of monopoles squeezes into flux tubes (CS) connecting pairs of monopoles and antimonopoles [411, 423]. The strings gradually shrink and lead to the annihilation of monopole and antimonopole pairs. Fig. 12, shows an example of a chain where

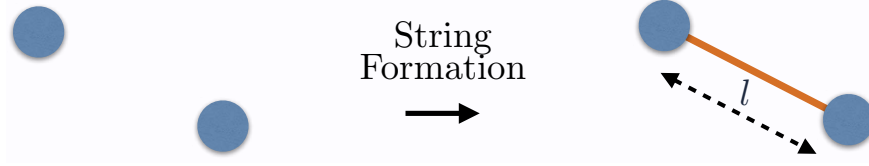


FIG. 15. A illustration of monopole squeezing into flux tubes or strings. The figure is taken from [344]

this gastronomy scenario occurs is $3221 \rightarrow 3211 \rightarrow 321$. While $3221 \rightarrow 3211$ results in the production of monopoles, the second breaking $3211 \rightarrow 321$ connects the monopoles to strings.

In a system where a string is attached to a pre-existing monopole [411, 418, 424, 425], the monopole's initial abundance is considered to be one per horizon at the formation as computed by Kibble [359] and as a result, there is no GW amplitude. In a recent work [344], it was shown that if the Kibble-Zurek mechanism [408] is considered and the monopole-antimonopole freeze-out occurring in between monopole and string formation is taken into account, the monopole-antimonopole pairs annihilate in less than a Hubble time with a non-relativistic velocity. This situation again does not generate any GWs. On the other hand, if some of the monopoles with mass m and string scale v_μ exist, then the monopole-bounded strings can be relativistic. They can generate GWs before decaying if the friction is not large.

Following the Kibble-Zurek mechanism, once formed, the monopole-antimonopole pairs start annihilating. Their freeze-out abundance at any temperature depends on the critical temperature T_c , [426]

$$\frac{n_m(T)}{T^3} = \left[\frac{T_c^3}{n_m(T_c)} + \frac{h^2}{\beta_m} \frac{CM_{Pl}}{m} \left(\frac{m}{T} - \frac{m}{T_c} \right) \right]^{-1} \quad (175)$$

With n_m being the number density of monopoles, $C = (8\pi^3 g_*/90)^{-1/2}$, critical temperature T_c corresponds to a temperature at which the vacua have degenerate energy and

$$\beta_m \simeq \frac{2\pi}{9} \sum_i b_i \left(\frac{he_i}{4\pi} \right)^2 \ln \Lambda \quad (176)$$

counts the particles of charge e_i in the background plasma that the monopole scatters off. The magnetic coupling is $h = 2\pi/e$, where e is the $U(1)$ gauge coupling constant, $\Lambda \sim 1/(g_* e^4/16\pi^2)$ is the ratio of maximum to minimum scattering angles of charged particles in the plasma, and $b_i = 1/2$ for fermions and 1 for bosons [418, 427]. With $e \sim 0.3$ and a comparable number of electromagnetic degrees of freedom as in the Standard Model, $\beta_m \sim 20$.

At a scale below v_μ , the magnetic fields of the monopoles squeeze into flux tubes. The string length here is set by the typical separation distance between monopoles,

$$l \approx \frac{1}{n_m(T = v_\mu)^{1/3}}. \quad (177)$$

Eq. 177 is valid when the correlation length of the string Higgs field denoted by ξ_μ follows the condition $\xi_\mu \geq l$ [418]. Since the string correlation length grows fast enough with time $\propto t^{5/4}$ [359, 418], the string-bounded monopole becomes straightened out within roughly a Hubble time of string formation and ends up with a length close to Eq. 177. For $T_c = v_m \lesssim 10^{17}$ GeV, l is far below the horizon scale. Consequently, l is not conformally stretched by Hubble expansion and only can decrease with time by energy losses from friction and gravitational waves.

Because the string rest mass is converted to monopole kinetic energy, the initial string length Eq. 177 determines whether or not the monopoles can potentially move relativistically. Relativistic monopoles can emit a brief pulse of gravitational radiation before annihilating while non-relativistic monopoles will generally not. This can be achieved in a situation where $\beta \sim 1$ and $T^2 \sim \mu$ (string tension) (see [344] for details). Here, the pulse of energy density emitted by relativistic monopoles in the form of gravitational waves is well approximated by the product of the power emitted ($P_{\text{GW}} = \Gamma G\mu^2$) by oscillating monopoles connected to strings, the number density ($n_m(v_\mu)$) of monopoles at $T = v_\mu$ and the lifetime of the string-bounded monopoles τ ,

$$\rho_{\text{GW,burst}} \approx n_m(v_\mu) P_{\text{GW}} \tau. \quad (178)$$

The GW amplitude from the burst is simply given by Eq. 178 and redshifted to the spectrum we see today,

$$\Omega_{\text{GW,burst}} = \frac{\rho_{\text{GW,burst}}}{\rho_c(v_\mu)} \Omega_r \left(\frac{g_{*0}}{g_*(v_\mu)} \right)^{\frac{1}{3}}$$

$$\approx \frac{30\pi^2}{g_*(v_\mu)\beta} \Gamma G\mu \left(\delta \frac{m}{M_{\text{Pl}}} \right)^{\frac{2}{3}}, \quad (179)$$

where

$$\delta = \frac{1}{C\beta_m h^2} \left(\frac{4\pi}{h^2} \right)^2 \text{Max} \left\{ 1, \frac{v_\mu}{m} \left(\frac{\beta_m h^2}{4\pi} \right)^2 \right\}. \quad (180)$$

and $\rho_c(v_\mu)$ is the critical energy density of the Universe at string formation, which is assumed to be in a radiation-dominated era. The amount of monopole-antimonopole annihilation that occurs before string formation at $T = v_\mu$ is characterized by the argument of the ‘Max’ function of Eq. 180. For a small v_μ/m , the freeze-out annihilating monopoles finishes before string formation, and the max function of Eq. 180 saturates at 1. In this situation, $\delta \approx 10^{-4} \beta_m^{-1} (e/0.5)^4$.

Similarly, the peak frequency for the burst is controlled by the inverse length which in turn is controlled by the symmetry-breaking scale,

$$f_{\text{burst}} \sim \frac{1}{l} \frac{a(t_\mu)}{a(t_0)} \approx 10^8 \text{ Hz} \left(\frac{v_m}{10^{14} \text{ GeV}} \frac{\delta}{10^{-4}} \frac{106.75}{g_*(v_\mu)} \right)^{\frac{1}{3}} \quad (181)$$

where $a(v_\mu)$ and $a(t_0)$ are the scale factors at string formation and today, respectively.

With the understanding of the monopole burst spectrum, one can compute Ω_{GW} for a situation where $\beta_m \sim 1$. Applying the chain rule, one can replace $\frac{dn(l,t')}{dl}$ in Eq.172 with

$$\frac{dn}{dl}(l, t') = \frac{dn}{dt_k} \frac{dt_k}{dl}. \quad (182)$$

where primed coordinates refer to the time of emission and unprimed refer to the present so that gravitational waves emitted from the monopoles at time t' with frequency f' will be observed today with frequency $f = f'a(t')/a(t)$. Further, t_k is the formation time of monopole-bounded strings of length $l(t_k)$,

$$\frac{dn}{dt_k} \simeq n_m(t_k) \delta(t_k - t_\mu) \left(\frac{a(t_k)}{a(t)} \right)^3 \quad (183)$$

is the string-bounded monopole production rate, which is localized in time to the string formation time, $t_\mu \simeq CM_{\text{Pl}}/v_\mu^2$. dt_k/dl is found by noting that the energy lost by relativistic monopoles separated by a string of length l which is given by the rate of change in string length and monopole mass,

$$\frac{dE}{dt} = \frac{d}{dt}(\mu l + 2m) \approx -\beta_m v^2 \mu. \quad (184)$$

A relativistic monopole can be achieved when $\mu l \gg 2m$ [344]. As a result, monopole-bounded strings that form at time t_k with initial size $l(t_k)$ decrease in length according to

$$l(t) \simeq l(t_k) - \beta_m v^2 (t - t_k) \quad (185)$$

so that

$$\frac{dt_k}{dl} \simeq \frac{1}{\beta_m v^2} \approx 1. \quad (186)$$

The normalized power spectrum for a discrete spectrum can be decomposed into the product of the delta function and fractional power radiated by the n^{th} mode of an oscillating string loop,

$$g(x) = \sum_n \mathcal{P}_n \delta(x - n\xi) \quad \xi \equiv \frac{l}{T} \quad (187)$$

ensures the emission frequency of the n th harmonic is $f' = n/T$, where T is the oscillation period of the monopoles. For pure string loops, $T = l/2$ ($\xi = 2$, reducing to Eq. 173), whereas for monopoles connected to strings, $T = 2m/\mu + l \simeq l$ [414, 415] ($\xi \approx 1$). $\mathcal{P}_n \approx n^{-1}$ is found [414, 415] for harmonics up to $n \approx \gamma_0^2$, where $\gamma_0 \simeq (1 + \mu l/2m)$, is the Lorentz factor of the monopoles. For $n > \gamma_0^2$, $\mathcal{P}_n \propto n^{-2}$, $\Gamma \approx 4 \ln \gamma_0^2$.

In this situation, a string eats the monopole, and the emitted GW spectrum looks like,

$$\Omega_{\text{GW}} = \sum_n \frac{8\pi(G\mu)^2}{3H_0^2} \left(\frac{a(t_\mu - l_*)}{a(t - 0)} \right)^5 \left(\frac{a(t_\mu)}{a(t_\mu - l_*)} \right)^3 \times \Gamma \mathcal{P}_n \frac{\zeta_n n_m(t_\mu)}{f \beta_m v^2} \quad (188)$$

where

$$l_* = \frac{\frac{\zeta_n n}{f} \frac{a(t_\mu)}{a(t_0)} - n_m(t_\mu)^{-1/3}}{\beta_m v^2} \quad (189)$$

The GW spectrum for this scenario is shown in the right panel of Fig. 14. Here, at high frequencies, the spectral shape goes as f^{-1} , prior to which a small plateau is observed where the spectrum goes as $\ln f$ and at low frequencies decays as f^3 .

- **String-Wall network:** Analogous to a string-monopole system, the hybrid defects associated with a string-wall network can also be categorized as either the destruction

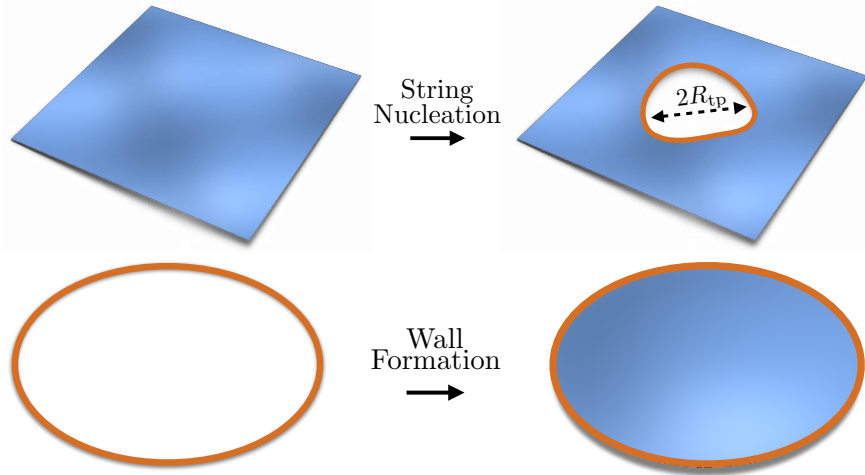


FIG. 16. A cartoon showing a string nucleation process in the top panel and wall formation in the bottom panel. The figure is taken from [344]

of a domain wall network by the nucleation of string-bounded holes on the wall that expand and eat the wall, or the collapse and decay of a string-bounded wall network by walls that eat the strings. If a vacuum manifold \mathcal{H}/\mathcal{K} is disconnected but \mathcal{G}/\mathcal{K} is connected, DWs are formed at transition from $\mathcal{H} \rightarrow \mathcal{K}$ and $\Pi_0(\mathcal{H}/\mathcal{K}) \neq \mathcal{I}$. The DWs of this nature are topologically unstable as $\Pi_0(\mathcal{G}/\mathcal{K}) = \mathcal{I}$. This instability is caused by the nucleation of string-bounded holes on the wall that expand and destroy the wall completely. As a consequence of Schwinger nucleation, a wall (formed after inflation) gets bounded by a string (formed before inflation) if both defects are related to the same discrete symmetry. Here, the wall's rest mass energy is transformed into the string's kinetic energy leading to its rapid expansion. This rapid expansion causes the collapse of the string wall system and produces GWs in the process.

To understand this, one can solve the Boltzmann equation [344] for the total energy density, ρ_{GW} in the gravitational wave background,

$$\frac{d\rho_{\text{GW}}}{dt} + 4H\rho_{\text{GW}} = \mathcal{A}\mathcal{B}\frac{G\sigma^2}{t}\theta(t_{\Gamma} - t) - x\frac{d\rho_{\text{DW}}}{dt}\theta(t - t_{\Gamma}). \quad (190)$$

While the first term on the RHS of Eq. 190 corresponds to the rate of energy density lost into GWs by DWs at time t in the scaling regime and prior to the nucleation, the second term shows the energy transferred into GWs after string began nucleating and eating the wall with $x \in [0, 1]$ denoting an efficiency parameter characterizing the

fraction of the energy density of the wall transferred into gravitational waves at time,

$$t_\Gamma \sim \frac{1}{\sigma A} e^{S_E} \sim \frac{1}{\sigma^{1/3}} \exp \frac{16\pi\kappa_s}{9}. \quad (191)$$

Here, we take the wall area, A at time t_Γ to be $\sim t_\Gamma^2$ following the scaling regime and $\kappa_s = \mu^3/\sigma^3$ where σ denotes the surface tension of the DW that depends on the breaking scale v_σ that leads to the formation of the DW (see section IV B for details). Also one needs to have $\mu^3 \sim \sigma^3$, otherwise, the DW remains long-lived. When the strings begin nucleating at t_Γ , they quickly expand from an initial radius $R_{\text{tp}} = 2R_c$ with $R_c \equiv \mu/\sigma$ according to [344]

$$R_s(t) = \sqrt{4R_c^2 + (t - t_\Gamma)^2}. \quad (192)$$

In the above, R_{tp} denotes the critical string radius that is obtained when the balance between string creation and domain wall destruction is balanced. Above this, it is energetically favorable for the string to nucleate and continue expanding and consuming the wall as shown in the top panel of Fig. 16. As a result, the strings rapidly accelerate to near the speed of light as they ‘eat’ the wall. The increase in string kinetic energy arises from the devoured wall mass. Thus, shortly after t_Γ , most of the energy density of the wall is transferred to strings and string kinetic energy.

Assuming a conservative limit $x = 0$ [344], the solution to Eq. 190 during an era with scale factor expansion $a(t) \propto t^\nu$ is then

$$\rho_{\text{GW}}(t) = \begin{cases} \mathcal{A}\mathcal{B} \frac{G\sigma^2}{4\nu} \left(1 - \left(\frac{t_{\text{scl}}}{t}\right)^{4\nu}\right) & t \leq t_\Gamma \\ \left(\rho_{\text{GW}}(t_\Gamma) + x\mathcal{A} \frac{\sigma}{t_\Gamma}\right) \left(\frac{a(t_\Gamma)}{a(t)}\right)^4 & t > t_\Gamma \end{cases} \quad (193)$$

Eq. 193 demonstrates that the gravitational wave energy density background quickly asymptotes to a constant value after reaching scaling at time t_{scl} and to a maximum at the nucleation time t_Γ . We thus expect a peak in the gravitational wave amplitude of approximately [344],

$$\Omega_{\text{GW, max}} = \frac{16\pi}{3} [(G\sigma t_\Gamma)^2 + 2xG\sigma t_\Gamma] \Omega_r \left(\frac{g_{*0}}{g_*(t_\Gamma)}\right)^{1/3}. \quad (194)$$

where we take $t_\Gamma > t_{\text{scl}}$, $\mathcal{A} = \mathcal{B} = 1$, and a radiation dominated background at the time of decay with $\nu = \frac{1}{2}$. $\Omega_r = 9.038 \times 10^{-5}$ is the critical energy in radiation today [428].

The first term in Eq. 194, the contribution to the peak amplitude from gravitational waves emitted prior to nucleation, agrees well with the numerical results of [353] if t_Γ maps to the decay time of unstable walls in the authors' simulations. The second term in Eq. 194, the contribution to the peak amplitude from GW emitted after nucleation, has not been considered in numerical simulations. The post-nucleation contribution dominates the pre-nucleation contribution if $x \gtrsim G\sigma t_\Gamma$, which may be important for short-lived walls. The complex dynamics of string collisions during the nucleation phase motivate further numerical simulations.

The frequency dependence on the gravitational wave amplitude may be extracted from numerical simulations of domain walls in the scaling regime. The form of the spectrum was found in [353] to scale as

$$\Omega_{\text{GW}}(f) \simeq \Omega_{\text{GW, max}} \begin{cases} \left(\frac{f}{f_p}\right)^{-1} & f > f_p \\ \left(\frac{f}{f_p}\right)^3 & f < f_p \end{cases} \quad (195)$$

where

$$f_{\text{peak}} \sim \frac{1}{t_\Gamma} \frac{a(t_\Gamma)}{a(t_0)} \quad (196)$$

The infrared f^3 dependence for $f < f_{\text{peak}}$ arises from causality arguments for an instantly decaying source [320]. This behavior is shown in Fig. 17.

Finally, consider the case of a string wall network where DWs get attached to pre-existing strings [344]. Here, both strings and DWs are formed after inflation. In this scenario, the strings are formed before the wall formations and once the walls are in the picture they fill the spaces between the strings. After the DW-bounded string system enters the horizon, the system oscillates with constant amplitude resulting in the production of the GWs.

Considering a string boundary of a circular wall with radius R , it was shown that while the wall tension dominates when the radius $R \gg R_c$ with $R_c \equiv \mu/\sigma$, the string dynamics reduces to the pure string loop motion for $R \ll R_c$ where the string dominates the dynamics and the power is independent of loop size which is in agreement

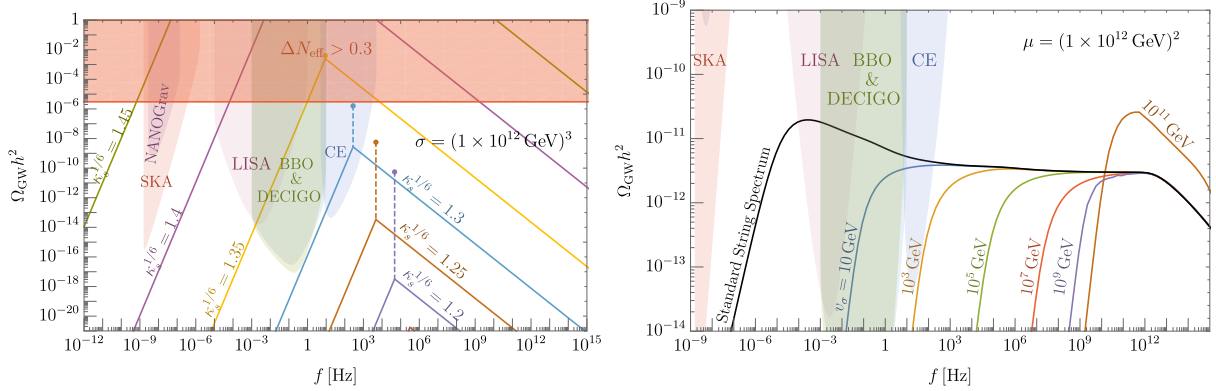


FIG. 17. Left Panel: GW spectrum emitted by domain walls that are eaten by nucleation of strings for fixed $\sigma^{1/3} = 10^{12}$ GeV. Right Panel: GW spectrum emitted by strings that are eaten by domain walls for fixed $\sqrt{\mu} = 10^{12}$ GeV. The figure is taken from [344].

with the pure string case. Using the VOS model of an infinite string-wall network they showed that the walls pull their attached strings into the horizon when the curvature radius of the hybrid network grows above R_c . Once this network is inside the horizon, it oscillates and radiates GWs. As expected, for $R \ll R_c$ (pure string limit), the power emitted in the GWs goes as $P_{\text{GW}} \propto G\mu^2$. On the other hand, for $R \gg R_c$, the domain wall dominates the dynamics and the power deviates from the pure string case, increasing quadratically with R/R_c . Since $R_c \equiv \mu/\sigma$, this is equivalent to $P_{\text{GW}} \propto G\sigma^2 R^2 \propto G\sigma M_{\text{DW}}$, in agreement with the quadrupole formula expectation for gravitational wave emission from domain walls.

With the idea of GW power emitted by a string-bounded domain wall system (see [344] for detail) one can now calculate the gravitational wave spectrum from a network of circular string-bounded walls. Here we briefly discuss the analytical estimate of the expected amplitude and frequency of the spectrum. For the numerical computation, we refer readers to [344].

To start with, first consider a pure string loop without walls that form at time t_k with initial length $l_k = \alpha t_k$, where $\alpha \simeq 0.1$. Once these loops are inside the horizon, they oscillate, and their energy density redshifts $\propto a^{-3}$ because their energy $E = \mu l$ is constant in the flat space limit. The loops radiate GW with power $P_{\text{GW}} = \Gamma_s G\mu^2$ as discussed above, where $\Gamma_s \approx 50$, and eventually decay from gravitational radiation

at time

$$t_\Gamma \approx \frac{\mu l_k}{\Gamma_s G \mu^2} \quad (\text{Pure string loop lifetime}). \quad (197)$$

When the pure string loops form and decay in a radiation-dominated era, their energy density at decay is

$$\rho(t_\Gamma) \approx \mu l_k n(t_k) \left(\frac{t_k}{t_\Gamma} \right)^{3/2} \quad (198)$$

with $n(t_k) \approx \frac{1}{3} \frac{\mathcal{F} C_{\text{eff}}}{\alpha t_k^3}$ being the initial number density of loops of size l_k that break off from the infinite string network in a scaling regime [398, 421, 429], $\mathcal{F} \approx 0.1$ [377] and $C_{\text{eff}} \approx 5.4$ in a radiation dominated era [430, 431]. Following Eq. 197 and Eq. 198, the gravitational wave amplitude coming from these pure string loops is approximately

$$\begin{aligned} \Omega_{\text{GW}}^{(\text{str})} &\approx \frac{\rho(t_\Gamma)}{\rho_c(t_\Gamma)} \Omega_r \left(\frac{g_{*0}}{g_*(t_\Gamma)} \right)^{\frac{1}{3}} \\ &= \frac{32\pi}{9} \mathcal{F} C_{\text{eff}} \sqrt{\frac{\alpha G \mu}{\Gamma_s}} \Omega_r \left(\frac{g_{*0}}{g_*(t_\Gamma)} \right)^{\frac{1}{3}} \end{aligned} \quad (199)$$

where $\rho_c(t_\Gamma)$ is the critical energy density of the Universe at t_Γ .

Before reaching $t = t_*$, the dynamics of the string-bounded walls are dominated by the strings and the spectrum must be approximately that of a pure string spectrum with Ω_{GW} given approximately by Eq. 199, independent of frequency. Now at time $t_k = t_*$, let us consider the formation of a near circular string-bounded wall with initial circumference $l_k = \alpha t_k$. While for $l_k \lesssim 2\pi R_c$, the power emitted and total mass of the system is effectively identical to the pure string case and Ω_{GW} remains the same as Eq. 199, for $l_k \gtrsim 2\pi R_c$, the power emitted and mass of the system is dominated by the DW contribution of the wall-string piece. In this situation, the wall-bounded string decays while radiating the GW at the time

$$t_\Gamma \approx \frac{\sigma l_k^2 / 4\pi}{\Gamma(l_k) G \mu^2} \approx \frac{1}{G \sigma} \quad (200)$$

For the wall-bounded strings forming and decaying in a radiation-dominated era, their energy density at decay is

$$\rho(t_\Gamma) \approx \frac{\sigma l_k^2}{4\pi} n(t_k) \left(\frac{t_k}{t_\Gamma} \right)^{3/2} \quad (201)$$

where $n(t_k) \approx \frac{1}{3} \frac{\mathcal{F}C_{\text{eff}}}{\alpha t_k^3}$ follows from the infinite string-wall network being in the scaling regime with \mathcal{F} and C_{eff} expected to be similar to the pure string values right before the infinite network collapses at t_* . Hence the GW amplitude in this scenario is controlled by the energy density of the string-wall system at decay,

$$\begin{aligned} \Omega_{\text{GW}} &\approx \frac{\rho(t_\Gamma)}{\rho_c(t_\Gamma)} \Omega_r \left(\frac{g_{*0}}{g_*(t_\Gamma)} \right)^{1/3} \\ &= \frac{8}{9} \mathcal{F} C_{\text{eff}} \alpha \sqrt{G\sigma t_k} \Omega_r \left(\frac{g_{*0}}{g_*(t_\Gamma)} \right)^{\frac{1}{3}}. \end{aligned} \quad (202)$$

The largest amplitude of Eq. 202 occurs at the latest formation time t_k , which is t_* , the time of the collapse of the infinite network. As a result of this, a ‘bump’ relative to the flat string amplitude appears if

$$\frac{\Omega_{\text{GW}}}{\Omega_{\text{GW}}^{(\text{str})}} \approx \frac{1}{4\pi} \sqrt{\frac{\Gamma_s \alpha t_*}{R_c}} \approx 0.2 \left(\frac{\alpha}{0.1} \right)^{\frac{1}{2}} \left(\frac{\Gamma_s}{50} \right)^{\frac{1}{2}} \left(\frac{t_*}{R_c} \right)^{\frac{1}{2}} \quad (203)$$

is greater than 1 and at a frequency

$$f_{\text{peak}} \sim \frac{1}{l_k} \frac{a(t_\Gamma)}{a(t_0)}. \quad (204)$$

since the walls remain the same size once inside the horizon and dominantly emit at the frequency of the harmonic, $f_{\text{emit}} \sim l_k^{-1}$. Here, $l_k \approx \alpha t_*$.

The estimation of Eq. 203 indicates that if $t_* \gg R_c$, then Ω_{GW} features a ‘bump’ relative to the flat string spectrum before decaying. In this situation, the walls are massive and large enough to live much longer than the pure string of the same size. Due to this, they have an enhanced energy density before decaying in comparison to the shorter-lived pure string loops. In a situation with $t_* \approx R_c$ no such enhancement is observed because string-bounded walls are smaller in size and decay quickly.

With the qualitative features of the spectrum understood, we turn to a numerical computation of Ω_{GW} . The GW spectrum obtained from the numerical computation of [344] for this system is shown in the right panel of Fig. 17 for a fixed value of $\sqrt{\mu} = 10^{12}$ GeV. It is also interesting to point out that, the spectrum here decays as f^3 (due to causality) rather than f^2 decay signal which was observed in the situation with the monopoles eating the strings.

F. Applications of gravitational waves from topological defects

Cosmic strings as discussed earlier, can play a vital role in understanding and testing the evolutionary history of the Universe. A string network continuously emits gravitational wave power for the entirety of its existence, and as the string network enters the scaling regime, the fraction of energy density in gravitational waves should remain constant for all frequencies unless there is some change in the energy budget of the Universe. GW signals emitted from the CS can therefore provide an unprecedented window into the evolution of the very early universe before BBN and the CMB. On the other hand, if a network of CS that was formed before or shortly after the start of inflation can regrow after getting diluted and generate GW signals that can be observed today. In this section, we will first cover how strings can be witnesses to a period of inflation before covering how they can be witnesses to dramatic changes in the Universe such as an early period of matter domination or kination. Finally, we will cover how topological defects can provide information about high-scale physics from leptogenesis to quantum gravity.

As is well known, primordial cosmological inflation dilutes all the relics that were generated before its commencement to a negligible level, hence one expects that a CS if produced before the onset of inflation will also be diluted. A recent study [432], has shown that a network of cosmic strings diluted by inflation can replenish to a level that can result in the generation of GW signals that can be probed by the present and future GW detectors. This is due to the energy density diluting slower than radiation. Unlike the signals that result from an undiluted CS which are of the form of SGWB, the signal resulting from the diluted CS can be distinctive bursts of GWs.

To understand this, we assume a constant Hubble parameter $H_I = V_I/3M_{\text{Pl}}^2$ during inflation that describes the inflationary energy density from the initial time t_I to end time t_E with $V_I = M^4$ ($M \leq 10^{16}$ GeV [433]), the cosmological scale factor grows as $a(t) \propto e^{H_I t}$. Once the inflation is completed, the radiation-dominated era is initiated with temperature $T_{RH} \leq (30/\pi^2 g_*)^{1/4} M$. Under the assumption that the temperature during the reheating remains below the symmetry breaking scale, the dilution of the pre-existing CS by thermal processes like symmetry restoration can be avoided. Once again following the VOS model used for describing the horizon-length long strings during and after inflation [434], one can study the evolution of the correlation length parameter L and the velocity parameter \bar{v} of a

long string [375, 376]. Starting with the initial conditions,

$$L(t_F) \equiv L_F = \frac{1}{\xi H_I}, \quad (205)$$

where ξ^2 corresponds approximately to the number of long strings within the Hubble volume at time t_F . $L(t)$ soon reaches an attractor solution during inflation after t_F ,

$$L(t) = L_F e^{H_I(t-t_F)}, \quad \bar{v}(t) = \frac{2\sqrt{2}}{\pi} \frac{1}{H_I L(t)}. \quad (206)$$

For $HL \gg 1$ and $\bar{v} \ll 1$, the above solution corresponds to the dilution of the long string network. As a result of this, the evolution of the string network after inflation takes a very simple form while $HL \gg 1$ with (L/a) approximately constant. It follows that HL decreases after inflation, corresponding to the gradual regrowth of the string network. If the network is to produce a potentially observable signal in GWs, at least a few strings are needed within our current Hubble volume corresponding to $HL \leq 1$ today. The conditions under which there is enough string regrowth for $HL \rightarrow 1$ while also maintaining a sufficient amount of inflation can be obtained by comparing the evolution of L before scaling to that of the curvature radius $R = 1/(H\sqrt{|\Omega - 1|})$ which evolves in precisely the same way, independently of the details of inflation or reheating. The total number of inflationary e-foldings can then be written as $N_{tot} = H_I(t_E - t_I) \equiv N_F + \Delta N$ with $\Delta N \geq 0$ being the number of e-foldings between t_I and t_F . Note that $\Delta N = 0$ corresponds to the string forming before or at the start of inflation. Applying the curvature limit $|\Omega_0 - 1| = 0.0007 \pm 0.0037$ [428], one finds,

$$\Delta N + \ln \xi \geq 2.7 + \frac{1}{2} \ln(|\Omega_I - 1|) + \frac{1}{2} \ln [\Omega_\Lambda(1+z)^{-2} + \Omega_m(1+z) + \Omega_r(1+z)^2] \quad (207)$$

where z is the redshift at which $HL \rightarrow 1$, Ω_a are the fractional energy densities in dark energy, matter, and radiation relative to critical today, $|\Omega - 1|$ is the deviation from flatness at the start of inflation, $\ln(|\Omega_0 - 1|)/2 \leq 2.7$ is the bound from Planck [428], and the last line describes the additional evolution of $(\Omega - 1)$ between z and now.

As discussed previously, the scaling solution produces larger string loops together with the smaller loops. The smaller loops are highly relativistic and most of the energy transferred to the smaller loops is in the form of kinetic energy that simply redshifts away, and thus larger loops are expected to be the dominant source of GWs. For a Nambu-Goto string large loops oscillate, emit energy in the form of GWs, and gradually shorten as shown in Eq. 157. Unlike the vanilla case discussed in section IV C, the GW in this situation is mostly emitted

by short, violent, collimated bursts involving cusps or kinks on the string loops. Bursts emitted by a cosmic string network over its cosmic history that are not resolved contribute to the characteristic stochastic gravitational wave background of the network. For comparing the GW signals with current and future detectors, one can separate the contributions of the recent burst (with large amplitude) and earlier bursts (unresolved). If a burst is to be resolved in a given frequency band f , it must produce a strain greater than the experimental sensitivity $h > h_{\text{exp}}$ with a rate less than f . The rate of such events is [381, 432, 435]

$$R_{\text{exp}}(f) = \int_0^{z_*} dz \int_{\max(h_{\min}, h_{\text{exp}})}^{h_{\max}} dh \frac{d^2 R}{dz dh}(h, z, f) \quad (208)$$

where z_* enforces the rate condition and is given by

$$f = \int_0^{z_*} dz \int_{h_{\min}}^{h_{\max}} dh \frac{d^2 R}{dz dh}(h, z, f). \quad (209)$$

Unresolved bursts contribute to the SGWB as [381, 435]

$$\Omega_{\text{GW}}(f) = \frac{4\pi^2 f^3}{3H_0^2} \int_{z_*}^{\infty} dz \int_{h_{\min}}^{h_{\max}} dh h^2 \frac{d^2 R}{dz dh}(h, z, f) \quad (210)$$

with $\Omega_{\text{GW}} = (f/\rho_c) d\rho_{\text{GW}}/df$ and

$$\frac{d^2 R}{dz dh} = \frac{2^{3(q-1)} \pi G\mu N_q}{(2-q)} \frac{r(z)}{(1+z)^5 H(z)} \frac{n(l, z)}{h^2 f^2} \quad (211)$$

where l is a function of h , f , and z , and

$$h_{\min} = \frac{1}{(1+z)f^2} \frac{G\mu}{r(z)}, \quad h_{\max} = \frac{[\alpha L(z)]^{q-2}}{f^q (1+z)^{q-1}} \frac{G\mu}{r(z)} \quad (212)$$

Since the total GW signal is expected to be dominated by bursts from cusps [378, 436], one can set $q = 4/3$ and $N_q = 2.13$ (to match $\Gamma = 50$ [381]) for the analysis purpose.

The top (bottom) panel of Fig. 18 shows the variation of the SGWB spectrum obtained from the unresolved (resolved) burst rate with frequency for diluted and undiluted string networks. The SGWB for the diluted networks falls off as $f^{-1/3}$ at high frequency due to the inclusion of the sufficient number of modes when computing the SGWB with the normal mode method (see [432]) for the details. At higher frequencies, a sharper drop is observed from the burst method that results from the subtraction of infrequent bursts from the SGWB.

Let us now turn our attention to how the GW emitted from the CS can help us understand the cosmic history of the Universe after the inflation but at times well before primordial

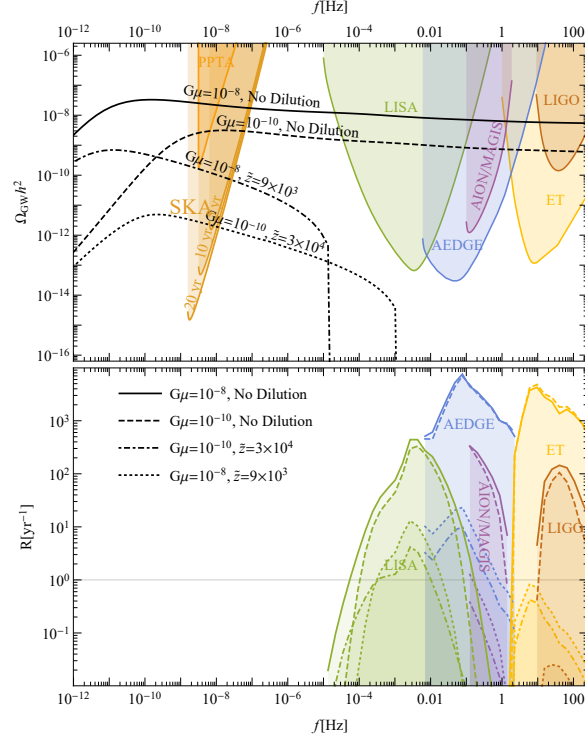


FIG. 18. GW spectrum from diluted and undiluted CS as a function of frequency observed today. While the top panel shows the stochastic GW background, the lower panel gives the event rates of resolved bursts. In both panels, the curves are shown for $G\mu = 10^{-8}$, 10^{-10} for undiluted networks as well as for two diluted networks with $z = 9 \times 10^3$ for $G\mu = 10^{-8}$, and $z = 3 \times 10^{-4}$ for $G\mu = 10^{-10}$. The figure is taken from [432]

nucleosynthesis and the cosmic microwave background where standard cosmology has yet to be tested. Recent studies like [429, 430], have demonstrated how the spectrum of GWs emitted by a Nambu-Goto cosmic string network depends on the energy content of the universe when they are produced. For example, if the Universe transitions from radiation domination at very high temperatures to matter domination and then back to radiation domination before the onset of BBN, a GW spectrum can be observed that is different from what is seen in the standard cosmology and hence can be distinguished.

In a scenario like this, one can use the cosmological time t_Δ (epoch of most recent radiation-domination era) to calculate the frequency f_Δ where such a deviation would appear. The first significant modification in the frequency spectrum will appear when the dominant emission time \tilde{t}_M comes from loops created at $t_i^{(k=1)} \simeq t_\Delta$. This results in an

approximate transition frequency f_Δ as the solution of

$$t_i(\tilde{t}_M(f_\Delta)) = t_\Delta . \quad (213)$$

Under the approximation $a(t) \propto t^{1/2}$ at the radiation dominated era one can obtain [429, 430]

$$\begin{aligned} f_\Delta &\simeq \sqrt{\frac{8 z_{\text{eq}}}{\alpha \Gamma G \mu}} \left(\frac{t_{\text{eq}}}{t_\Delta}\right)^{1/2} t_0^{-1} \\ &\simeq \sqrt{\frac{8}{z_{\text{eq}} \alpha \Gamma G \mu}} \left[\frac{g_*(T_\Delta)}{g_*(T_0)}\right]^{1/4} \left(\frac{T_\Delta}{T_0}\right) t_0^{-1} \end{aligned} \quad (214)$$

where $z_{\text{eq}} \simeq 3387$ is the redshift at matter-radiation equality, and $T_0 = 2.725$ K is the temperature today. A more accurate dependence is obtained by fitting it to a full numerical the calculation that properly accounts for variations in g_* gives [429, 430]

$$f_\Delta = (8.67 \times 10^{-3} \text{ Hz}) \left(\frac{T_\Delta}{\text{Gev}}\right) \left(\frac{0.1 \times 50 \times 10^{-11}}{\alpha \Gamma G \mu}\right)^{1/2} \left(\frac{g_*(T_\Delta)}{g_*(T_0)}\right)^{\frac{8}{6}} \left(\frac{g_{*S}(T_0)}{g_{*S}(T_\Delta)}\right)^{-\frac{7}{6}} . \quad (215)$$

This is found to be accurate to about 10%. One can reinterpret this f_Δ as a frequency required to test cosmology up to temperature T_Δ . This is because the measured GW spectrum obtained from the CS will remain approximately flat till f_Δ for a given value of α and $\Gamma G \mu$ and hence would provide strong evidence for radiation domination up to the corresponding temperature T_Δ .

Such cosmological modification can be observed in a scenario having a very large number of additional degrees of freedom present in the spectrum at high energy. If additional degrees of freedom exist till temperature T_Δ , the energy density of GW will be altered above f_Δ in comparison to what is expected in a standard cosmology with only SM degrees of freedom. In such a scenario, one obtains a standard $\Omega_{\text{GW}}(f)$ vs. f for cosmic strings behaviour up to f_Δ and thereafter fall-off is observed for $f > f_\Delta$. For a detailed discussion see [429, 430].

The refs. [429, 430] also discuss scenarios where GWs from cosmic strings evolve in a non-standard phase, either of an early matter domination phase ($n = 3$) or an early kination ($n = 6$) phase. The early matter domination can result from the presence of a new degree of freedom whose late decay brings the Universe back to the radiation domination era. Such slow decay should also satisfy BBN constraints. In other words, the universe transitions from radiation domination at very high temperatures to matter domination (at T comparable to the mass of long-lived heavy new particles) and then back to radiation domination (by the decay of said particles) before the onset of BBN. On the other hand, a kination ($n = 6$)

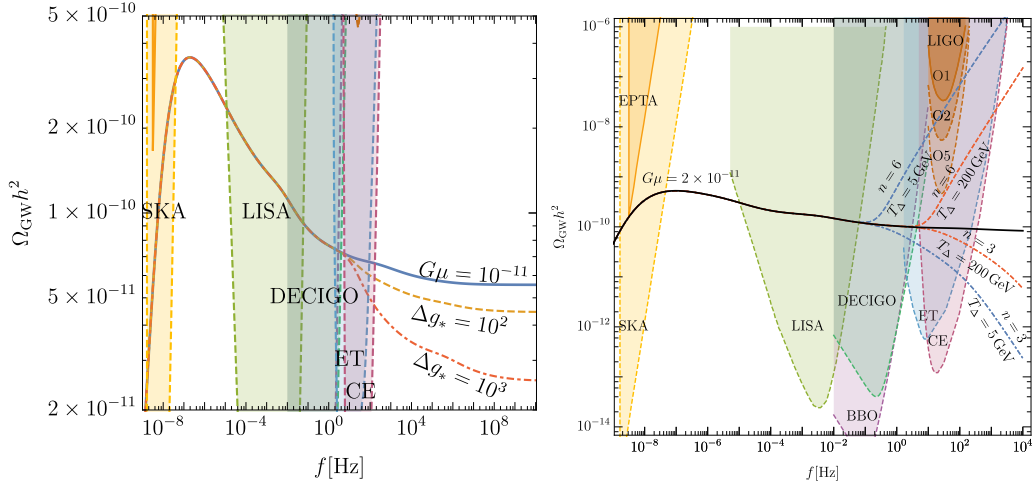


FIG. 19. Left panel: Modification of the GW spectrum obtained from the CS by changing the number of DOFs. Here $G\mu = 10^{-11}$ GeV and $T_\Delta = 200$ GeV. Right panel: GW spectrum resulting from the early period of kination ($n=6$), matter ($n=3$) domination lasting until temperature T_Δ . The figure is taken from [429]

phase can arise from oscillating scalar moduli in the early Universe, which then decay. This leads to a cosmological history of very early radiation domination to kination domination (oscillation energy dominating) and back to radiation (by the decay of the moduli). CS can act as a tool to probe these scenarios of alternate cosmologies, this is because they rapidly enter a scaling regime *i.e.* their energy density scales with scale factor a the same as the dominant energy density of the Universe. While for an early matter domination era, the CS will scale like a^3 during that phase, an early kination phase will make cosmic strings scale as a^6 . The modified scaling behavior of CS will alter the energy density of the GWs emitted through its non-standard redshifting. [429, 430] shows these effects quantitatively, which leads to a sharp fall-off in $\Omega_{\text{GW}}(f)$ at high frequency f (corresponding to the new phase era) if there is early matter domination and a sharp rise in $\Omega_{\text{GW}}(f)$ if there is an early kination phase.

Apart from testing the scenarios of modified cosmologies, a GW emitted from the CS can also help in testing the other early Universe physics like why there exists a plethora of matter over anti-matter in our Universe. Arguably the most elegant way to understand this issue is through leptogenesis [437–439], using type I seesaw mechanism [440–450]. Here an out-of-equilibrium decay of a heavy state generates an asymmetry in between leptons and their

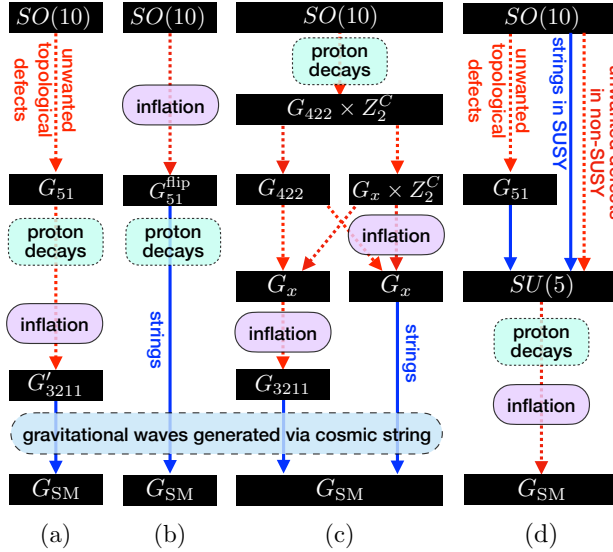


FIG. 20. The breaking chains of $SO(10) \rightarrow G_{SM}$ are shown along with their terrestrial and cosmological signatures where G_x represents either G_{3221} or G_{421} . The figure is taken from [362]

antiparticles. Once generated, the lepton asymmetry catalyzes a baryon asymmetry through sphaleron transitions [451–453]. Unfortunately, the scale of leptogenesis is much beyond the scales that can be tested on present-day earth-based detectors. The mass of the Right-handed neutrinos (RHN) responsible for explaining the light neutrino masses lies below the Planck or a possible GUT scale suggesting some symmetry that survives below these scales to protect the right-handed neutrino mass. Thermal leptogenesis demands the breaking of this symmetry to be below the scale of inflation or the asymmetry will be catastrophically diluted. Such a breaking can be observed through its predicted cosmological defects. In [409], a $B - L$ that protects the RHN masses is spontaneously broken to generate the RHN masses, this process also results in the generation of CS that radiates a spectrum of stochastic gravitational waves. When embedding this symmetry into a grand unified group, one finds that the majority of viable symmetry-breaking paths admit cosmic strings. The GW signal is expected to be tested using future detectors that are expected to probe the entire mass range relevant to the paradigm of thermal leptogenesis.⁹ Symmetry breaking paths that do not admit cosmic strings could result in a signal from proton decay [362, 455, 456]. Recent work has also considered the complementarity of gravitational waves and neutrino oscillation experiments within the concrete framework of an $SO(10)$ model [457].

⁹ If it is a global symmetry protecting the seesaw mass, it is still possible a signal is visible if the seesaw scale is very high [454]

Like CS, the GW resulting from the DW can also play an interesting role in understanding the physics of the early Universe. For example, recent works like [350, 352], have explored the phenomenological consequences of breaking discrete global symmetries in quantum gravity (QG). Motivated by Swampland global symmetry conjecture [458–460] which says that there exists no exact global symmetry in effective field theories (EFTs) arising from UV theories of QG, they studied how quantum gravity effects, manifested through the breaking of discrete symmetry responsible for both Dark Matter and Domain Walls, can have observational effects through CMB observations and gravitational waves. They show that the existence of very small bias terms stems from the QG¹⁰ which allows DWs to annihilate, thus stopping them from dominating the energy density of the Universe. To illustrate this idea, in [350], they considered a simple model with two singlet scalar fields together with two Z_2 symmetries, one being responsible for DM stability, and the other spontaneously broken and responsible for DWs.¹¹ Moreover, both the Z_2 symmetries are assumed to be explicitly broken by QG effects by operators at the same mass dimension and with the same effective Planck scale. They showed that this hypothesis led to observable GW signatures from the annihilation of DWs, which are correlated with the decaying DM signatures constrained by CMB observations.¹² Fig. 21 shows constraints obtained on the QG scale.

GW detectors have given us a window to early universe cosmology complementary to any other probes previously developed. A strong and well-understood source of GWs in the early universe could give us unprecedented ability to probe cosmological energy evolution of the early universe far earlier than previously attainable. These works have also demonstrated that topological defects if they exist, would be excellent standard candles to achieve these aims.

¹⁰ Work like [351] showed that a small bias can also be achieved in a clockwork axion model where the QCD axion potential induced by the QCD phase transition can serve as an energy bias leading to the annihilation of DW

¹¹ For the fermionic DM see [352]. Explicit due to QG causes the DM to allowed to mix with the SM neutrinos after the electroweak symmetry breaking. This causes the DM to become unstable. Such DM decay puts constraints on the QG operator from the CMB, BBN, galactic and extragalactic diffuse X/γ -ray background, SKA, neutrinoless double beta decay.

¹² This is also a possible explanation for the results of the North American Nanohertz Observatory for Gravitational Waves (NANOGrav) [461, 462], the European PTA [463, 464], the Parkes PTA [465] and the Chinese PTA [466]

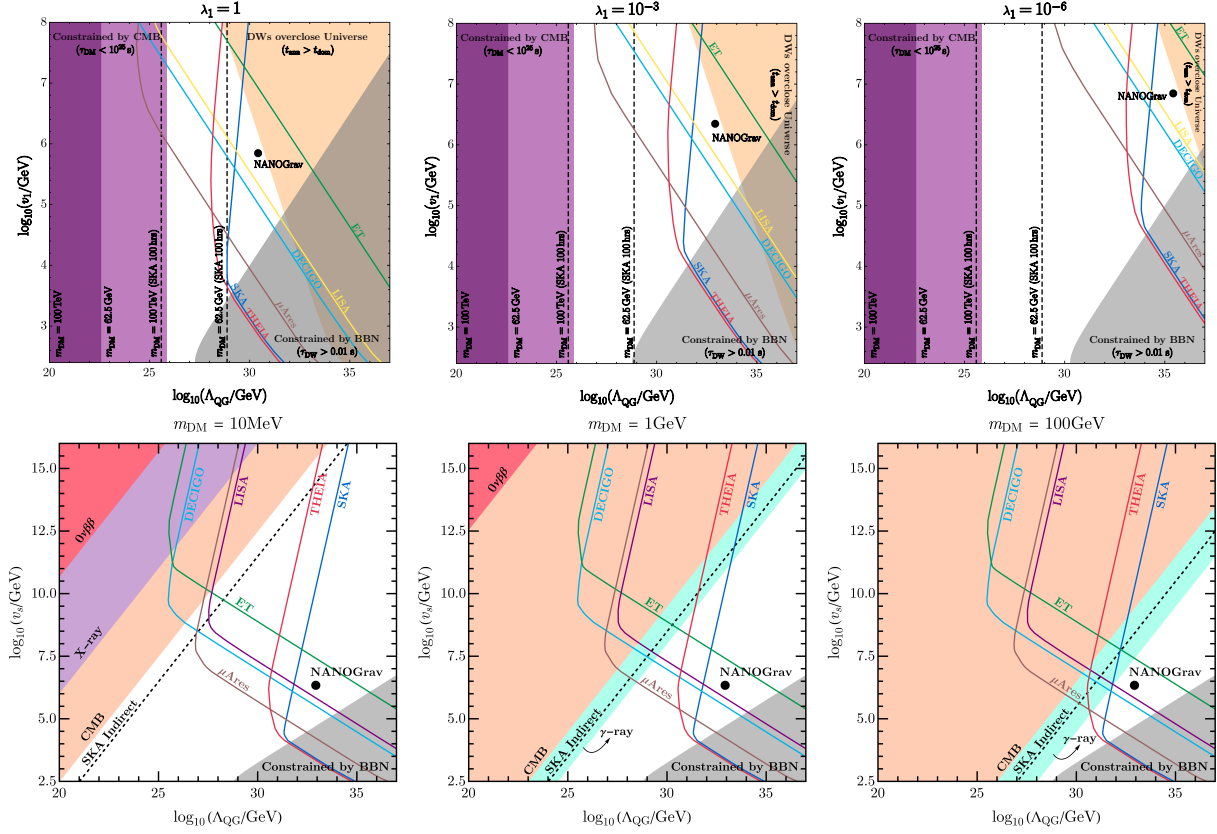


FIG. 21. Combined constraints on Λ_{QG} and v_1 from indirect DM detection and GWs observations with varying model parameter λ_1 of [350] in the top panel while varying DM mass of freeze-in DM of [352] in the bottom panel. The top panel is taken from [350] and the bottom panel is taken from [352]

V. SCALAR INDUCED GRAVITATIONAL WAVES

It was first mentioned by Tomita [467] then rediscovered by Matarrese, Pantano, and Saez [468, 469] that large scalar perturbations can act as a source for tensor perturbations at second order. For a curvature perturbation power spectrum, $\mathcal{P}_{\mathcal{R}}$, the approximate scaling of scalar induced gravitational waves are

$$\Omega_{\text{GW}}^{\text{induced}} h^2 \sim \frac{1}{12} \Omega_{r,0} h^2 \mathcal{P}_{\mathcal{R}}^2 \sim 10^{-6} \mathcal{P}_{\mathcal{R}}^2. \quad (216)$$

In vanilla cosmology, the scalar power spectrum after inflation can be inferred from CMB extrapolation $\mathcal{P}_{\mathcal{R}} \sim 10^{-9}$ [470] which means that absent any enhancement, $\Omega_{\text{GW}}^{\text{induced}} h^2 \sim 10^{-24}$, which is far too small for any detector in the foreseeable future. The enhancement can occur during a period of ultra-slow roll inflation, or due to the evolution of scalar perturbations after inflation [471]. For example, a sudden change in the equation of state can dramatically enhance the gravitational wave spectrum [472–475]. Scalar-induced gravitational waves have a remarkable range of applications. For instance, if there exists an instability scale as hinted at in the Standard Model [476–488], there should be a scalar induced gravitational wave spectrum [489]. As the running of the Higgs quartic self-interaction could be affected by any number of hypothetical particles in the mass range between the weak scale and the instability scale, gravitational wave detectors may be the only way to tell if the electroweak vacuum is stable. Further, if the Baryon asymmetry was produced during the Affleck Dine mechanism, there was likely a period of Q-ball domination whose sudden decay results in a gravitational wave spectrum, one of the few ways to test this paradigm [490]. Finally, if one produces primordial Black holes that are too small to survive after Big Bang nucleosynthesis before evaporating via Hawking radiation, these black holes can dominate the Universe and their decay rate is again surface-to-volume suppressed which results in a sudden transition from matter to radiation [491]. We summarize the range of applications in section [VE](#) in slightly more depth. For now, we emphasize the extraordinary promise of this source of gravitational waves.

In this section, we review the current formalism and our understanding of both causes of scalar-induced gravitational waves and present some recent applications.

A. Enhanced scalar power spectrum during inflation

When large scalar perturbations reenter the horizon after inflation they can produce a detectable source of gravitational waves [492–494] (for a review, see [471]). Consider the slow roll parameters for a scalar field in an expanding background

$$\epsilon = -\frac{\dot{H}}{H}, \epsilon_2 = \frac{2\ddot{\phi}}{H\dot{\phi}} + 2\epsilon. \quad (217)$$

The slow roll conditions are of course that the above parameters are small. However, near an inflection point when $V' \rightarrow 0$, the Klein Gordon equation in an expanding background yields $\ddot{\phi} = -3H\dot{\phi}$ and we have

$$\epsilon_2 = -6 + 2\epsilon \rightarrow |\epsilon_2| \gg 1. \quad (218)$$

So we have the surprising result that on the one hand, the slow roll (SR) approximation assumes that the potential is flat, but if it is too flat the approximation breaks down. In this “ultra slow roll” (USR) regime the potential barely affects the evolution and the number of e-folds contrasts with slow roll as follows

$$\Delta N = \begin{cases} \frac{1}{m_{\text{pl}}} \int_{\phi_1}^{\phi_2} \frac{d\phi}{2\epsilon} & \text{SR} \\ -\int \frac{dH}{\epsilon H} & \text{USR} \end{cases} \quad (219)$$

and the scalar power spectrum grows exponentially for modes near the Hubble scale during the period of USR, $\mathcal{P}_{\mathcal{R}} \sim e^{6\Delta N}$. To calculate the scalar power spectrum accurately during ultra-slow roll inflation, one needs to solve the equations of motion of the inflaton potential. Writing this equation at second order in perturbations and transforming to Fourier space yields the Mukhanov-Sasaki equations [495, 496]

$$\frac{d^2 u_k}{d\eta^2} + \left(k^2 - \frac{1}{z} \frac{d^2 z}{d\eta^2} \right) u_k = 0 \quad (220)$$

where $u = -z\mathcal{R}$ and $z = \frac{1}{H} \frac{d\phi}{d\eta}$. If the second term in brackets dominates, we have an exponentially growing mode. It is clear that this is achieved when $\dot{\phi}$ is small, that is the ultra-slow roll regime. With the possibility of such large fluctuations, it is worth noting that if the fluctuations are large enough, one might not only induce gravitational waves at second order, but primordial black holes [497–500] which themselves can leave a gravitational wave signal [501–503]. This means that if one sees PBHs, one can see the corresponding

primordial GW background. In particular, the scalar power spectrum can be enhanced if there is a period where the scalar field is near an inflection point. In this review we focus on cosmological sources of gravitational waves, so will only make brief comments about PBHs through this mechanism. PBHs are formed when $\delta\rho/\rho \gtrsim \delta_c$. Fluctuations during inflation follow a Gaussian distribution around zero, so the support for a large enough fluctuation is negligible in vanilla inflation unless there is an enhancement in the scalar power spectrum. One typically needs $\mathcal{P}_{\mathcal{R}} \gtrsim 10^{-2}$ to have a substantial abundance of pbhs, implying $\Omega_{\text{GW}}h^2 \gtrsim 10^{-10}$ which is expected to be detectable. Conversely, the absence of such an observable gravitational wave spectrum can rule out the production of PBHs through inflation. There is a debate about whether this is achievable during single-field inflation and one might need a multifield inflation model to realize this mechanism [504–508].

B. Models of scalar induced gravitational waves

The precise shape of the scalar power spectrum, and therefore the gravitational wave spectrum, will depend upon the specifics of the potential. So in principle, this leads to a wide range of possible signal shapes to search for. Fortunately, there are several ways to parametrize categories of power spectra. Common categories are delta function spectra, log normal spectral, and a broken power law. Let us begin with the delta function case. A sharply peaked, almost monochromatic spectra appear to be only possible in multifield inflation,[509–517] (to see a discussion of this cannot be achieved during single field inflation, see [518–520]). In such a case we can parametrize the curvature perturbation power spectrum as follows,

$$\mathcal{P}_{\mathcal{R}} = \mathcal{A}_{\mathcal{R}}\delta(\ln(k/k_p)) \quad (221)$$

where k_p is the typical scale at which scalar fluctuations are occurring and $\mathcal{A}_{\mathcal{R}}$ is the amplitude of the fluctuations. The resulting GW spectrum for instantaneous reheating occurring at time τ_{rh} and $k_{\text{rh}} = \mathcal{H}_{\text{rh}}$ is,

$$\Omega_{\text{GW,rh}}(k) = \frac{2}{3} \left(\frac{k_p}{k_{\text{rh}}} \right)^2 \left(1 - \frac{k}{4k_p^2} \right)^2 I_{\text{RD}}(k/k_{\text{rh}}, k/k_p)\Theta(2k_p - k) . \quad (222)$$

More generally, one can model a finite width with a log normal peak,

$$\mathcal{P}_{\mathcal{R}} = \frac{\mathcal{A}_{\mathcal{R}}}{\sqrt{2\pi}\Delta} \exp \left[-\frac{\ln^2(k/k_p)}{2\Delta^2} \right] . \quad (223)$$

For example, refs [509–517, 521] considered narrow peaks and for broad peaks see refs. [511, 522–527]. In this case the gravitational wave spectrum has the form

$$\Omega_{\text{GW},\Delta}(k) = \text{erf}\left(\frac{1}{\Delta} \sinh^{-1} \frac{k}{2k_p}\right) \frac{2}{3} \left(\frac{k_p}{k_{\text{rh}}}\right)^2 \left(1 - \frac{k}{4k_p^2}\right)^2 I_{\text{RD}}(k/k_{\text{rh}}^-, k/k_p) \Theta(2k_p - k) \quad (224)$$

Finally, in the case of single field inflation [518–520, 528], we have more predictability and the power spectrum can be described by a broken power law

$$\mathcal{P}_{\text{calR}} = \mathcal{A}_{\mathcal{R}} \begin{cases} \left(\frac{k}{k_p}\right)^{n_{\text{IR}}} & k \leq k_p \\ \left(\frac{k}{k_p}\right)^{-n_{\text{UV}}} & k \geq k_p \end{cases} \quad (225)$$

with a resulting gravitational wave spectrum [529–533],

$$\Omega_{\text{GW,rh}}(k \ll k_p) \sim 12\mathcal{A}_{\mathcal{R}}^2 \left(\frac{1}{2n_{\text{IR}} - 3} + \frac{1}{2n_{\text{UV}} + 3}\right) \left(\frac{k}{k_p}\right)^2 \ln^2\left(\frac{k}{k_p}\right) \quad (226)$$

$$\Omega_{\text{GW,rh}}(k \gg k_p, n_{\text{UV}} < 4) \sim \frac{1}{12}\mathcal{A}_{\mathcal{R}}^2 \left(41 + \frac{16n_{\text{UV}}}{\sqrt{16 - n_{\text{UV}}^2}}\right) \left(\frac{k}{k_p}\right)^{-2n_{\text{UV}}} \quad (227)$$

Clearly, in all cases, we require the amplitude to be much larger than the CMB extrapolation, $A_s \gg 10^{-9}$ as occurs in vanilla inflation where the slow roll conditions never become invalid due to a period of ultra slow roll. The gravitational wave spectra of all three types of sources we show in Fig. 22 with the benchmarks taken from ref [471].

C. Sudden changes in the equation of state

Even if the curvature power spectrum is no larger than the CMB extrapolation, if there is an early period of matter domination that suddenly decays faster than the Hubble time one can induce a sizeable gravitational wave spectrum. During matter domination, the scalar perturbations grow and if the transition to radiation is faster than a Hubble time, there is a resonant enhancement of the induced gravitational waves which can result in a striking sharp gravitational wave spectrum [475]. Let us consider the scenario where there was an early period of matter domination which suddenly ends when $\eta = \eta_R$.¹³

The power spectrum of tensor modes sourced by curvature perturbations is given by,

$$\overline{\mathcal{P}(\eta, k)} = 4 \int_0^\infty dv \int_{|1-v|}^{1+v} du \left(\frac{4v^2 - (1 + v^2 - u^2)^2}{4vu}\right)^2 \overline{I^2(u, v, k, \eta, \eta_R)} \mathcal{P}_\zeta(uk) \mathcal{P}_\zeta(vk) \quad (228)$$

¹³ For the gravitational wave signal involving a transition from/to kination see ref. [534]

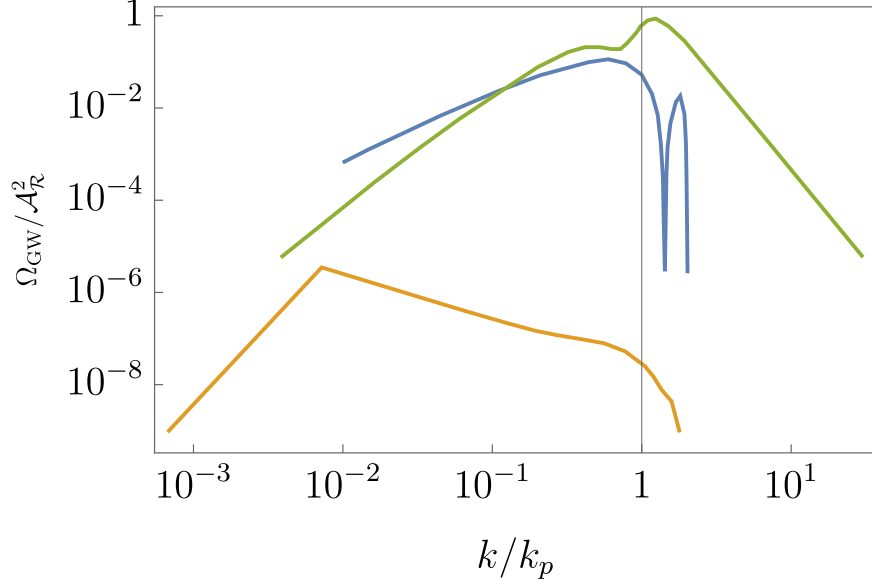


FIG. 22. Gravitational wave spectrum from induced gravitational waves from benchmarks involving a Dirac delta function power spectrum and a speed of sound near unity (blue curve) a Gaussian power spectrum (yellow) and a broken power law spectrum (Green). Data taken from ref. [471] and the references therein.

where the power spectrum of curvature perturbations is given by

$$\mathcal{P}_\zeta(k) = \Theta(k_{\text{max}} - k) A_s \left(\frac{k}{k_*} \right)^{n_s - 1} \quad (229)$$

with $A_s = 2.1 \times 10^{-9}$ the amplitude of the pivot scale, $n_s = 0.97$ is the spectral tilt, $k_* = 0.05 \text{Mpc}^{-1}$ the pivot scale where all of these values we take from ref. [10]. As the scalar perturbations grow during matter domination, we eventually enter a regime where it is no longer valid to consider linear perturbations. This occurs when $k_{\text{max}} \leq 470/\eta_r$ and there is no accessible way to calculate the spectrum in this case. A recent simulation seemed to show that the gravitational wave spectrum continues to grow as on enters the non-linear regime [535]. The I function in the above describes the time dependence of the gravitational waves and is the convolution of the appropriate greens function⁻¹ and a source function, f ,

$$I(u, v, k, \eta, \eta_R) = \int_0^x d\bar{x} \frac{a(\bar{\eta})}{a(\eta)} k G_k(\eta, \bar{\eta}) f(u, v, \bar{x}, x_R) \quad (230)$$

with $(x, x_R) = (k\eta, k\eta_R)$ and the source function is given by the expression

$$f(u, v, \bar{x}, x_R) =$$

$$\frac{3(2(5 + 3w)\Phi(u\bar{x})\Phi(v\bar{x}) + 4\mathcal{H}^{-1}(\Phi'(u\bar{x})\Phi(v\bar{x}) + \Phi(u\bar{x})\Phi'(v\bar{x})) + 4\mathcal{H}^{-2}\Phi'(u\bar{x})\Phi'(v\bar{x}))}{25(1 + w)} \quad (231)$$

Here, Φ is the transfer function of the gravitational potential. The Green functions for radiation and matter domination have different functional forms, so it is convenient to split Eq. 230,

$$I(u, v, k, \eta, \eta_R) = \int_0^{x_r} d\bar{x} \frac{1}{2(x/x_r) - 1} \left(\frac{\bar{x}}{x_r}\right)^2 k G_k^{\text{MD}}(\eta, \bar{\eta}) f(u, v, \bar{x}, x_r) + \int_{x_r}^x \bar{x} \left(\frac{2(\bar{x}/x_r) - 1}{2(x/x_r) - 1}\right) k G_k^{\text{RD}}(\eta, \bar{\eta}) f(u, v, \bar{x}, x_r) \quad (232)$$

$$= I_{\text{MD}}(u, v, x, x_R) + I_{\text{RD}}(u, v, x, x_R) . \quad (233)$$

As the power spectrum involves the square of the above, the scalar-induced gravitational waves will involve a radiation term, a matter term, and a cross term,

$$\Omega_{\text{GW}} = \Omega_{\text{RD}} + \Omega_{\text{MD}} + \Omega_{\text{cross}} . \quad (234)$$

The cross term is negative definite and vanishes when the transition is instantaneous. So the faster the transition, the stronger the gravitational waves. For a sudden transition, the gravitational wave spectrum we expect has the approximate form,

$$\frac{\Omega_{\text{GW}}(\eta_c, k)}{A_s^2} \sim \begin{cases} 0.8 & (x_R \lesssim 150x_{\text{max,R}}^{-5/3}) \\ 3 \times 10^{-7} x_R^3 x_{\text{max,R}}^5 & (150x_{\text{max,R}}^{-5/3} \lesssim x_R \ll 1) \\ 1 \times 10^{-6} X_R x_{\text{max,R}}^5 & (1 \ll x_R \lesssim x_{\text{max,R}}^{5/6}) \\ 7 \times 10^{-7} x_R^7 & (x_{\text{max,R}} \lesssim x_R \lesssim x_{\text{max,R}}) \\ \text{sharpdrop} & (x_{\text{max,R}} \lesssim X_R \leq 2x_{\text{max,R}}) \end{cases} \quad (235)$$

This approach of course assumes an instantaneous transition from matter to radiation, and that the period of matter domination did not last so long that it is no longer valid to make use of linear perturbations. One might naturally ask what happens to the signal if these two assumptions break down. This question is only just being probed by the community, nonetheless, let us briefly make some qualitative remarks based on some recent work. First, if one enters the non-linear regime, the peak of the gravitational wave spectrum does not grow as quickly with respect to the duration of the matter domination. Further, the resonance

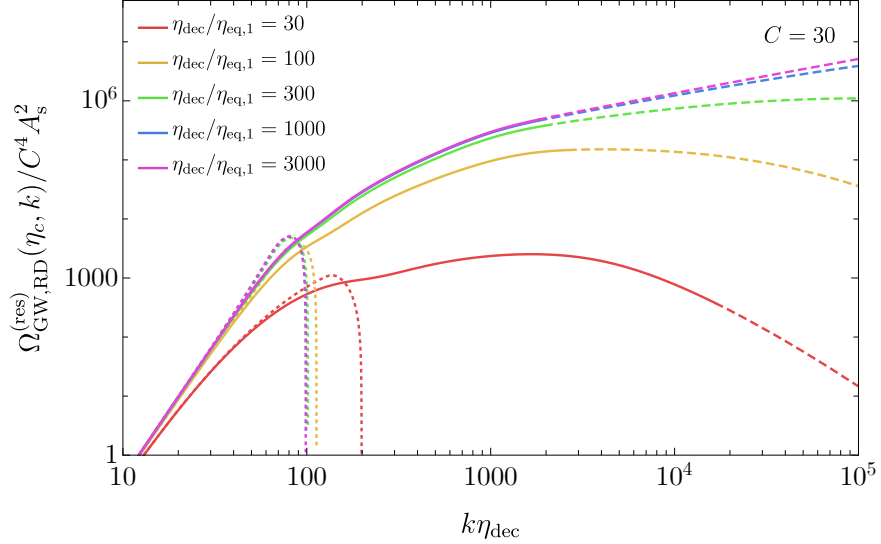


FIG. 23. Shape of the gravitational wave spectrum for periods of matter domination that last so long as to render linear perturbations inadequate. The dotted line is the component of the spectrum arising from the linear regime, the solid from the non-linear regime, and the dashed line refers to a period where the calculations in the figure are inaccurate. Figure taken from ref. [535] with parameter C explained within

flattens out considerably, see Fig. 23. When the timescale of transition is in between the limits of instantaneous and Hubble time, the signal flattens out and the peak becomes smaller as seen in 24. Such a smooth interpolation between the signals predicted in the instantaneous and gradual limits lends hope to the possibility that one can distinguish between differing scenarios that result in an early period of matter domination.

D. Gauge invariance

Early work found that the predictions of second-order gravitational waves can vary by orders of magnitude due to an unphysical gauge dependence [537]. The issue is that tensor modes are gauge-independent, so if we define

$$\rho_{\text{GW}} \sim \langle h'^{ij} h'_{ij} \rangle \quad (236)$$

and perform a gauge transformation

$$x^\mu \rightarrow x^\mu - \xi^\mu, \quad \text{where } \xi^\mu = (T, \partial^i L) \quad (237)$$

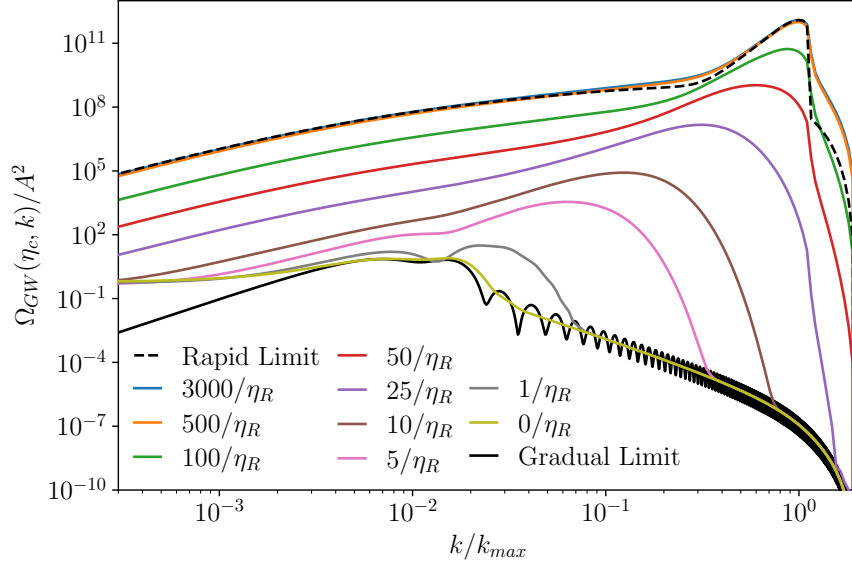


FIG. 24. Shape of scalar induced gravitational wave spectra as a function of how rapidly the matter disappears. Figure taken from ref [536]

one gets a gauge dependence in our prediction of the gravitational wave spectrum,

$$\rho_{\text{GW}} \rightarrow \rho_{\text{GW}} + \langle \partial_i T \partial_j T \partial^i T \partial^j T \rangle . \quad (238)$$

There is no obvious way to remove the spurious gauge dependence by choosing a gauge invariant variable, as it is not clear which gauge invariant variables should go in the above equation to correspond to the real gravitational wave a detector would observe. As yet the issue is unsolved, yet a partial solution discussed in [538–542]. One finds in a Universe with a fixed equation of state and a non-zero speed of sound, the Newtonian gauge and synchronous gauge yield the same predictions for gravitational waves. In general, there are a class of gauges that yield the same results under a set of conditions [543]

- 1 We consider only sub-horizon scales
- 2 tensor modes can be approximated as freely propagating
- 3 The gauge we use is suitable for small distance calculations.

The second condition is essentially insisting that we calculate the gravitational wave energy density after the source has become negligible. If such conditions are satisfied then the correction to the tensor mode from a gauge transformation is suppressed by a factor H^2/k^2

and the gravitational wave spectrum is roughly gauge invariant. As yet, a more satisfying and complete answer remains elusive and is one of the challenges facing the field.

E. Applications of scalar induced gravitational waves

Let us conclude this section by sampling the range of applications scalar-induced gravitational waves have. We will begin with one of the most striking applications of scalar-induced gravitational waves - that it may be possible to discern whether the Higgs vacuum is absolutely stable [544]. During inflation, so long as the Higgs mass is less than Hubble, its vacuum expectation value will randomly walk with kicks of $\pm O(H/2\pi)$ until the Higgs field ends up in the catastrophic vacuum. The classical motion of the Higgs begins to dominate and the Higgs rapidly descends into the abyss. At the end of inflation, the Higgs potential obtains thermal corrections to its potential which can shift the catastrophic vacuum to begin at a larger field value [24] and the Higgs may harmlessly oscillate around its minimum with an amplitude that decays as the Universe expands. The situation is slightly different from the ultra-slow roll scenario as the Higgs is a spectator field during inflation. Nonetheless, the motion of the Higgs field at the end of inflation causes curvature perturbations

$$\mathcal{P}_\zeta(t_{\text{dec}}) = \frac{\rho_h^2(t_{\text{dec}})}{\rho_{\text{tot}}^2 4} \left(\frac{H}{2\pi} \right)^2 \left(\frac{\dot{h}_c(t_e)}{h_c(t_e) \dot{h}_c(t_k)} \right)^2 \quad (239)$$

where t_{dec} is the time at the end of inflation. The shape of the resulting gravitational wave spectrum is highly sensitive to the precise instability scale.

Another application is the so-called poltergeist mechanism [491] (see also [545–552]). Black holes below a threshold mass of 10^9g evaporate before the onset of Big Bang nucleosynthesis. However, they can dominate the energy budget of the Universe as their density dilutes like matter rather than radiation. When they evaporate, it is only through Hawking radiation at the event Horizon. This means the evaporation rate is surface-to-volume suppressed and accelerates once the rate of mass loss is comparable to the expansion of the Universe. This is precisely the conditions needed to create scalar-induced gravitational waves. Such light, evaporating black holes could partly explain the Hubble tension [553–555], be crucial in the explanation for why there is more matter than anti-matter [556–566] or generate dark matter particles [565, 567–570]. The poltergeist mechanism can also be used to probe high-scale supersymmetry, as the flat directions in SUSY tend to fragment

into Q-balls which, for much of the parameter space relevant to high-scale SUSY, merge and collapse into primordial black holes that are light enough to create a signal [571]

Q-balls are another source of early matter domination [572]. One of the core paradigms for explaining why there is more matter than anti-matter relies on the existence of flat directions during Supersymmetry having a non-zero lepton or baryon number. Such directions fragment into Q-balls with a finite baryon or lepton charge. Much like primordial black holes, the Q-balls can only decay at the surface of the soliton leading to a surface-to-volume suppression. The rate of decay is slightly different from primordial black holes which means that there is hope in distinguishing the signals. Recent work found that the mechanism generally resulted in a visible scalar-induced gravitational wave spectrum [490].

VI. OTHER SIGNIFICANT SOURCES

In this review, we have focused on three types of gravitational wave sources that we see as the most promising as well as the most relevant to next-generation gravitational wave detectors, predicting signals in the nanoHz to kHz frequency band. There are many other sources, some of which are too significant to omit, though we neglect a full section on them because the likely signal is high frequency or there has been little recent progress. For the sake of brevity, we regret that we do not cover some of the more exotic sources in the literature including oscillons [573–589], brane worlds [590–593] and pre-big bang cosmology [594–596]. We refer the reader to these references for more information. However, in this section, we cover the case of blue-tilted gravitational wave spectra from inflation, gravitational waves as a Big Bang thermometer - perhaps the only measure of the reheating temperature, and gravitational waves from (p)reheating.

A. Inflation

It is well known that gravitational waves arising from inflation result in B modes in the CMB [597–601]. For single-field inflation, the actual signal from the CMB peaks at an ultralow frequency, many orders of magnitude below what even pulsar timing arrays are sensitive to. Worse, the spectrum of tensor modes predicted by single field inflation is red-tilted, meaning that excluding probes of the CMB, the prediction of the amplitude of a SGWB is formidably small in the frequency range relevant to next-generation experiments. However, in multifield inflation, it is possible to have a blue-tilted spectrum. The usual notation is to denote the tensor spectral index as n_t and the scalar-tensor ratio as r , in which case we can write the gravitational wave spectrum in the case of a constant spectral tilt as a simple power law,

$$\Omega_{\text{GW}}(f) = 2.1 \times 10^{-6} g_*(f) \left(\frac{g_{*,s}^0}{g_{*,s}(f)} \right)^{4/3} r A_s \left(\frac{f}{f_{\text{cmb}}} \right)^{n_t} \mathcal{T}(f) . \quad (240)$$

where $g_{*,s}^0 = 3.93$ is the number of effective relativistic degrees of freedom today, $g_*(f), g_{*,s}(f)$ is the number of relativistic degrees of freedom when mode $k = 2\pi f$ re-entered the horizon, $A_s = 2.1 \times 10^{-9}$ [10] is the amplitude of the scalar power spectrum and \mathcal{T} is a transfer

function connecting reheating to radiation domination [602]

$$\mathcal{T}(f) \sim \frac{\Theta(f_{\text{end}} - f)}{1 - 0.22(f/r_{\text{rh}})^{3/2} + 0.64(f/f_{\text{rh}})^2}. \quad (241)$$

The high-frequency cutoff of the gravitational wave spectrum, which marks the end of inflation is set by the reheating temperature and the Hubble rate at the end of inflation,

$$f_{\text{end}} = \frac{1}{2\pi} \left(\frac{g_{*,s}^0}{g_{*,s}^{\text{rh}}} \right)^{1/3} \left(\frac{\pi^2 g_*^{\text{rh}}}{90} \right)^{1/3} \frac{T_{\text{rh}}^{1/3} H_{\text{end}}^{1/3} T_0}{M_p^{2/3}} \quad (242)$$

with $T_0 = 2.73K$ today's CMB temperature. Naively, it is not easy to generate a positive value of n_t , as in single field inflation at lowest order in slow-roll parameters, one finds a negative tilt $n_T = -2\epsilon$ [603]. However, in axion vector inflation [604–608], massive gravity [609] and other non-minimal scenarios [609–613] it is possible to have a blue tilted spectrum.

B. (p)reheating

Khlebnikov and Tkachev first pointed out the production of GW during the era of reheating [614]. Since reheating is an outcome of all the inflationary scenarios, a GW generated during this period carries all the information of the inflationary period together with the reheating era. This is because they remain decoupled after they are produced and hence can act as a probe of the interaction strength between the inflation and the other fields. See [615] and the references therein for the details.

Once the inflation has ended, the inflaton field oscillates around its minimum to produce the elementary particles that interact among themselves to reach thermal equilibrium. In scenarios like chaotic inflation [616–618], if these oscillations are huge and coherent, the particles can be produced rapidly through resonant enhancement and the mechanism is popularly known as the parametric resonance [619–621]. During this phase, the amplitudes of the inflaton field grow exponentially and the growth rate is dominated by the Mathieu characteristic exponent. This stage of rapid particle production is known as *preheating*. Here the particles produced are not in equilibrium and another phase is needed to thermalize the radiation. On the other hand, in the case of hybrid inflation [622] one can have a different kind of preheating known as *tachyonic preheating* [622, 623]. Here, the secondary field (waterfall field) descends from the maxima of its potential and oscillates around its minimum. In principle, around the maxima of the potential, there might exist a region where

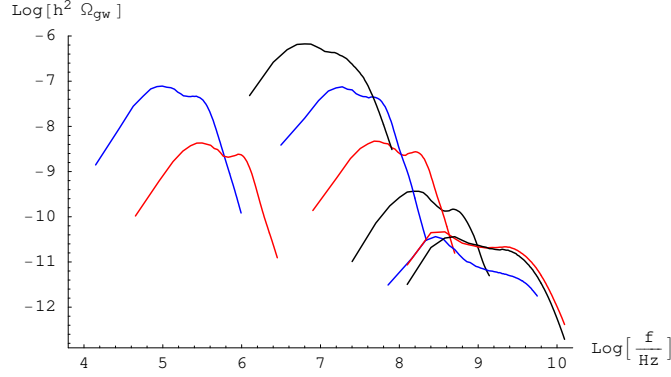


FIG. 25. GW spectra from numerical simulations generated after hybrid inflation. The figure is taken from [624].

the quadratic mass of the field turns negative and the field fluctuations grow exponentially. Chaotic inflation and hybrid inflation are the most studied inflationary scenarios in which GW production during the following preheating phase has been investigated. The process of production of GWs in both scenarios is almost the same. Here, the GW production is sourced from inhomogeneities that cannot be neglected as they act as a source term in the GW equation of motion. These inhomogeneities in the energy density of the Universe are produced as a result of the highly pumped modes (large oscillations of the fields) during this phase.

Including the rate of expansion of the Universe between the time of emission and the present time, the GW that we see today is rescaled as [625],

$$\Omega_{\text{GW}} h^2 = \frac{S_k(\tau_f)}{a_j^4 \rho_j} \left(\frac{a_j}{a_*} \right)^{1-3w} \left(\frac{g_*}{g_0} \right)^{-1/3} \Omega_{\text{rad}} h^2, \quad (243)$$

where $\Omega_{\text{rad}} h^2 = 4.3 \times 10^{-5}$ and ρ_j is the total energy-density at $t = t_j$. While τ_f denotes the time when the GW source becomes negligible, S_k carries the information about the amount of GW produced at the time the source was present. The frequency evaluated today is,

$$f \equiv \frac{k}{a_j \rho_j^{1/4}} \left(\frac{a_j}{a_*} \right)^{1-\frac{3}{4}(1+w)} 4 \times 10^{10} \text{ Hz}, \quad (244)$$

where k is the comoving wave number of a given fluctuation.

For preheating following chaotic inflation or hybrid inflation, the mean value of w in the intermediate stage reaches $w = 1/3$ soon after the end of inflation [625, 626], so that the

factor $(a_j/a_*)^{1-3w}$ can be neglected. In this case the previous relations read

$$f = \frac{k}{a_j \rho_j^{1/4}} 4 \times 10^{10} \text{ Hz} \quad \text{and} \quad \Omega_{\text{GW}} h^2 = \frac{S_k(\tau_f)}{a_j^4 \rho_j} 9.3 \times 10^{-6}. \quad (245)$$

Fig. 25 shows the variation of GW spectrum with frequency for the case of hybrid inflation. As can be seen from Fig. 25, the GW spectra generated during the preheating are mostly blue-tilted and lies beyond the accessible range of the present and future detectors. At this stage, we would like to point out that in recent times it was shown that one can get GW signals during the preheating era that lies within the sensitivity of some present and future GW experiments. We will not delve into the details of these scenarios but we refer readers to [627, 628] and the references therein for details.

C. Graviton production as a big bang thermometer

Production of SGWB by thermal plasma is guaranteed in the early Universe. The energy density of this SGWB scales with the maximum temperature T_{max} of the plasma attained at the initial time of the Big Bang era, then peaks in the microwave range. The standard hot Big Bang cosmology gives a very good description of the Universe when the SM bath was radiation-dominated and the Universe's temperature was around a few MeV [629–632]. Unfortunately, it fails to predict the temperature of the bath before the radiation-dominated era and hence the temperature before this era could be arbitrarily large. However, one can provide an upper bound on this maximum temperature from the Planck scale *i.e.* $T_{\text{max}} \lesssim M_P$ [633]. For a temperature higher than this bound the quantum gravity effect cannot be ignored. In the regime where $T_{\text{max}} > M_P$, the gravitons reach thermal equilibrium and attain a black body spectrum that would decouple around $T_{\text{dec}} \simeq M_P$ [340]¹⁴ and thereafter, the black body spectrum redshifts with the expansion of the Universe. The prediction for the relative abundance of gravitational waves in this scenario is that of a blackbody spectrum with an effective temperature obtained by redshifting the decoupling temperature M_P by the expansion of the universe between the decoupling time and the present [340]. This follows simply from noting that after decoupling, gravitons would stop interacting and start to propagate freely, with their momenta redshifting due to the expansion and hence [90]

$$\Omega_{\text{Eq.}}(f) = \frac{16\pi^2}{3M_P^2 H_0^2} \frac{f^4}{e^{2\pi f/T_{\text{grav}}} - 1}, T_{\text{grav}} = \frac{a(T = M_P)}{a(T = T_0)} M_P = \left(\frac{g_{*s}(\text{fin})}{g_{*s}(M_P)} \right)^{1/3} T_0. \quad (246)$$

¹⁴ If there is a SM instability scale, the T_{max} is around GUT scale [24]

where $g_{*s}(\text{fin}) = 3.931 \pm 0.004$ [634] is the number of effective degrees of freedom of the entropy density after neutrino decoupling. Here, T_0 is the current CMB temperature, and for the equilibrated spectrum with the peak frequency,

$$f_{\text{peak}}^{\Omega} \approx \frac{3.92}{2\pi} \left[\frac{g_{*s}(\text{fin})}{g_{*s}(M_P)} \right]^{1/3} T_0 \simeq 74 \text{ GHz} \left[\frac{g_{*s}(M_P)}{106.75} \right]^{-1/3}. \quad (247)$$

On the other hand, for $T_{\text{max}} < M_P$, when the Planck suppressed gravitational interaction rates are slower than the expansion rate of the Universe the gravitons are not expected to thermalize. Even in this scenario, the out-of-equilibrium gravitational excitations can still be generated from the thermal plasma, and T_{max} can be probed by the GW with the redshifted GW spectrum given as [90],

$$\begin{aligned} h^2 \Omega(f) &\approx \frac{1440\sqrt{10}}{2\pi^2} h^2 \Omega_{\gamma} \frac{[g_{*s}(\text{fin})]^{1/3}}{[g_{*s}(T_{\text{max}})]^{5/6}} \frac{f^3}{T_0^3} \frac{T_{\text{max}}}{M_P} \hat{\eta} \left(T_{\text{max}}, 2\pi \left[\frac{g_{*s}(T_{\text{max}})}{g_{*s}(\text{fin})} \right]^{1/3} \frac{f}{T_0} \right) \\ &= 4.03 \times 10^{-12} \left[\frac{T_{\text{max}}}{M_P} \right] \left[\frac{g_{*s}(T_{\text{max}})}{106.75} \right]^{-5/6} \left[\frac{f}{\text{GHz}} \right]^3 \hat{\eta} \left(T_{\text{max}}, 2\pi \left[\frac{g_{*s}(T_{\text{max}})}{g_{*s}(\text{fin})} \right]^{1/3} \frac{f}{T_0} \right). \end{aligned} \quad (248)$$

with peak frequency,

$$f_{\text{peak}}^{\Omega} \approx \frac{3.92}{2\pi} \left[\frac{g_{*s}(\text{fin})}{g_{*s}(T_{\text{max}})} \right]^{1/3} T_0 \simeq 74 \text{ GHz} \left[\frac{g_{*s}(T_{\text{max}})}{106.75} \right]^{-1/3}, \quad (249)$$

$\Omega_{\gamma} \equiv 2.4728(21) \times 10^{-5}/h^2$ the present fractional energy density of the CMB photons, with temperature $T_0 = 2.72548(57)$ K and f being the present day GW frequency. Finally, $\hat{\eta}$ is a dimensionless source term the details of which can be found in [90]. As seen from Eq. 248, the amplitude scales approximately linearly with T_{max} and hence can play the role of a hot Big Bang thermometer. Considering the broken power law and using Eq. 248 and Eq. 249, one can plot the variation of the GW spectra with the frequency for different values T_{max} as shown in Fig. 26 and as expected a larger T_{max} corresponds to a larger amplitude of the GW spectrum. It is interesting to point out that, up to the factor $\left[\frac{g_{*s}(\text{fin})}{g_{*s}(T_{\text{max}})} \right]^{1/3}$, the peak frequency coincides with the CMB peak frequency,

$$f_{\text{peak}}^{\Omega_{\text{CMB}}} \simeq \frac{3.92}{2\pi} T_0 \simeq 223 \text{ GHz}, \quad (250)$$

of the present energy fraction of the CMB per logarithmic frequency,

$$\Omega_{\text{CMB}}(f) = \frac{16 \pi^2}{3H_0^2 M_P^2} \frac{f^4}{e^{2\pi f/T_0} - 1}. \quad (251)$$

As can be seen, these high-frequency GW spectra remain out of reach of the current and future GW experiments.

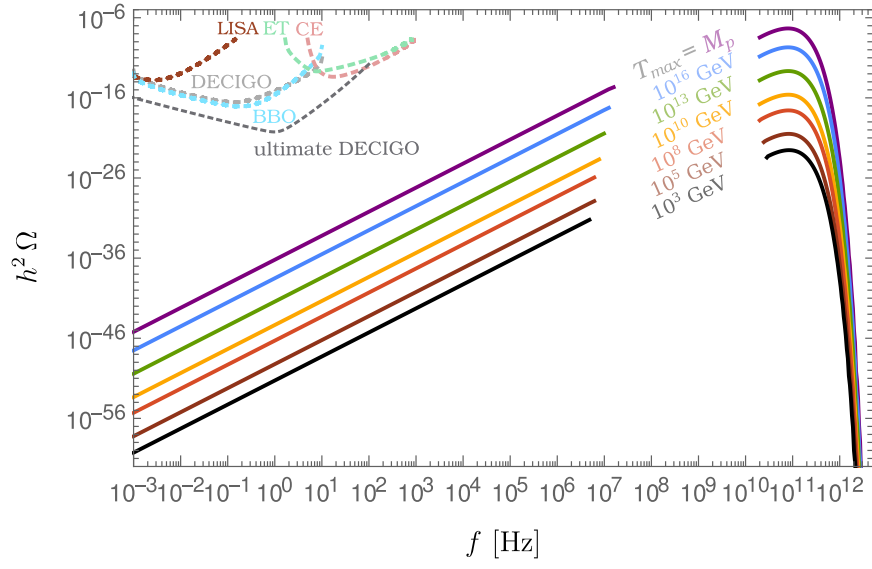


FIG. 26. Shape of gravitational wave spectra generated from the primordial thermal plasma for different values of maximum temperature T_{\max} . Figure is taken from ref [90]

VII. CONCLUSIONS

Gravitational wave cosmology is one of the most promising avenues for discovering physics beyond the Standard Model. Next-generation detectors promise to have cosmologically significant strain sensitivities over 12 decades of frequencies - from the nanoHz to the kHz. In section II we outlined three major strategies for gravitational wave detection - pulsar timing arrays, astrometry, and of course interferometry both terrestrial and in space.

In sections III-V we covered three very active subfields in gravitational cosmology which cover, in this review's opinion, the three major sources that next-generation detectors will be sensitive to. First-order cosmic phase transitions can produce a source from the collision of bubbles, the explosion of sound, and the aftermath of turbulence. We surveyed the many possible scenarios that can produce a cosmological phase transition, though the electroweak phase transition continues to inspire the most interest. This source is arguably the most difficult to understand as it requires taming of finite temperature perturbation theory and understanding how the behaviour of bubbles and sound shells translates to precise predictions of spectra. So far, the community requires simulations to shed light on both issues and the theory is still maturing.

We covered an array of topological defects including hybrid defects in section IV. The string signals are expected to grow with the scale of spontaneous symmetry breaking, as is the case of textures. Domain walls by contrast have a peak frequency and strength that is determined not just by the surface tension, but the lifetimes of the walls. In all three cases, there can be a detectable signal arising from physics at scales many orders of magnitude higher than what can be reached at the LHC. Successive symmetry-breaking steps can result in hybrid defects, with each possible combination having its own unique gravitational wave signature, indicating the possibility of learning about a potentially rich cosmic history. The most severe source of theoretical uncertainty is undoubtedly the mismatch between field-theoretic and string simulations of cosmic strings. This conflict appears to still be in flux and needs to be resolved. We conclude this section by discussing some of the applications of GW from topological defects.

Finally, in section V we considered scalar-induced gravitational waves. Despite being lumped under the same category, two radically different types of scenarios can result in scalar-induced gravitational waves - a period of ultra-slow roll inflation and a sudden change

in the equation of state. Both sources have a theoretical uncertainty due to gauge invariance and it is hard to rigorously pin down the severity of this issue. There are, however, plausible arguments that we at least qualitatively understand the gravitational wave signal.

In the case of all three signals, there are no known mechanisms under which the Standard Model could provide the conditions needed to generate such a primordial source. So any detection of such a background would be a smoking gun of new physics. Moreover, all three sources potentially can involve physics at a higher scale than we can reach at the LHC. In the case of phase transitions, the frequency is loosely proportional to the scale of the transition, meaning that it is not a probe of very high-scale physics. However, the other two scenarios are less constrained. In the case of strings, the signal is expected to grow with the scale of symmetry breaking, whereas the peak frequency of signals from domain walls and resonantly enhanced scalar-induced gravitational waves corresponds to the lifetime of a macroscopic object. The range of applications to test high-scale physics is already quite broad and we expect it to grow over the next few decades.

There are other sources of gravitational waves, some of which we grouped together in section VI, which we only briefly summarized due to the fact that their detection is loosely connected to next-generation detectors such as inflation,¹⁵ or because the source is high frequency.

The discovery of gravitational waves has provided a method for observing the first moment of creating, where deficiencies in our understanding of what lies beyond the Standard Model matter the most. Gravitational wave cosmology is a new and rapidly growing field that has recently arisen in response to this challenge and opportunity and it feels as though we are just beginning to understand the potential of this field.

¹⁵ We say that is loosely connected rather than unconnected due to the possibility of a blue tilted spectrum

Acknowledgements. We are grateful to David Dunsy and Qaisir Shafi for some useful discussions. GW acknowledges the STFC Consolidated Grant ST/L000296/1 and RR acknowledges financial support from the STFC Consolidated Grant ST/T000775/1.

-
- [1] Albert Einstein. Näherungsweise integration der feldgleichungen der gravitation. *Sitzungsberichte der Königlich Preussischen Akademie der Wissenschaften*, pages 688–696, 1916.
 - [2] Albert Einstein. Über gravitationswellen. *Sitzungsberichte der Königlich Preussischen Akademie der Wissenschaften*, pages 154–167, 1918.
 - [3] Henri Poincaré. *La dynamique de l'électron*. A. Dumas, 1913.
 - [4] Daniel Kennefick. *Traveling at the speed of thought: Einstein and the quest for gravitational waves*. Princeton university press, 2007.
 - [5] Alexander S Blum. Einstein's second-biggest blunder: the mistake in the 1936 gravitational-wave manuscript of albert einstein and nathan rosen. *Archive for History of Exact Sciences*, 76(6):623–632, 2022.
 - [6] Albert Einstein and Nathan Rosen. On gravitational waves. *Journal of the Franklin Institute*, 223(1):43–54, 1937.
 - [7] B. P. Abbott et al. Observation of Gravitational Waves from a Binary Black Hole Merger. *Phys. Rev. Lett.*, 116(6):061102, 2016. doi:10.1103/PhysRevLett.116.061102.
 - [8] Georges Lemaître. The beginning of the world from the point of view of quantum theory. *Nature*, 127(3210):706–706, 1931.
 - [9] Arno A Penzias and Robert W Wilson. A measurement of excess antenna temperature at 4080 mhz. In *A Source Book in Astronomy and Astrophysics, 1900–1975*, pages 873–876. Harvard University Press, 1979.
 - [10] N. Aghanim et al. Planck 2018 results. VI. Cosmological parameters. *Astron. Astrophys.*, 641: A6, 2020. doi:10.1051/0004-6361/201833910. [Erratum: *Astron. Astrophys.* 652, C4 (2021)].
 - [11] Antonio Riotto. Theories of baryogenesis. In *ICTP Summer School in High-Energy Physics and Cosmology*, pages 326–436, 7 1998.
 - [12] Antonio Riotto and Mark Trodden. Recent progress in baryogenesis. *Ann. Rev. Nucl. Part. Sci.*, 49:35–75, 1999. doi:10.1146/annurev.nucl.49.1.35.
 - [13] Michael Dine and Alexander Kusenko. The Origin of the matter - antimatter asymmetry.

- Rev. Mod. Phys.*, 76:1, 2003. doi:10.1103/RevModPhys.76.1.
- [14] James M. Cline. Baryogenesis. In *Les Houches Summer School - Session 86: Particle Physics and Cosmology: The Fabric of Spacetime*, 9 2006.
- [15] Laurent Canetti, Marco Drewes, and Mikhail Shaposhnikov. Matter and Antimatter in the Universe. *New J. Phys.*, 14:095012, 2012. doi:10.1088/1367-2630/14/9/095012.
- [16] David E. Morrissey and Michael J. Ramsey-Musolf. Electroweak baryogenesis. *New J. Phys.*, 14:125003, 2012. doi:10.1088/1367-2630/14/12/125003.
- [17] Csaba Balazs. Baryogenesis: A small review of the big picture. *arXiv preprint arXiv:1411.3398*, 2014.
- [18] Graham Albert White. A Pedagogical Introduction to Electroweak Baryogenesis. 11 2016. doi:10.1088/978-1-6817-4457-5.
- [19] Dietrich Bodeker and Wilfried Buchmuller. Baryogenesis from the weak scale to the grand unification scale. *Rev. Mod. Phys.*, 93(3):035004, 2021. doi:10.1103/RevModPhys.93.035004.
- [20] Richard H Cyburt, Brian D Fields, Keith A Olive, and Tsung-Han Yeh. Big bang nucleosynthesis: Present status. *Reviews of Modern Physics*, 88(1):015004, 2016.
- [21] S. Eidelman et al. Review of particle physics. Particle Data Group. *Phys. Lett. B*, 592(1-4): 1, 2004. doi:10.1016/j.physletb.2004.06.001.
- [22] Eleonora Di Valentino, Olga Mena, Supriya Pan, Luca Visinelli, Weiqiang Yang, Alessandro Melchiorri, David F Mota, Adam G Riess, and Joseph Silk. In the realm of the hubble tension—a review of solutions. *Classical and Quantum Gravity*, 38(15):153001, 2021.
- [23] P. F. de Salas, M. Lattanzi, G. Mangano, G. Miele, S. Pastor, and O. Pisanti. Bounds on very low reheating scenarios after Planck. *Phys. Rev. D*, 92(12):123534, 2015. doi:10.1103/PhysRevD.92.123534.
- [24] Luigi Delle Rose, Carlo Marzo, and Alfredo Urbano. On the fate of the Standard Model at finite temperature. *JHEP*, 05:050, 2016. doi:10.1007/JHEP05(2016)050.
- [25] Lars Bergström. Nonbaryonic dark matter: Observational evidence and detection methods. *Rept. Prog. Phys.*, 63:793, 2000. doi:10.1088/0034-4885/63/5/2r3.
- [26] Gianfranco Bertone, Dan Hooper, and Joseph Silk. Particle dark matter: Evidence, candidates and constraints. *Phys. Rept.*, 405:279–390, 2005. doi:10.1016/j.physrep.2004.08.031.
- [27] Jonathan L. Feng. Dark Matter Candidates from Particle Physics and Methods of Detection. *Ann. Rev. Astron. Astrophys.*, 48:495–545, 2010. doi:10.1146/annurev-astro-082708-101659.

- [28] Katherine Garrett and Gintaras Duda. Dark matter: A primer. *Advances in Astronomy*, 2011:1–22, 2011.
- [29] Annika HG Peter. Dark matter: a brief review. *arXiv preprint arXiv:1201.3942*, 2012.
- [30] Gianfranco Bertone and Dan Hooper. History of dark matter. *Rev. Mod. Phys.*, 90(4):045002, 2018. doi:10.1103/RevModPhys.90.045002.
- [31] Kenath Arun, SB Gudennavar, and Ch Sivaram. Dark matter, dark energy, and alternate models: A review. *Advances in Space Research*, 60(1):166–186, 2017.
- [32] Gianfranco Bertone and Tim MP Tait. A new era in the search for dark matter. *Nature*, 562(7725):51–56, 2018.
- [33] A Arbey and F Mahmoudi. Dark matter and the early universe: a review. *Progress in Particle and Nuclear Physics*, 119:103865, 2021.
- [34] Bruce A Bassett, Shinji Tsujikawa, and David Wands. Inflation dynamics and reheating. *Reviews of Modern Physics*, 78(2):537, 2006.
- [35] Rouzbeh Allahverdi, Robert Brandenberger, Francis-Yan Cyr-Racine, and Anupam Mazumdar. Reheating in Inflationary Cosmology: Theory and Applications. *Ann. Rev. Nucl. Part. Sci.*, 60:27–51, 2010. doi:10.1146/annurev.nucl.012809.104511.
- [36] Rouzbeh Allahverdi, Mustafa A Amin, Asher Berlin, Nicolás Bernal, Christian T Byrnes, M Sten Delos, Adrienne L Erickcek, Miguel Escudero, Daniel G Figueroa, Katherine Freese, et al. The first three seconds: a review of possible expansion histories of the early universe. *arXiv preprint arXiv:2006.16182*, 2020.
- [37] Andrei D Linde. Phase transitions in gauge theories and cosmology. *Reports on Progress in Physics*, 42(3):389, 1979.
- [38] Christophe Grojean and Geraldine Servant. Gravitational waves from phase transitions at the electroweak scale and beyond. *Physical Review D*, 75(4):043507, 2007.
- [39] D Boyanovsky, HJ De Vega, and DJ Schwarz. Phase transitions in the early and present universe. *Annu. Rev. Nucl. Part. Sci.*, 56:441–500, 2006.
- [40] David J Weir. Gravitational waves from a first-order electroweak phase transition: a brief review. *Philosophical Transactions of the Royal Society A: Mathematical, Physical and Engineering Sciences*, 376(2114):20170126, 2018.
- [41] Anupam Mazumdar and Graham White. Review of cosmic phase transitions: their significance and experimental signatures. *Reports on Progress in Physics*, 82(7):076901, 2019.

- [42] Chiara Caprini, Mikael Chala, Glauber C Dorsch, Mark Hindmarsh, Stephan J Huber, Thomas Konstandin, Jonathan Kozaczuk, Germano Nardini, Jose Miguel No, Kari Rummukainen, et al. Detecting gravitational waves from cosmological phase transitions with lisa: an update. *Journal of Cosmology and Astroparticle Physics*, 2020(03):024, 2020.
- [43] J. Aasi et al. Advanced LIGO. *Class. Quant. Grav.*, 32:074001, 2015. doi:10.1088/0264-9381/32/7/074001.
- [44] B. P. Abbott et al. GW150914: The Advanced LIGO Detectors in the Era of First Discoveries. *Phys. Rev. Lett.*, 116(13):131103, 2016. doi:10.1103/PhysRevLett.116.131103.
- [45] Aaron Buikema et al. Sensitivity and performance of the Advanced LIGO detectors in the third observing run. *Phys. Rev. D*, 102(6):062003, 2020. doi:10.1103/PhysRevD.102.062003.
- [46] M. Tse et al. Quantum-Enhanced Advanced LIGO Detectors in the Era of Gravitational-Wave Astronomy. *Phys. Rev. Lett.*, 123(23):231107, 2019. doi:10.1103/PhysRevLett.123.231107.
- [47] F. Acernese et al. Advanced Virgo: a second-generation interferometric gravitational wave detector. *Class. Quant. Grav.*, 32(2):024001, 2015. doi:10.1088/0264-9381/32/2/024001.
- [48] F. Acernese et al. Increasing the Astrophysical Reach of the Advanced Virgo Detector via the Application of Squeezed Vacuum States of Light. *Phys. Rev. Lett.*, 123(23):231108, 2019. doi:10.1103/PhysRevLett.123.231108.
- [49] T. Akutsu et al. KAGRA: 2.5 Generation Interferometric Gravitational Wave Detector. *Nature Astron.*, 3(1):35–40, 2019. doi:10.1038/s41550-018-0658-y.
- [50] Yoichi Aso, Yuta Michimura, Kentaro Somiya, Masaki Ando, Osamu Miyakawa, Takanori Sekiguchi, Daisuke Tatsumi, and Hiroaki Yamamoto. Interferometer design of the KAGRA gravitational wave detector. *Phys. Rev. D*, 88(4):043007, 2013. doi:10.1103/PhysRevD.88.043007.
- [51] David Reitze et al. Cosmic Explorer: The U.S. Contribution to Gravitational-Wave Astronomy beyond LIGO. *Bull. Am. Astron. Soc.*, 51(7):035, 2019.
- [52] Pau Amaro-Seoane et al. Laser Interferometer Space Antenna. 2 2017.
- [53] Alberto Sesana et al. Unveiling the gravitational universe at μ -Hz frequencies. *Exper. Astron.*, 51(3):1333–1383, 2021. doi:10.1007/s10686-021-09709-9.
- [54] Seiji Kawamura. Primordial gravitational wave and DECIGO. *PoS*, KMI2019:019, 2019. doi:10.22323/1.356.0019.

- [55] Nick Kaiser and Andrew H. Jaffe. Bending of light by gravity waves. *Astrophys. J.*, 484: 545–554, 1997. doi:10.1086/304357.
- [56] A. G. A. Brown et al. Gaia Data Release 2: Summary of the contents and survey properties. *Astron. Astrophys.*, 616:A1, 2018. doi:10.1051/0004-6361/201833051.
- [57] Céline Boehm et al. Theia: Faint objects in motion or the new astrometry frontier. 7 2017.
- [58] Laura G. Book and Eanna E. Flanagan. Astrometric Effects of a Stochastic Gravitational Wave Background. *Phys. Rev. D*, 83:024024, 2011. doi:10.1103/PhysRevD.83.024024.
- [59] Christopher J. Moore, Deyan P. Mihaylov, Anthony Lasenby, and Gerard Gilmore. Astrometric Search Method for Individually Resolvable Gravitational Wave Sources with Gaia. *Phys. Rev. Lett.*, 119(26):261102, 2017. doi:10.1103/PhysRevLett.119.261102.
- [60] Deyan P. Mihaylov, Christopher J. Moore, Jonathan R. Gair, Anthony Lasenby, and Gerard Gilmore. Astrometric Effects of Gravitational Wave Backgrounds with non-Einsteinian Polarizations. *Phys. Rev. D*, 97(12):124058, 2018. doi:10.1103/PhysRevD.97.124058.
- [61] Deyan P. Mihaylov, Christopher J. Moore, Jonathan Gair, Anthony Lasenby, and Gerard Gilmore. Astrometric effects of gravitational wave backgrounds with nonluminal propagation speeds. *Phys. Rev. D*, 101(2):024038, 2020. doi:10.1103/PhysRevD.101.024038.
- [62] Juan Garcia-Bellido, Hitoshi Murayama, and Graham White. Exploring the Early Universe with Gaia and THEIA. 4 2021.
- [63] Michael A. Fedderke, Peter W. Graham, and Surjeet Rajendran. Asteroids for μHz gravitational-wave detection. *Phys. Rev. D*, 105(10):103018, 2022. doi:10.1103/PhysRevD.105.103018.
- [64] Mesut Çalışkan, Yifan Chen, Liang Dai, Neha Anil Kumar, Isak Stomberg, and Xiao Xue. Dissecting Stochastic Gravitational Wave Background with Astrometry. 12 2023.
- [65] Sergei A. Klioner. Gaia-like astrometry and gravitational waves. *Class. Quant. Grav.*, 35(4): 045005, 2018. doi:10.1088/1361-6382/aa9f57.
- [66] Yijun Wang, Kris Pardo, Tzu-Ching Chang, and Olivier Doré. Gravitational Wave Detection with Photometric Surveys. *Phys. Rev. D*, 103(8):084007, 2021. doi:10.1103/PhysRevD.103.084007.
- [67] Yijun Wang, Kris Pardo, Tzu-Ching Chang, and Olivier Doré. Constraining the stochastic gravitational wave background with photometric surveys. *Phys. Rev. D*, 106(8):084006, 2022. doi:10.1103/PhysRevD.106.084006.

- [68] J. Antoniadis et al. The second data release from the European Pulsar Timing Array - I. The dataset and timing analysis. *Astron. Astrophys.*, 678:A48, 2023. doi:10.1051/0004-6361/202346841.
- [69] Gabriella Agazie et al. The NANOGrav 15 yr Data Set: Observations and Timing of 68 Millisecond Pulsars. *Astrophys. J. Lett.*, 951(1):L9, 2023. doi:10.3847/2041-8213/acda9a.
- [70] Andrew Zic et al. The Parkes Pulsar Timing Array Third Data Release. 6 2023.
- [71] A. Weltman et al. Fundamental physics with the Square Kilometre Array. *Publ. Astron. Soc. Austral.*, 37:e002, 2020. doi:10.1017/pasa.2019.42.
- [72] Xing-Jiang Zhu, Linqing Wen, George Hobbs, Richard N. Manchester, and Ryan M. Shannon. Detecting nanohertz gravitational waves with pulsar timing arrays. 9 2015.
- [73] Sarah Burke-Spolaor et al. The Astrophysics of Nanohertz Gravitational Waves. *Astron. Astrophys. Rev.*, 27(1):5, 2019. doi:10.1007/s00159-019-0115-7.
- [74] Pravin Kumar Dahal. Review of Pulsar Timing Array for Gravitational Wave Research. *J. Astrophys. Astron.*, 41(1):8, 2020. doi:10.1007/s12036-020-9625-y.
- [75] MV Sazhin. Opportunities for detecting ultralong gravitational waves. *Sov. Astron.*, 22: 36–38, 1978.
- [76] Nancy Aggarwal et al. Challenges and opportunities of gravitational-wave searches at MHz to GHz frequencies. *Living Rev. Rel.*, 24(1):4, 2021. doi:10.1007/s41114-021-00032-5.
- [77] G. Hobbs et al. The international pulsar timing array project: using pulsars as a gravitational wave detector. *Class. Quant. Grav.*, 27:084013, 2010. doi:10.1088/0264-9381/27/8/084013.
- [78] Seiji Kawamura et al. Current status of space gravitational wave antenna DECIGO and B-DECIGO. 6 2020.
- [79] Michele Maggiore et al. Science Case for the Einstein Telescope. *JCAP*, 03:050, 2020. doi:10.1088/1475-7516/2020/03/050.
- [80] Michele Maggiore. *Gravitational waves: Volume 1: Theory and experiments*. OUP Oxford, 2007.
- [81] Fulvio Ricci and Alain Brillet. A review of gravitational wave detectors. *Ann. Rev. Nucl. Part. Sci.*, 47:111–156, 1997. doi:10.1146/annurev.nucl.47.1.111.
- [82] P. Aufmuth and K. Danzmann. Gravitational wave detectors. *New J. Phys.*, 7:202, 2005. doi:10.1088/1367-2630/7/1/202.
- [83] Joseph D. Romano and Neil J. Cornish. Detection methods for stochastic gravitational-wave

- backgrounds: a unified treatment. *Living Rev. Rel.*, 20(1):2, 2017. doi:10.1007/s41114-017-0004-1.
- [84] RW Hellings and GS Downs. Upper limits on the isotropic gravitational radiation background from pulsar timing analysis. *The Astrophysical Journal*, 265:L39–L42, 1983.
- [85] Pratik Tarafdar et al. The Indian Pulsar Timing Array: First data release. *Publ. Astron. Soc. Austral.*, 39:e053, 2022. doi:10.1017/pasa.2022.46.
- [86] Albert A Michelson. Art. xxi.—the relative motion of the earth and the luminiferous ether. *American Journal of Science (1880-1910)*, 22(128):120, 1881.
- [87] Cyril Pitrou, Alain Coc, Jean-Philippe Uzan, and Elisabeth Vangioni. Precision big bang nucleosynthesis with improved Helium-4 predictions. *Phys. Rept.*, 754:1–66, 2018. doi:10.1016/j.physrep.2018.04.005.
- [88] Marc Kamionkowski and Ely D. Kovetz. The Quest for B Modes from Inflationary Gravitational Waves. *Ann. Rev. Astron. Astrophys.*, 54:227–269, 2016. doi:10.1146/annurev-astro-081915-023433.
- [89] Paul D. Lasky et al. Gravitational-wave cosmology across 29 decades in frequency. *Phys. Rev. X*, 6(1):011035, 2016. doi:10.1103/PhysRevX.6.011035.
- [90] Andreas Ringwald, Jan Schütte-Engel, and Carlos Tamarit. Gravitational Waves as a Big Bang Thermometer. *JCAP*, 03:054, 2021. doi:10.1088/1475-7516/2021/03/054.
- [91] Farid F Abraham. *Homogeneous nucleation theory*, volume 263. Elsevier, 1974.
- [92] Sidney Coleman. Fate of the false vacuum: Semiclassical theory. *Physical Review D*, 15(10):2929, 1977.
- [93] Curtis G Callan Jr and Sidney Coleman. Fate of the false vacuum. ii. first quantum corrections. *Physical Review D*, 16(6):1762, 1977.
- [94] Andrei D Linde. Fate of the false vacuum at finite temperature: theory and applications. *Phys. Lett., B*, 100(1):37–40, 1981.
- [95] Djuna Croon, Rachel Houtz, and Verónica Sanz. Dynamical Axions and Gravitational Waves. *JHEP*, 07:146, 2019. doi:10.1007/JHEP07(2019)146.
- [96] Biagio Lucini, Michael Teper, and Urs Wenger. Properties of the deconfining phase transition in SU(N) gauge theories. *JHEP*, 02:033, 2005. doi:10.1088/1126-6708/2005/02/033.
- [97] Saumen Datta and Sourendu Gupta. Continuum Thermodynamics of the Gluo N_c Plasma. *Phys. Rev. D*, 82:114505, 2010. doi:10.1103/PhysRevD.82.114505.

- [98] Peter Athron, Csaba Balázs, Tomás E. Gonzalo, and Matthew Pearce. Falsifying Pati-Salam models with LIGO. 7 2023.
- [99] Bjorn Garbrecht and Peter Millington. Self-consistent radiative corrections to false vacuum decay. *J. Phys. Conf. Ser.*, 873(1):012041, 2017. doi:10.1088/1742-6596/873/1/012041.
- [100] K. Kajantie, M. Laine, K. Rummukainen, and Mikhail E. Shaposhnikov. The Electroweak phase transition: A Nonperturbative analysis. *Nucl. Phys. B*, 466:189–258, 1996. doi:10.1016/0550-3213(96)00052-1.
- [101] K. Kajantie, M. Laine, K. Rummukainen, and Mikhail E. Shaposhnikov. Is there a hot electroweak phase transition at $m_H \gtrsim m_W$? *Phys. Rev. Lett.*, 77:2887–2890, 1996. doi:10.1103/PhysRevLett.77.2887.
- [102] K. Kajantie, M. Laine, K. Rummukainen, and Mikhail E. Shaposhnikov. A Nonperturbative analysis of the finite T phase transition in SU(2) x U(1) electroweak theory. *Nucl. Phys.*, B493:413–438, 1997. doi:10.1016/S0550-3213(97)00164-8.
- [103] F. Csikor, Z. Fodor, and J. Heitger. Endpoint of the hot electroweak phase transition. *Phys. Rev. Lett.*, 82:21–24, 1999. doi:10.1103/PhysRevLett.82.21.
- [104] Michela D’Onofrio and Kari Rummukainen. Standard model cross-over on the lattice. *Phys. Rev. D*, 93(2):025003, 2016. doi:10.1103/PhysRevD.93.025003.
- [105] Y. Aoki, G. Endrodi, Z. Fodor, S. D. Katz, and K. K. Szabo. The Order of the quantum chromodynamics transition predicted by the standard model of particle physics. *Nature*, 443:675–678, 2006. doi:10.1038/nature05120.
- [106] Tanmoy Bhattacharya et al. QCD Phase Transition with Chiral Quarks and Physical Quark Masses. *Phys. Rev. Lett.*, 113(8):082001, 2014. doi:10.1103/PhysRevLett.113.082001.
- [107] G. C. Dorsch, S. J. Huber, and J. M. No. A strong electroweak phase transition in the 2HDM after LHC8. *JHEP*, 10:029, 2013. doi:10.1007/JHEP10(2013)029.
- [108] P. Basler, M. Krause, M. Muhlleitner, J. Wittbrodt, and A. Wlotzka. Strong First Order Electroweak Phase Transition in the CP-Conserving 2HDM Revisited. *JHEP*, 02:121, 2017. doi:10.1007/JHEP02(2017)121.
- [109] G. C. Dorsch, S. J. Huber, K. Mimasu, and J. M. No. Hierarchical versus degenerate 2HDM: The LHC run 1 legacy at the onset of run 2. *Phys. Rev. D*, 93(11):115033, 2016. doi:10.1103/PhysRevD.93.115033.
- [110] G. C. Dorsch, S. J. Huber, T. Konstandin, and J. M. No. A Second Higgs Doublet in the Early

- Universe: Baryogenesis and Gravitational Waves. *JCAP*, 05:052, 2017. doi:10.1088/1475-7516/2017/05/052.
- [111] J er emy Bernon, Ligong Bian, and Yun Jiang. A new insight into the phase transition in the early Universe with two Higgs doublets. *JHEP*, 05:151, 2018. doi:10.1007/JHEP05(2018)151.
- [112] G. C. Dorsch, S. J. Huber, K. Mimasu, and J. M. No. The Higgs Vacuum Uplifted: Revisiting the Electroweak Phase Transition with a Second Higgs Doublet. *JHEP*, 12:086, 2017. doi:10.1007/JHEP12(2017)086.
- [113] Jens O. Andersen, Tyler Gorda, Andreas Helset, Lauri Niemi, Tuomas V. I. Tenkanen, Anders Tranberg, Alekski Vuorinen, and David J. Weir. Nonperturbative Analysis of the Electroweak Phase Transition in the Two Higgs Doublet Model. *Phys. Rev. Lett.*, 121(19):191802, 2018. doi:10.1103/PhysRevLett.121.191802.
- [114] Kimmo Kainulainen, Venus Keus, Lauri Niemi, Kari Rummukainen, Tuomas V. I. Tenkanen, and Ville Vaskonen. On the validity of perturbative studies of the electroweak phase transition in the Two Higgs Doublet model. *JHEP*, 06:075, 2019. doi:10.1007/JHEP06(2019)075.
- [115] Xiao Wang, Fa Peng Huang, and Xinmin Zhang. Gravitational wave and collider signals in complex two-Higgs doublet model with dynamical CP-violation at finite temperature. *Phys. Rev. D*, 101(1):015015, 2020. doi:10.1103/PhysRevD.101.015015.
- [116] Wei Su, Anthony G. Williams, and Mengchao Zhang. Strong first order electroweak phase transition in 2HDM confronting future Z & Higgs factories. *JHEP*, 04:219, 2021. doi:10.1007/JHEP04(2021)219.
- [117] Hooman Davoudiasl, Ian M. Lewis, and Matthew Sullivan. Multi-TeV signals of baryogenesis in a Higgs troika model. *Phys. Rev. D*, 104(1):015024, 2021. doi:10.1103/PhysRevD.104.015024.
- [118] Thomas Biek otter, Sven Heinemeyer, Jos e Miguel No, Mar ıa Olalla Olea, and Georg Weiglein. Fate of electroweak symmetry in the early Universe: Non-restoration and trapped vacua in the N2HDM. *JCAP*, 06:018, 2021. doi:10.1088/1475-7516/2021/06/018.
- [119] Zhao Zhang, Chengfeng Cai, Xue-Min Jiang, Yi-Lei Tang, Zhao-Huan Yu, and Hong-Hao Zhang. Phase transition gravitational waves from pseudo-Nambu-Goldstone dark matter and two Higgs doublets. *JHEP*, 05:160, 2021. doi:10.1007/JHEP05(2021)160.
- [120] Mayumi Aoki, Takatoshi Komatsu, and Hiroto Shibuya. Possibility of a multi-step electroweak phase transition in the two-Higgs doublet models. *PTEP*, 2022(6):063B05, 2022.

- doi:10.1093/ptep/ptac068.
- [121] Dorival Gonçalves, Ajay Kaladharan, and Yongcheng Wu. Electroweak phase transition in the 2HDM: Collider and gravitational wave complementarity. *Phys. Rev. D*, 105(9):095041, 2022. doi:10.1103/PhysRevD.105.095041.
- [122] Vo Quoc Phong, Nguyen Minh Anh, and Hoang Ngoc Long. Dual electroweak phase transition in the two-Higgs-doublet model with the S3 discrete symmetry. *Phys. Rev. D*, 107(3):035020, 2023. doi:10.1103/PhysRevD.107.035020.
- [123] Thomas Biekötter, Sven Heinemeyer, José Miguel No, María Olalla Olea-Romacho, and Georg Weiglein. The trap in the early Universe: impact on the interplay between gravitational waves and LHC physics in the 2HDM. *JCAP*, 03:031, 2023. doi:10.1088/1475-7516/2023/03/031.
- [124] Anisha, Lisa Biermann, Christoph Englert, and Margarete Mühlleitner. Two Higgs doublets, effective interactions and a strong first-order electroweak phase transition. *JHEP*, 08:091, 2022. doi:10.1007/JHEP08(2022)091.
- [125] Oliver Atkinson, Matthew Black, Christoph Englert, Alexander Lenz, Aleksey Rusov, and James Wynne. The flavourful present and future of 2HDMs at the collider energy frontier. *JHEP*, 11:139, 2022. doi:10.1007/JHEP11(2022)139.
- [126] Thomas Biekötter, Sven Heinemeyer, Jose Miguel No, Kateryna Radchenko, María Olalla Olea Romacho, and Georg Weiglein. First shot of the smoking gun: probing the electroweak phase transition in the 2HDM with novel searches for $A \rightarrow ZH$ in $\ell^+\ell^-t\bar{t}$ and $\nu\nu b\bar{b}$ final states. 9 2023.
- [127] Dorival Gonçalves, Ajay Kaladharan, and Yongcheng Wu. Gravitational waves, bubble profile, and baryon asymmetry in the complex 2HDM. *Phys. Rev. D*, 108(7):075010, 2023. doi:10.1103/PhysRevD.108.075010.
- [128] Nikita Blinov, Stefano Profumo, and Tim Stefaniak. The Electroweak Phase Transition in the Inert Doublet Model. *JCAP*, 07:028, 2015. doi:10.1088/1475-7516/2015/07/028.
- [129] Fa Peng Huang and Jiang-Hao Yu. Exploring inert dark matter blind spots with gravitational wave signatures. *Phys. Rev. D*, 98(9):095022, 2018. doi:10.1103/PhysRevD.98.095022.
- [130] Avik Paul, Biswajit Banerjee, and Debasish Majumdar. Gravitational wave signatures from an extended inert doublet dark matter model. *JCAP*, 10:062, 2019. doi:10.1088/1475-7516/2019/10/062.

- [131] Sven Fabian, Florian Goertz, and Yun Jiang. Dark matter and nature of electroweak phase transition with an inert doublet. *JCAP*, 09:011, 2021. doi:10.1088/1475-7516/2021/09/011.
- [132] Nico Benincasa, Luigi Delle Rose, Kristjan Kannike, and Luca Marzola. Multi-step phase transitions and gravitational waves in the inert doublet model. *JCAP*, 12:025, 2022. doi:10.1088/1475-7516/2022/12/025.
- [133] Avik Paul, Debasish Majumdar, and Biswajit Banerjee. Gravitational Wave Signatures from First-Order Phase Transitions in an Extended Inert Doublet Dark Matter Model. *Springer Proc. Phys.*, 277:73–77, 2022. doi:10.1007/978-981-19-2354-8_13.
- [134] Siyu Jiang, Fa Peng Huang, and Xiao Wang. Bubble wall velocity during electroweak phase transition in the inert doublet model. *Phys. Rev. D*, 107(9):095005, 2023. doi:10.1103/PhysRevD.107.095005.
- [135] María Dias Astros, Sven Fabian, and Florian Goertz. Minimal Inert Doublet Benchmark for Dark Matter and the Baryon Asymmetry. 7 2023.
- [136] Marcela Carena, M. Quiros, and C. E. M. Wagner. Opening the window for electroweak baryogenesis. *Phys. Lett. B*, 380:81–91, 1996. doi:10.1016/0370-2693(96)00475-3.
- [137] J. R. Espinosa. Dominant two loop corrections to the MSSM finite temperature effective potential. *Nucl. Phys. B*, 475:273–292, 1996. doi:10.1016/0550-3213(96)00297-0.
- [138] D. Delepine, J. M. Gerard, R. Gonzalez Felipe, and J. Weyers. A Light stop and electroweak baryogenesis. *Phys. Lett. B*, 386:183–188, 1996. doi:10.1016/0370-2693(96)00921-5.
- [139] James M. Cline and Kimmo Kainulainen. Supersymmetric electroweak phase transition: Beyond perturbation theory. *Nucl. Phys. B*, 482:73–91, 1996. doi:10.1016/S0550-3213(96)00519-6.
- [140] Marta Losada. High temperature dimensional reduction of the MSSM and other multiscalar models. *Phys. Rev. D*, 56:2893–2913, 1997. doi:10.1103/PhysRevD.56.2893.
- [141] M. Laine. Effective theories of MSSM at high temperature. *Nucl. Phys. B*, 481:43–84, 1996. doi:10.1016/S0550-3213(96)90121-2. [Erratum: Nucl.Phys.B 548, 637–638 (1999)].
- [142] D. Bodeker, P. John, M. Laine, and M. G. Schmidt. The Two loop MSSM finite temperature effective potential with stop condensation. *Nucl. Phys. B*, 497:387–414, 1997. doi:10.1016/S0550-3213(97)00252-6.
- [143] B. de Carlos and J. R. Espinosa. The Baryogenesis window in the MSSM. *Nucl. Phys. B*, 503:24–54, 1997. doi:10.1016/S0550-3213(97)00437-9.

- [144] James M. Cline and Guy D. Moore. Supersymmetric electroweak phase transition: Baryogenesis versus experimental constraints. *Phys. Rev. Lett.*, 81:3315–3318, 1998. doi:10.1103/PhysRevLett.81.3315.
- [145] Marta Losada. The Two loop finite temperature effective potential of the MSSM and baryogenesis. *Nucl. Phys. B*, 537:3–31, 1999. doi:10.1016/S0550-3213(98)00563-X.
- [146] M. Laine and K. Rummukainen. Two Higgs doublet dynamics at the electroweak phase transition: A Nonperturbative study. *Nucl. Phys. B*, 597:23–69, 2001. doi:10.1016/S0550-3213(00)00736-7.
- [147] M. Carena, Germano Nardini, M. Quiros, and C. E. M. Wagner. The Baryogenesis Window in the MSSM. *Nucl. Phys. B*, 812:243–263, 2009. doi:10.1016/j.nuclphysb.2008.12.014.
- [148] Antonio Delgado, Germano Nardini, and Mariano Quiros. The Light Stop Scenario from Gauge Mediation. *JHEP*, 04:137, 2012. doi:10.1007/JHEP04(2012)137.
- [149] Marcela Carena, Germano Nardini, Mariano Quiros, and Carlos E. M. Wagner. MSSM Electroweak Baryogenesis and LHC Data. *JHEP*, 02:001, 2013. doi:10.1007/JHEP02(2013)001.
- [150] Daniel J. H. Chung, Andrew J. Long, and Lian-Tao Wang. 125 GeV Higgs boson and electroweak phase transition model classes. *Phys. Rev. D*, 87(2):023509, 2013. doi:10.1103/PhysRevD.87.023509.
- [151] Weicong Huang, Jing Shu, and Yue Zhang. On the Higgs Fit and Electroweak Phase Transition. *JHEP*, 03:164, 2013. doi:10.1007/JHEP03(2013)164.
- [152] M. Laine, G. Nardini, and K. Rummukainen. Lattice study of an electroweak phase transition at $m_h \simeq 126$ GeV. *JCAP*, 01:011, 2013. doi:10.1088/1475-7516/2013/01/011.
- [153] Stefan Liebler, Stefano Profumo, and Tim Stefaniak. Light Stop Mass Limits from Higgs Rate Measurements in the MSSM: Is MSSM Electroweak Baryogenesis Still Alive After All? *JHEP*, 04:143, 2016. doi:10.1007/JHEP04(2016)143.
- [154] Hiren H. Patel and Michael J. Ramsey-Musolf. Stepping Into Electroweak Symmetry Breaking: Phase Transitions and Higgs Phenomenology. *Phys. Rev. D*, 88:035013, 2013. doi:10.1103/PhysRevD.88.035013.
- [155] Mikael Chala, Maria Ramos, and Michael Spannowsky. Gravitational wave and collider probes of a triplet Higgs sector with a low cutoff. *Eur. Phys. J. C*, 79(2):156, 2019. doi:10.1140/epjc/s10052-019-6655-1.
- [156] Sebastian Baum, Marcela Carena, Nausheen R. Shah, Carlos E. M. Wagner, and Yikun

- Wang. Nucleation is more than critical: A case study of the electroweak phase transition in the NMSSM. *JHEP*, 03:055, 2021. doi:10.1007/JHEP03(2021)055.
- [157] M. J. Kazemi and S. S. Abdussalam. Electroweak Phase Transition in an Inert Complex Triplet Model. *Phys. Rev. D*, 103(7):075012, 2021. doi:10.1103/PhysRevD.103.075012.
- [158] Minyuan Jiang, Ligong Bian, Weicong Huang, and Jing Shu. Impact of a complex singlet: Electroweak baryogenesis and dark matter. *Phys. Rev. D*, 93(6):065032, 2016. doi:10.1103/PhysRevD.93.065032.
- [159] Cheng-Wei Chiang, Michael J. Ramsey-Musolf, and Eibun Senaha. Standard Model with a Complex Scalar Singlet: Cosmological Implications and Theoretical Considerations. *Phys. Rev. D*, 97(1):015005, 2018. doi:10.1103/PhysRevD.97.015005.
- [160] Amine Ahriche, Katsuya Hashino, Shinya Kanemura, and Salah Nasri. Gravitational Waves from Phase Transitions in Models with Charged Singlets. *Phys. Lett. B*, 789:119–126, 2019. doi:10.1016/j.physletb.2018.12.013.
- [161] Ning Chen, Tong Li, Yongcheng Wu, and Ligong Bian. Complementarity of the future e^+e^- colliders and gravitational waves in the probe of complex singlet extension to the standard model. *Phys. Rev. D*, 101(7):075047, 2020. doi:10.1103/PhysRevD.101.075047.
- [162] Gi-Chol Cho, Chikako Idegawa, and Eibun Senaha. Electroweak phase transition in a complex singlet extension of the Standard Model with degenerate scalars. *Phys. Lett. B*, 823:136787, 2021. doi:10.1016/j.physletb.2021.136787.
- [163] Philipp Schicho, Tuomas V. I. Tenkanen, and Graham White. Combining thermal resummation and gauge invariance for electroweak phase transition. *JHEP*, 11:047, 2022. doi:10.1007/JHEP11(2022)047.
- [164] J. R. Espinosa and M. Quiros. The Electroweak phase transition with a singlet. *Phys. Lett. B*, 305:98–105, 1993. doi:10.1016/0370-2693(93)91111-Y.
- [165] Stefano Profumo, Michael J. Ramsey-Musolf, and Gabe Shaughnessy. Singlet Higgs phenomenology and the electroweak phase transition. *JHEP*, 08:010, 2007. doi:10.1088/1126-6708/2007/08/010.
- [166] James M. Cline, Guillaume Laporte, Hiroki Yamashita, and Sabine Kraml. Electroweak Phase Transition and LHC Signatures in the Singlet Majoron Model. *JHEP*, 07:040, 2009. doi:10.1088/1126-6708/2009/07/040.
- [167] James M. Cline and Kimmo Kainulainen. Electroweak baryogenesis and dark matter from a

- singlet Higgs. *JCAP*, 1301:012, 2013. doi:10.1088/1475-7516/2013/01/012.
- [168] James M. Cline, Kimmo Kainulainen, Pat Scott, and Christoph Weniger. Update on scalar singlet dark matter. *Phys. Rev.*, D88:055025, 2013. doi:10.1103/PhysRevD.92.039906, 10.1103/PhysRevD.88.055025. [Erratum: *Phys. Rev.D*92,no.3,039906(2015)].
- [169] Andrey Katz and Maxim Perelstein. Higgs Couplings and Electroweak Phase Transition. *JHEP*, 07:108, 2014. doi:10.1007/JHEP07(2014)108.
- [170] Stefano Profumo, Michael J. Ramsey-Musolf, Carroll L. Wainwright, and Peter Winslow. Singlet-catalyzed electroweak phase transitions and precision Higgs boson studies. *Phys. Rev. D*, 91(3):035018, 2015. doi:10.1103/PhysRevD.91.035018.
- [171] Ville Vaskonen. Electroweak baryogenesis and gravitational waves from a real scalar singlet. 2016.
- [172] Katsuya Hashino, Mitsuru Kakizaki, Shinya Kanemura, Pyungwon Ko, and Toshinori Matsui. Gravitational waves and Higgs boson couplings for exploring first order phase transition in the model with a singlet scalar field. 2016.
- [173] Wei Chao, Huai-Ke Guo, and Jing Shu. Gravitational Wave Signals of Electroweak Phase Transition Triggered by Dark Matter. 2017.
- [174] Toshinori Matsui. Gravitational waves from the first order electroweak phase transition in the Z_3 symmetric singlet scalar model. *EPJ Web Conf.*, 168:05001, 2018. doi:10.1051/epjconf/201816805001.
- [175] Zhaofeng Kang, P. Ko, and Toshinori Matsui. Strong first order EWPT & strong gravitational waves in Z_3 -symmetric singlet scalar extension. *JHEP*, 02:115, 2018. doi:10.1007/JHEP02(2018)115.
- [176] Alexandre Alves, Tathagata Ghosh, Huai-Ke Guo, Kuver Sinha, and Daniel Vagie. Collider and Gravitational Wave Complementarity in Exploring the Singlet Extension of the Standard Model. *JHEP*, 04:052, 2019. doi:10.1007/JHEP04(2019)052.
- [177] Vahid Reza Shajiee and Ali Tofghi. Electroweak Phase Transition, Gravitational Waves and Dark Matter in Two Scalar Singlet Extension of The Standard Model. *Eur. Phys. J. C*, 79(4):360, 2019. doi:10.1140/epjc/s10052-019-6881-6.
- [178] Ankit Beniwal, Marek Lewicki, Martin White, and Anthony G. Williams. Gravitational waves and electroweak baryogenesis in a global study of the extended scalar singlet model. *JHEP*, 02:183, 2019. doi:10.1007/JHEP02(2019)183.

- [179] Toshinori Matsui. Gravitational waves from the first order electroweak phase transition in the Z_3 symmetric singlet scalar model. *PoS*, CORFU2017:092, 2018. doi:10.22323/1.318.0092.
- [180] S. Demidov, D. Gorbunov, and E. Kriukova. Gravitational waves from first-order electroweak phase transition in a model with light sgoldstinos. *JHEP*, 07:061, 2022. doi:10.1007/JHEP07(2022)061.
- [181] James M. Cline, Avi Friedlander, Dong-Ming He, Kimmo Kainulainen, Benoit Laurent, and David Tucker-Smith. Baryogenesis and gravity waves from a UV-completed electroweak phase transition. *Phys. Rev. D*, 103(12):123529, 2021. doi:10.1103/PhysRevD.103.123529.
- [182] Qing-Hong Cao, Katsuya Hashino, Xu-Xiang Li, and Jiang-Hao Yue. Multi-step phase transition and gravitational wave from general Z_2 scalar extensions. 12 2022.
- [183] Peter Athron, Csaba Balázs, Andrew Fowlie, Lachlan Morris, and Lei Wu. Cosmological phase transitions: from perturbative particle physics to gravitational waves. 5 2023.
- [184] Christophe Grojean, Geraldine Servant, and James D. Wells. First-order electroweak phase transition in the standard model with a low cutoff. *Phys. Rev.*, D71:036001, 2005. doi:10.1103/PhysRevD.71.036001.
- [185] Dietrich Bodeker, Lars Fromme, Stephan J. Huber, and Michael Seniuch. The Baryon asymmetry in the standard model with a low cut-off. *JHEP*, 02:026, 2005. doi:10.1088/1126-6708/2005/02/026.
- [186] Cedric Delaunay, Christophe Grojean, and James D. Wells. Dynamics of Non-renormalizable Electroweak Symmetry Breaking. *JHEP*, 04:029, 2008. doi:10.1088/1126-6708/2008/04/029.
- [187] Csaba Balazs, Graham White, and Jason Yue. Effective field theory, electric dipole moments and electroweak baryogenesis. *JHEP*, 03:030, 2017. doi:10.1007/JHEP03(2017)030.
- [188] Jordy de Vries, Marieke Postma, Jorinde van de Vis, and Graham White. Electroweak Baryogenesis and the Standard Model Effective Field Theory. *JHEP*, 01:089, 2018. doi:10.1007/JHEP01(2018)089.
- [189] Jordy De Vries, Marieke Postma, and Jorinde van de Vis. The role of leptons in electroweak baryogenesis. *JHEP*, 04:024, 2019. doi:10.1007/JHEP04(2019)024.
- [190] Mikael Chala, Claudius Krause, and Germano Nardini. Signals of the electroweak phase transition at colliders and gravitational wave observatories. *JHEP*, 07:062, 2018. doi:10.1007/JHEP07(2018)062.
- [191] Sebastian A. R. Ellis, Seyda Ipek, and Graham White. Electroweak Baryogenesis from

- Temperature-Varying Couplings. *JHEP*, 08:002, 2019. doi:10.1007/JHEP08(2019)002.
- [192] Marieke Postma and Graham White. Cosmological phase transitions: is effective field theory just a toy? *JHEP*, 03:280, 2021. doi:10.1007/JHEP03(2021)280.
- [193] Steven Weinberg. Gauge and Global Symmetries at High Temperature. *Phys. Rev. D*, 9:3357–3378, 1974. doi:10.1103/PhysRevD.9.3357.
- [194] David Land and Eric D. Carlson. Two stage phase transition in two Higgs models. *Phys. Lett. B*, 292:107–112, 1992. doi:10.1016/0370-2693(92)90616-C.
- [195] A. Hammerschmitt, J. Kripfganz, and M. G. Schmidt. Baryon asymmetry from a two stage electroweak phase transition? *Z. Phys. C*, 64:105–110, 1994. doi:10.1007/BF01557241.
- [196] Hiren H. Patel, Michael J. Ramsey-Musolf, and Mark B. Wise. Color Breaking in the Early Universe. *Phys. Rev. D*, 88(1):015003, 2013. doi:10.1103/PhysRevD.88.015003.
- [197] Nikita Blinov, Jonathan Kozaczuk, David E. Morrissey, and Carlos Tamarit. Electroweak Baryogenesis from Exotic Electroweak Symmetry Breaking. *Phys. Rev. D*, 92(3):035012, 2015. doi:10.1103/PhysRevD.92.035012.
- [198] Satoru Inoue, Grigory Ovanesyan, and Michael J. Ramsey-Musolf. Two-Step Electroweak Baryogenesis. *Phys. Rev. D*, 93:015013, 2016. doi:10.1103/PhysRevD.93.015013.
- [199] Michael J. Ramsey-Musolf, Peter Winslow, and Graham White. Color Breaking Baryogenesis. *Phys. Rev. D*, 97(12):123509, 2018. doi:10.1103/PhysRevD.97.123509.
- [200] Djuna Croon and Graham White. Exotic Gravitational Wave Signatures from Simultaneous Phase Transitions. *JHEP*, 05:210, 2018. doi:10.1007/JHEP05(2018)210.
- [201] Andrei Angelescu and Peisi Huang. Multistep Strongly First Order Phase Transitions from New Fermions at the TeV Scale. *Phys. Rev. D*, 99(5):055023, 2019. doi:10.1103/PhysRevD.99.055023.
- [202] Lauri Niemi, Hiren H. Patel, Michael J. Ramsey-Musolf, Tuomas V. I. Tenkanen, and David J. Weir. Electroweak phase transition in the real triplet extension of the SM: Dimensional reduction. *Phys. Rev. D*, 100(3):035002, 2019. doi:10.1103/PhysRevD.100.035002.
- [203] António P. Morais, Roman Pasechnik, and Thibault Vieu. Multi-peaked signatures of primordial gravitational waves from multi-step electroweak phase transition. *PoS, EPS-HEP2019*:054, 2020. doi:10.22323/1.364.0054.
- [204] António P. Morais and Roman Pasechnik. Probing multi-step electroweak phase transition with multi-peaked primordial gravitational waves spectra. *JCAP*, 04:036, 2020. doi:

- 10.1088/1475-7516/2020/04/036.
- [205] Lauri Niemi, Michael J. Ramsey-Musolf, Tuomas V. I. Tenkanen, and David J. Weir. Thermodynamics of a Two-Step Electroweak Phase Transition. *Phys. Rev. Lett.*, 126(17):171802, 2021. doi:10.1103/PhysRevLett.126.171802.
- [206] Robert D. Pisarski and Frank Wilczek. Remarks on the Chiral Phase Transition in Chromodynamics. *Phys. Rev. D*, 29:338–341, 1984. doi:10.1103/PhysRevD.29.338.
- [207] Pedro Costa, C. A. de Sousa, M. C. Ruivo, and H. Hansen. The QCD critical end point in the PNJL model. *EPL*, 86(3):31001, 2009. doi:10.1209/0295-5075/86/31001.
- [208] F. Marquez and R. Zamora. Critical end point in a thermomagnetic nonlocal NJL model. *Int. J. Mod. Phys. A*, 32(26):1750162, 2017. doi:10.1142/S0217751X17501627.
- [209] Volodymyr Vovchenko, Mark I. Gorenstein, Carsten Greiner, and Horst Stoecker. Hagedorn bag-like model with a crossover transition meets lattice QCD. *Phys. Rev. C*, 99(4):045204, 2019. doi:10.1103/PhysRevC.99.045204.
- [210] Xun Chen, Danning Li, and Mei Huang. Criticality of qcd in a holographic qcd model with critical end point. *Chinese Physics C*, 43(2):023105, 2019.
- [211] Renan Câmara Pereira, João Moreira, and Pedro Costa. The strange critical endpoint and isentropic trajectories in an extended PNJL model with eight Quark interactions. *Eur. Phys. J. A*, 56(8):214, 2020. doi:10.1140/epja/s10050-020-00223-8.
- [212] Fei Gao and Jan M. Pawłowski. QCD phase structure from functional methods. *Phys. Rev. D*, 102(3):034027, 2020. doi:10.1103/PhysRevD.102.034027.
- [213] Fei Gao and Jan M. Pawłowski. Chiral phase structure and critical end point in QCD. *Phys. Lett. B*, 820:136584, 2021. doi:10.1016/j.physletb.2021.136584.
- [214] Fei Gao and Isabel M. Oldengott. Cosmology Meets Functional QCD: First-Order Cosmic QCD Transition Induced by Large Lepton Asymmetries. *Phys. Rev. Lett.*, 128(13):131301, 2022. doi:10.1103/PhysRevLett.128.131301.
- [215] Fei Gao, Julia Harz, Chandan Hati, Yi Lu, Isabel M. Oldengott, and Graham White. Sphaleron freeze-in baryogenesis with gravitational waves from the QCD transition. 9 2023.
- [216] A. Bazavov et al. The QCD Equation of State to $\mathcal{O}(\mu_B^6)$ from Lattice QCD. *Phys. Rev. D*, 95(5):054504, 2017. doi:10.1103/PhysRevD.95.054504.
- [217] Heng-Tong Ding. New developments in lattice QCD on equilibrium physics and phase diagram. *Nucl. Phys. A*, 1005:121940, 2021. doi:10.1016/j.nuclphysa.2020.121940.

- [218] Hooman Davoudiasl. LIGO/Virgo Black Holes from a First Order Quark Confinement Phase Transition. *Phys. Rev. Lett.*, 123(10):101102, 2019. doi:10.1103/PhysRevLett.123.101102.
- [219] Benedict von Harling and Geraldine Servant. QCD-induced Electroweak Phase Transition. *JHEP*, 01:159, 2018. doi:10.1007/JHEP01(2018)159.
- [220] James Halverson, Cody Long, Anindita Maiti, Brent Nelson, and Gustavo Salinas. Gravitational waves from dark Yang-Mills sectors. *JHEP*, 05:154, 2021. doi:10.1007/JHEP05(2021)154.
- [221] Francesco Bigazzi, Alessio Caddeo, Aldo L. Cotrone, and Angel Paredes. Fate of false vacua in holographic first-order phase transitions. *JHEP*, 12:200, 2020. doi:10.1007/JHEP12(2020)200.
- [222] Francesco Bigazzi, Alessio Caddeo, Aldo L. Cotrone, and Angel Paredes. Dark Holograms and Gravitational Waves. *JHEP*, 04:094, 2021. doi:10.1007/JHEP04(2021)094.
- [223] Wei-Chih Huang, Manuel Reichert, Francesco Sannino, and Zhi-Wei Wang. Testing the dark SU(N) Yang-Mills theory confined landscape: From the lattice to gravitational waves. *Phys. Rev. D*, 104(3):035005, 2021. doi:10.1103/PhysRevD.104.035005.
- [224] Xiao Wang, Fa Peng Huang, and Xinmin Zhang. Bubble wall velocity beyond leading-log approximation in electroweak phase transition. 11 2020.
- [225] Zhaofeng Kang, Jiang Zhu, and Shinya Matsuzaki. Dark confinement-deconfinement phase transition: a roadmap from Polyakov loop models to gravitational waves. *JHEP*, 09:060, 2021. doi:10.1007/JHEP09(2021)060.
- [226] Enrico Morgante, Nicklas Ramberg, and Pedro Schwaller. Gravitational waves from dark SU(3) Yang-Mills theory. *Phys. Rev. D*, 107(3):036010, 2023. doi:10.1103/PhysRevD.107.036010.
- [227] Dominik J. Schwarz and Maik Stuke. Lepton asymmetry and the cosmic QCD transition. *JCAP*, 11:025, 2009. doi:10.1088/1475-7516/2009/11/025. [Erratum: JCAP 10, E01 (2010)].
- [228] Chiara Caprini, Ruth Durrer, and Xavier Siemens. Detection of gravitational waves from the QCD phase transition with pulsar timing arrays. *Phys. Rev. D*, 82:063511, 2010. doi:10.1103/PhysRevD.82.063511.
- [229] Mandy M. Middeldorf-Wygas, Isabel M. Oldengott, Dietrich Bödeker, and Dominik J. Schwarz. Cosmic QCD transition for large lepton flavor asymmetries. *Phys. Rev. D*, 105(12):123533, 2022. doi:10.1103/PhysRevD.105.123533.

- [230] Ryusuke Jinno and Masahiro Takimoto. Probing a classically conformal B-L model with gravitational waves. *Phys. Rev. D*, 95(1):015020, 2017. doi:10.1103/PhysRevD.95.015020.
- [231] Wei Chao, Wen-Feng Cui, Huai-Ke Guo, and Jing Shu. Gravitational wave imprint of new symmetry breaking. *Chin. Phys. C*, 44(12):123102, 2020. doi:10.1088/1674-1137/abb4cb.
- [232] Vedran Brdar, Alexander J. Helmboldt, and Jisuke Kubo. Gravitational Waves from First-Order Phase Transitions: LIGO as a Window to Unexplored Seesaw Scales. *JCAP*, 02:021, 2019. doi:10.1088/1475-7516/2019/02/021.
- [233] Nobuchika Okada and Osamu Seto. Probing the seesaw scale with gravitational waves. *Phys. Rev. D*, 98(6):063532, 2018. doi:10.1103/PhysRevD.98.063532.
- [234] Carlo Marzo, Luca Marzola, and Ville Vaskonen. Phase transition and vacuum stability in the classically conformal B-L model. *Eur. Phys. J. C*, 79(7):601, 2019. doi:10.1140/epjc/s10052-019-7076-x.
- [235] Ligong Bian, Wei Cheng, Huai-Ke Guo, and Yongchao Zhang. Cosmological implications of a B - L charged hidden scalar: leptogenesis and gravitational waves. *Chin. Phys. C*, 45(11):113104, 2021. doi:10.1088/1674-1137/ac1e09.
- [236] Taiki Hasegawa, Nobuchika Okada, and Osamu Seto. Gravitational waves from the minimal gauged $U(1)_{B-L}$ model. *Phys. Rev. D*, 99(9):095039, 2019. doi:10.1103/PhysRevD.99.095039.
- [237] John Ellis, Marek Lewicki, José Miguel No, and Ville Vaskonen. Gravitational wave energy budget in strongly supercooled phase transitions. *JCAP*, 06:024, 2019. doi:10.1088/1475-7516/2019/06/024.
- [238] Nobuchika Okada, Osamu Seto, and Hikaru Uchida. Gravitational waves from breaking of an extra $U(1)$ in $SO(10)$ grand unification. 6 2020.
- [239] Bartosz Fornal and Barmak Shams Es Haghi. Baryon and Lepton Number Violation from Gravitational Waves. *Phys. Rev. D*, 102(11):115037, 2020. doi:10.1103/PhysRevD.102.115037.
- [240] Mingqiu Li, Qi-Shu Yan, Yongchao Zhang, and Zhijie Zhao. Prospects of gravitational waves in the minimal left-right symmetric model. *JHEP*, 03:267, 2021. doi:10.1007/JHEP03(2021)267.
- [241] Pasquale Di Bari, Danny Marfatia, and Ye-Ling Zhou. Gravitational waves from first-order phase transitions in Majoron models of neutrino mass. *JHEP*, 10:193, 2021. doi:10.1007/JHEP10(2021)193.

- [242] Ruiyu Zhou, Ligong Bian, and Yong Du. Electroweak phase transition and gravitational waves in the type-II seesaw model. *JHEP*, 08:205, 2022. doi:10.1007/JHEP08(2022)205.
- [243] Katsuya Hashino, Mitsuru Kakizaki, Shinya Kanemura, Pyungwon Ko, and Toshinori Matsui. Gravitational waves from first order electroweak phase transition in models with the $U(1)_X$ gauge symmetry. *JHEP*, 06:088, 2018. doi:10.1007/JHEP06(2018)088.
- [244] Fa Peng Huang and Xinmin Zhang. Probing the gauge symmetry breaking of the early universe in 3-3-1 models and beyond by gravitational waves. *Phys. Lett. B*, 788:288–294, 2019. doi:10.1016/j.physletb.2018.11.024.
- [245] Djuna Croon, Tomás E. Gonzalo, and Graham White. Gravitational Waves from a Pati-Salam Phase Transition. *JHEP*, 02:083, 2019. doi:10.1007/JHEP02(2019)083.
- [246] Vedran Brdar, Lukas Graf, Alexander J. Helmboldt, and Xun-Jie Xu. Gravitational Waves as a Probe of Left-Right Symmetry Breaking. *JCAP*, 12:027, 2019. doi:10.1088/1475-7516/2019/12/027.
- [247] Wei-Chih Huang, Francesco Sannino, and Zhi-Wei Wang. Gravitational Waves from Pati-Salam Dynamics. *Phys. Rev. D*, 102(9):095025, 2020. doi:10.1103/PhysRevD.102.095025.
- [248] Admir Greljo, Toby Opferkuch, and Ben A. Stefanek. Gravitational Imprints of Flavor Hierarchies. *Phys. Rev. Lett.*, 124(17):171802, 2020. doi:10.1103/PhysRevLett.124.171802.
- [249] Bartosz Fornal. Gravitational Wave Signatures of Lepton Universality Violation. *Phys. Rev. D*, 103(1):015018, 2021. doi:10.1103/PhysRevD.103.015018.
- [250] Bartosz Fornal, Barmak Shams Es Haghi, Jiang-Hao Yu, and Yue Zhao. Gravitational waves from minisplit SUSY. *Phys. Rev. D*, 104(11):115005, 2021. doi:10.1103/PhysRevD.104.115005.
- [251] Nathaniel Craig, Noam Levi, Alberto Mariotti, and Diego Redigolo. Ripples in Spacetime from Broken Supersymmetry. *JHEP*, 21:184, 2020. doi:10.1007/JHEP02(2021)184.
- [252] Riccardo Apreda, Michele Maggiore, Alberto Nicolis, and Antonio Riotto. Gravitational waves from electroweak phase transitions. *Nucl. Phys. B*, 631:342–368, 2002. doi:10.1016/S0550-3213(02)00264-X.
- [253] Ligong Bian, Huai-Ke Guo, and Jing Shu. Gravitational Waves, baryon asymmetry of the universe and electric dipole moment in the CP-violating NMSSM. *Chin. Phys. C*, 42(9):093106, 2018. doi:10.1088/1674-1137/42/9/093106. [Erratum: *Chin.Phys.C* 43, 129101 (2019)].
- [254] Pedro Schwaller. Gravitational Waves from a Dark Phase Transition. *Phys. Rev. Lett.*, 115

- (18):181101, 2015. doi:10.1103/PhysRevLett.115.181101.
- [255] Jason Baldes and Camilo Garcia-Cely. Strong gravitational radiation from a simple dark matter model. *JHEP*, 05:190, 2019. doi:10.1007/JHEP05(2019)190.
- [256] Moritz Breitbach, Joachim Kopp, Eric Madge, Toby Opferkuch, and Pedro Schwaller. Dark, Cold, and Noisy: Constraining Secluded Hidden Sectors with Gravitational Waves. *JCAP*, 07:007, 2019. doi:10.1088/1475-7516/2019/07/007.
- [257] Djuna Croon, Verónica Sanz, and Graham White. Model Discrimination in Gravitational Wave spectra from Dark Phase Transitions. *JHEP*, 08:203, 2018. doi:10.1007/JHEP08(2018)203.
- [258] Eleanor Hall, Thomas Konstandin, Robert McGehee, Hitoshi Murayama, and Géraldine Servant. Baryogenesis From a Dark First-Order Phase Transition. *JHEP*, 04:042, 2020. doi:10.1007/JHEP04(2020)042.
- [259] Jason Baldes. Gravitational waves from the asymmetric-dark-matter generating phase transition. *JCAP*, 05:028, 2017. doi:10.1088/1475-7516/2017/05/028.
- [260] Djuna Croon, Alexander Kusenko, Anupam Mazumdar, and Graham White. Solitogenesis and Gravitational Waves. *Phys. Rev. D*, 101(8):085010, 2020. doi:10.1103/PhysRevD.101.085010.
- [261] Eleanor Hall, Thomas Konstandin, Robert McGehee, and Hitoshi Murayama. Asymmetric matter from a dark first-order phase transition. *Phys. Rev. D*, 107(5):055011, 2023. doi:10.1103/PhysRevD.107.055011.
- [262] Wei Chao, Xiu-Fei Li, and Lei Wang. Filtered pseudo-scalar dark matter and gravitational waves from first order phase transition. *JCAP*, 06:038, 2021. doi:10.1088/1475-7516/2021/06/038.
- [263] James B. Dent, Bhaskar Dutta, Sumit Ghosh, Jason Kumar, and Jack Runburg. Sensitivity to dark sector scales from gravitational wave signatures. *JHEP*, 08:300, 2022. doi:10.1007/JHEP08(2022)300.
- [264] Alexander J. Helmboldt, Jisuke Kubo, and Susan van der Woude. Observational prospects for gravitational waves from hidden or dark chiral phase transitions. *Phys. Rev. D*, 100(5):055025, 2019. doi:10.1103/PhysRevD.100.055025.
- [265] Mayumi Aoki and Jisuke Kubo. Gravitational waves from chiral phase transition in a conformally extended standard model. *JCAP*, 04:001, 2020. doi:10.1088/1475-7516/2020/04/001.

- [266] Djuna Croon, Jessica N. Howard, Seyda Ipek, and Timothy M. P. Tait. QCD baryogenesis. *Phys. Rev. D*, 101(5):055042, 2020. doi:10.1103/PhysRevD.101.055042.
- [267] P. S. Bhupal Dev, Francesc Ferrer, Yiyang Zhang, and Yongchao Zhang. Gravitational Waves from First-Order Phase Transition in a Simple Axion-Like Particle Model. *JCAP*, 11:006, 2019. doi:10.1088/1475-7516/2019/11/006.
- [268] Benedict Von Harling, Alex Pomarol, Oriol Pujolàs, and Fabrizio Rompineve. Peccei-Quinn Phase Transition at LIGO. *JHEP*, 04:195, 2020. doi:10.1007/JHEP04(2020)195.
- [269] Luigi Delle Rose, Giuliano Panico, Michele Redi, and Andrea Tesi. Gravitational Waves from Supercool Axions. *JHEP*, 04:025, 2020. doi:10.1007/JHEP04(2020)025.
- [270] Yoichiro Nambu and G. Jona-Lasinio. Dynamical Model of Elementary Particles Based on an Analogy with Superconductivity. 1. *Phys. Rev.*, 122:345–358, 1961. doi:10.1103/PhysRev.122.345.
- [271] Yoichiro Nambu and G. Jona-Lasinio. Dynamical model of elementary particles based on an analogy with superconductivity. II. *Phys. Rev.*, 124:246–254, 1961. doi:10.1103/PhysRev.124.246.
- [272] S. P. Klevansky. The Nambu-Jona-Lasinio model of quantum chromodynamics. *Rev. Mod. Phys.*, 64:649–708, 1992. doi:10.1103/RevModPhys.64.649.
- [273] Martin Holthausen, Jisuke Kubo, Kher Sham Lim, and Manfred Lindner. Electroweak and Conformal Symmetry Breaking by a Strongly Coupled Hidden Sector. *JHEP*, 12:076, 2013. doi:10.1007/JHEP12(2013)076.
- [274] Kenji Fukushima and Vladimir Skokov. Polyakov loop modeling for hot QCD. *Prog. Part. Nucl. Phys.*, 96:154–199, 2017. doi:10.1016/j.ppnp.2017.05.002.
- [275] Arthur Kosowsky, Michael S. Turner, and Richard Watkins. Gravitational radiation from colliding vacuum bubbles. *Phys. Rev.*, D45:4514–4535, 1992. doi:10.1103/PhysRevD.45.4514.
- [276] Arthur Kosowsky and Michael S. Turner. Gravitational radiation from colliding vacuum bubbles: envelope approximation to many bubble collisions. *Phys. Rev. D*, 47:4372–4391, 1993. doi:10.1103/PhysRevD.47.4372.
- [277] Mark Hindmarsh. Sound shell model for acoustic gravitational wave production at a first-order phase transition in the early Universe. *Phys. Rev. Lett.*, 120(7):071301, 2018. doi:10.1103/PhysRevLett.120.071301.
- [278] Ue-Li Pen and Neil Turok. Shocks in the Early Universe. *Phys. Rev. Lett.*, 117(13):131301,

2016. doi:10.1103/PhysRevLett.117.131301.
- [279] Pierre Auclair, Chiara Caprini, Daniel Cutting, Mark Hindmarsh, Kari Rummukainen, Danièle A. Steer, and David J. Weir. Generation of gravitational waves from freely decaying turbulence. *JCAP*, 09:029, 2022. doi:10.1088/1475-7516/2022/09/029.
- [280] Mark Hindmarsh, Stephan J. Huber, Kari Rummukainen, and David J. Weir. Shape of the acoustic gravitational wave power spectrum from a first order phase transition. *Phys. Rev. D*, 96(10):103520, 2017. doi:10.1103/PhysRevD.96.103520. [Erratum: Phys.Rev.D 101, 089902 (2020)].
- [281] Huai-Ke Guo, Kuver Sinha, Daniel Vagie, and Graham White. Phase Transitions in an Expanding Universe: Stochastic Gravitational Waves in Standard and Non-Standard Histories. *JCAP*, 01:001, 2021. doi:10.1088/1475-7516/2021/01/001.
- [282] Daniel Cutting, Mark Hindmarsh, and David J. Weir. Vorticity, kinetic energy, and suppressed gravitational wave production in strong first order phase transitions. *Phys. Rev. Lett.*, 125(2):021302, 2019. doi:10.1103/PhysRevLett.125.021302.
- [283] Graham White. *Electroweak Baryogenesis (Second Edition): An introduction*. IOP, 4 2022. ISBN 978-0-7503-3569-0, 978-0-7503-3570-6, 978-0-7503-3571-3. doi:10.1088/978-0-7503-3571-3.
- [284] Chloe Gowling and Mark Hindmarsh. Observational prospects for phase transitions at LISA: Fisher matrix analysis. *JCAP*, 10:039, 2021. doi:10.1088/1475-7516/2021/10/039.
- [285] Mark Hindmarsh and Mulham Hijazi. Gravitational waves from first order cosmological phase transitions in the Sound Shell Model. *JCAP*, 12:062, 2019. doi:10.1088/1475-7516/2019/12/062.
- [286] Felix Giese, Thomas Konstandin, and Jorinde van de Vis. Model-independent energy budget of cosmological first-order phase transitions—A sound argument to go beyond the bag model. *JCAP*, 07(07):057, 2020. doi:10.1088/1475-7516/2020/07/057.
- [287] Tuomas V. I. Tenkanen and Jorinde van de Vis. Speed of sound in cosmological phase transitions and effect on gravitational waves. *JHEP*, 08:302, 2022. doi:10.1007/JHEP08(2022)302.
- [288] Ryusuke Jinno, Thomas Konstandin, Henrique Rubira, and Jorinde van de Vis. Effect of density fluctuations on gravitational wave production in first-order phase transitions. *JCAP*, 12(12):019, 2021. doi:10.1088/1475-7516/2021/12/019.
- [289] Dietrich Bodeker and Guy D. Moore. Electroweak Bubble Wall Speed Limit. *JCAP*, 05:025,

2017. doi:10.1088/1475-7516/2017/05/025.
- [290] Stefan H ocher, Jonathan Kozaczuk, Andrew J. Long, Jessica Turner, and Yikun Wang. Towards an all-orders calculation of the electroweak bubble wall velocity. *JCAP*, 03:009, 2021. doi:10.1088/1475-7516/2021/03/009.
- [291] Wen-Yuan Ai, Bjorn Garbrecht, and Carlos Tamarit. Bubble wall velocities in local equilibrium. *JCAP*, 03(03):015, 2022. doi:10.1088/1475-7516/2022/03/015.
- [292] Jose Ramon Espinosa and Mariano Quiros. Novel Effects in Electroweak Breaking from a Hidden Sector. *Phys. Rev. D*, 76:076004, 2007. doi:10.1103/PhysRevD.76.076004.
- [293] J. R. Espinosa, T. Konstandin, J. M. No, and M. Quiros. Some Cosmological Implications of Hidden Sectors. *Phys. Rev. D*, 78:123528, 2008. doi:10.1103/PhysRevD.78.123528.
- [294] Thomas Konstandin and Geraldine Servant. Cosmological Consequences of Nearly Conformal Dynamics at the TeV scale. *JCAP*, 12:009, 2011. doi:10.1088/1475-7516/2011/12/009.
- [295] Thomas Konstandin and Geraldine Servant. Natural Cold Baryogenesis from Strongly Interacting Electroweak Symmetry Breaking. *JCAP*, 07:024, 2011. doi:10.1088/1475-7516/2011/07/024.
- [296] Geraldine Servant. Baryogenesis from Strong CP Violation and the QCD Axion. *Phys. Rev. Lett.*, 113(17):171803, 2014. doi:10.1103/PhysRevLett.113.171803.
- [297] Kaori Fuyuto and Eibun Senaha. Sphaleron and critical bubble in the scale invariant two Higgs doublet model. *Phys. Lett. B*, 747:152–157, 2015. doi:10.1016/j.physletb.2015.05.061.
- [298] Francesco Sannino and Jussi Virkaj arvi. First Order Electroweak Phase Transition from (Non)Conformal Extensions of the Standard Model. *Phys. Rev. D*, 92(4):045015, 2015. doi:10.1103/PhysRevD.92.045015.
- [299] Marek Lewicki and Ville Vaskonen. Gravitational waves from colliding vacuum bubbles in gauge theories. *Eur. Phys. J. C*, 81(5):437, 2021. doi:10.1140/epjc/s10052-021-09232-3. [Erratum: *Eur.Phys.J.C* 81, 1077 (2021)].
- [300] Marek Lewicki and Ville Vaskonen. Gravitational waves from bubble collisions and fluid motion in strongly supercooled phase transitions. *Eur. Phys. J. C*, 83(2):109, 2023. doi:10.1140/epjc/s10052-023-11241-3.
- [301] Paul H. Ginsparg. First Order and Second Order Phase Transitions in Gauge Theories at Finite Temperature. *Nucl. Phys. B*, 170:388–408, 1980. doi:10.1016/0550-3213(80)90418-6.
- [302] Thomas Appelquist and Robert D. Pisarski. High-Temperature Yang-Mills Theories

- and Three-Dimensional Quantum Chromodynamics. *Phys. Rev. D*, 23:2305, 1981. doi:10.1103/PhysRevD.23.2305.
- [303] Sudhir Nadkarni. Dimensional Reduction in Hot QCD. *Phys. Rev. D*, 27:917, 1983. doi:10.1103/PhysRevD.27.917.
- [304] N. P. Landsman. Limitations to Dimensional Reduction at High Temperature. *Nucl. Phys. B*, 322:498–530, 1989. doi:10.1016/0550-3213(89)90424-0.
- [305] K. Farakos, K. Kajantie, K. Rummukainen, and Mikhail E. Shaposhnikov. 3-D physics and the electroweak phase transition: Perturbation theory. *Nucl. Phys. B*, 425:67–109, 1994. doi:10.1016/0550-3213(94)90173-2.
- [306] Eric Braaten and Agustin Nieto. Effective field theory approach to high temperature thermodynamics. *Phys. Rev. D*, 51:6990–7006, 1995. doi:10.1103/PhysRevD.51.6990.
- [307] Eric Braaten and Agustin Nieto. Free energy of QCD at high temperature. *Phys. Rev. D*, 53:3421–3437, 1996. doi:10.1103/PhysRevD.53.3421.
- [308] K. Kajantie, M. Laine, K. Rummukainen, and Mikhail E. Shaposhnikov. Generic rules for high temperature dimensional reduction and their application to the standard model. *Nucl. Phys. B*, 458:90–136, 1996. doi:10.1016/0550-3213(95)00549-8.
- [309] David Curtin, Jyotirmoy Roy, and Graham White. Gravitational waves and tadpole resummation: Efficient and easy convergence of finite temperature QFT. 11 2022.
- [310] Michael Dine, Robert G. Leigh, Patrick Y. Huet, Andrei D. Linde, and Dmitri A. Linde. Towards the theory of the electroweak phase transition. *Phys. Rev. D*, 46:550–571, 1992. doi:10.1103/PhysRevD.46.550.
- [311] J. R. Espinosa, M. Quiros, and F. Zwirner. On the phase transition in the scalar theory. *Phys. Lett. B*, 291:115–124, 1992. doi:10.1016/0370-2693(92)90129-R.
- [312] C. Glenn Boyd, David E. Brahm, and Stephen D. H. Hsu. Corrections to the electroweak effective action at finite temperature. *Phys. Rev. D*, 48:4952–4962, 1993. doi:10.1103/PhysRevD.48.4952.
- [313] J. R. Espinosa, M. Quiros, and F. Zwirner. On the nature of the electroweak phase transition. *Phys. Lett. B*, 314:206–216, 1993. doi:10.1016/0370-2693(93)90450-V.
- [314] C. Glenn Boyd, David E. Brahm, and Stephen D. H. Hsu. Resummation methods at finite temperature: The Tadpole way. *Phys. Rev. D*, 48:4963–4973, 1993. doi:10.1103/PhysRevD.48.4963.

- [315] David Curtin, Patrick Meade, and Harikrishnan Ramani. Thermal Resummation and Phase Transitions. *Eur. Phys. J. C*, 78(9):787, 2018. doi:10.1140/epjc/s10052-018-6268-0.
- [316] Dietrich Bodeker and Guy D. Moore. Can electroweak bubble walls run away? *JCAP*, 0905:009, 2009. doi:10.1088/1475-7516/2009/05/009.
- [317] Wen-Yuan Ai. Logarithmically divergent friction on ultrarelativistic bubble walls. 8 2023.
- [318] Chiara Caprini, Ruth Durrer, and Geraldine Servant. Gravitational wave generation from bubble collisions in first-order phase transitions: An analytic approach. *Phys. Rev. D*, 77:124015, 2008. doi:10.1103/PhysRevD.77.124015.
- [319] Stephan J. Huber and Thomas Konstandin. Gravitational Wave Production by Collisions: More Bubbles. *JCAP*, 0809:022, 2008. doi:10.1088/1475-7516/2008/09/022.
- [320] Chiara Caprini, Ruth Durrer, Thomas Konstandin, and Geraldine Servant. General Properties of the Gravitational Wave Spectrum from Phase Transitions. *Phys. Rev.*, D79:083519, 2009. doi:10.1103/PhysRevD.79.083519.
- [321] Ryusuke Jinno and Masahiro Takimoto. Gravitational waves from bubble collisions: analytic derivation. *Phys. Rev.*, D95(2):024009, 2017. doi:10.1103/PhysRevD.95.024009.
- [322] Andreĭ Nikolaevich Kolmogorov. *Turbulence: the legacy of AN Kolmogorov*. Cambridge university press, 1995.
- [323] Arthur Kosowsky, Andrew Mack, and Tinatin Kahniashvili. Gravitational radiation from cosmological turbulence. *Phys. Rev. D*, 66:024030, 2002. doi:10.1103/PhysRevD.66.024030.
- [324] Chiara Caprini, Ruth Durrer, and Geraldine Servant. The stochastic gravitational wave background from turbulence and magnetic fields generated by a first-order phase transition. *JCAP*, 0912:024, 2009. doi:10.1088/1475-7516/2009/12/024.
- [325] Andrei D. Linde. Infrared Problem in Thermodynamics of the Yang-Mills Gas. *Phys. Lett. B*, 96:289–292, 1980. doi:10.1016/0370-2693(80)90769-8.
- [326] Michael Dine, Robert G Leigh, Patrick Huet, Andrei Linde, and Dmitri Linde. Towards the theory of the electroweak phase transition. *Physical Review D*, 46(2):550, 1992.
- [327] Oliver Gould, Sinan Güyer, and Kari Rummukainen. First-order electroweak phase transitions: A nonperturbative update. *Phys. Rev. D*, 106(11):114507, 2022. doi:10.1103/PhysRevD.106.114507.
- [328] Andreas Ekstedt, Oliver Gould, and Johan Löfgren. Radiative first-order phase transitions to next-to-next-to-leading order. *Phys. Rev. D*, 106(3):036012, 2022. doi:

- 10.1103/PhysRevD.106.036012.
- [329] Djuna Croon, Oliver Gould, Philipp Schicho, Tuomas V. I. Tenkanen, and Graham White. Theoretical uncertainties for cosmological first-order phase transitions. *JHEP*, 04:055, 2021. doi:10.1007/JHEP04(2021)055.
- [330] Oliver Gould and Tuomas V. I. Tenkanen. On the perturbative expansion at high temperature and implications for cosmological phase transitions. *JHEP*, 06:069, 2021. doi:10.1007/JHEP06(2021)069.
- [331] Fei Gao, Jing Chen, Yu-Xin Liu, Si-Xue Qin, Craig D. Roberts, and Sebastian M. Schmidt. Phase diagram and thermal properties of strong-interaction matter. *Phys. Rev. D*, 93(9):094019, 2016. doi:10.1103/PhysRevD.93.094019.
- [332] Mark Hindmarsh, Stephan J. Huber, Kari Rummukainen, and David J. Weir. Numerical simulations of acoustically generated gravitational waves at a first order phase transition. *Phys. Rev.*, D92(12):123009, 2015. doi:10.1103/PhysRevD.92.123009.
- [333] Hillary L. Child and John T. Giblin, Jr. Gravitational Radiation from First-Order Phase Transitions. *JCAP*, 10:001, 2012. doi:10.1088/1475-7516/2012/10/001.
- [334] Daniel Cutting, Mark Hindmarsh, and David J. Weir. Gravitational waves from vacuum first-order phase transitions: from the envelope to the lattice. *Phys. Rev. D*, 97(12):123513, 2018. doi:10.1103/PhysRevD.97.123513.
- [335] Daniel Cutting, Elba Granados Escartin, Mark Hindmarsh, and David J. Weir. Gravitational waves from vacuum first order phase transitions II: from thin to thick walls. *Phys. Rev. D*, 103(2):023531, 2021. doi:10.1103/PhysRevD.103.023531.
- [336] Ryusuke Jinno and Masahiro Takimoto. Gravitational waves from bubble dynamics: Beyond the Envelope. *JCAP*, 01:060, 2019. doi:10.1088/1475-7516/2019/01/060.
- [337] Thomas Konstandin. Gravitational radiation from a bulk flow model. *JCAP*, 03:047, 2018. doi:10.1088/1475-7516/2018/03/047.
- [338] Ryusuke Jinno, Hyeonseok Seong, Masahiro Takimoto, and Choong Min Um. Gravitational waves from first-order phase transitions: Ultra-supercooled transitions and the fate of relativistic shocks. *JCAP*, 10:033, 2019. doi:10.1088/1475-7516/2019/10/033.
- [339] Ryusuke Jinno, Thomas Konstandin, and Henrique Rubira. A hybrid simulation of gravitational wave production in first-order phase transitions. *JCAP*, 04:014, 2021. doi:10.1088/1475-7516/2021/04/014.

- [340] Edward W. Kolb and Michael S. Turner. *The Early Universe*, volume 69. 1990. ISBN 978-0-201-62674-2. doi:10.1201/9780429492860.
- [341] A. Vilenkin and E. P. S. Shellard. *Cosmic Strings and Other Topological Defects*. Cambridge University Press, 7 2000. ISBN 978-0-521-65476-0.
- [342] Michele Maggiore. *Gravitational Waves. Vol. 2: Astrophysics and Cosmology*. Oxford University Press, 3 2018. ISBN 978-0-19-857089-9.
- [343] Ken'ichi Saikawa. A review of gravitational waves from cosmic domain walls. *Universe*, 3 (2):40, 2017. doi:10.3390/universe3020040.
- [344] David I. Dunsky, Anish Ghoshal, Hitoshi Murayama, Yuki Sakakihara, and Graham White. GUTs, hybrid topological defects, and gravitational waves. *Phys. Rev. D*, 106(7):075030, 2022. doi:10.1103/PhysRevD.106.075030.
- [345] Ya. B. Zeldovich, I. Yu. Kobzarev, and L. B. Okun. Cosmological Consequences of the Spontaneous Breakdown of Discrete Symmetry. *Zh. Eksp. Teor. Fiz.*, 67:3–11, 1974.
- [346] A. Vilenkin. Gravitational Field of Vacuum Domain Walls and Strings. *Phys. Rev. D*, 23: 852–857, 1981. doi:10.1103/PhysRevD.23.852.
- [347] Graciela B. Gelmini, Marcelo Gleiser, and Edward W. Kolb. Cosmology of Biased Discrete Symmetry Breaking. *Phys. Rev. D*, 39:1558, 1989. doi:10.1103/PhysRevD.39.1558.
- [348] Sebastian E. Larsson, Subir Sarkar, and Peter L. White. Evading the cosmological domain wall problem. *Phys. Rev. D*, 55:5129–5135, 1997. doi:10.1103/PhysRevD.55.5129.
- [349] Cheng-Wei Chiang and Bo-Qiang Lu. Testing clockwork axion with gravitational waves. *JCAP*, 05:049, 2021. doi:10.1088/1475-7516/2021/05/049.
- [350] Stephen F. King, Rishav Roshan, Xin Wang, Graham White, and Masahito Yamazaki. Quantum Gravity Effects on Dark Matter and Gravitational Waves. 8 2023.
- [351] Bo-Qiang Lu and Cheng-Wei Chiang. Nano-Hertz stochastic gravitational wave background from domain wall annihilation. 7 2023.
- [352] Stephen F. King, Rishav Roshan, Xin Wang, Graham White, and Masahito Yamazaki. Quantum Gravity Effects on Fermionic Dark Matter and Gravitational Waves. 11 2023.
- [353] Takashi Hiramatsu, Masahiro Kawasaki, and Ken'ichi Saikawa. On the estimation of gravitational wave spectrum from cosmic domain walls. *JCAP*, 02:031, 2014. doi:10.1088/1475-7516/2014/02/031.
- [354] Takashi Hiramatsu, Masahiro Kawasaki, Ken'ichi Saikawa, and Toyokazu Sekiguchi. Ax-

- ion cosmology with long-lived domain walls. *JCAP*, 01:001, 2013. doi:10.1088/1475-7516/2013/01/001.
- [355] P. P. Avelino, C. J. A. P. Martins, and J. C. R. E. Oliveira. One-scale model for domain wall network evolution. *Phys. Rev. D*, 72:083506, 2005. doi:10.1103/PhysRevD.72.083506.
- [356] Chiara Caprini et al. Detecting gravitational waves from cosmological phase transitions with LISA: an update. *JCAP*, 03:024, 2020. doi:10.1088/1475-7516/2020/03/024.
- [357] Ricardo Z. Ferreira, Alessio Notari, Oriol Pujolas, and Fabrizio Rompineve. Gravitational waves from domain walls in Pulsar Timing Array datasets. *JCAP*, 02:001, 2023. doi:10.1088/1475-7516/2023/02/001.
- [358] Yongcheng Wu, Ke-Pan Xie, and Ye-Ling Zhou. Collapsing domain walls beyond Z2. *Phys. Rev. D*, 105(9):095013, 2022. doi:10.1103/PhysRevD.105.095013.
- [359] T.W.B. Kibble. Topology of Cosmic Domains and Strings. *J. Phys. A*, 9:1387–1398, 1976. doi:10.1088/0305-4470/9/8/029.
- [360] Holger Bech Nielsen and P. Olesen. Vortex Line Models for Dual Strings. *Nucl. Phys.*, B61:45–61, 1973. doi:10.1016/0550-3213(73)90350-7.
- [361] Tanmay Vachaspati and Alexander Vilenkin. Formation and Evolution of Cosmic Strings. *Phys. Rev. D*, 30:2036, 1984. doi:10.1103/PhysRevD.30.2036.
- [362] Stephen F. King, Silvia Pascoli, Jessica Turner, and Ye-Ling Zhou. Gravitational Waves and Proton Decay: Complementary Windows into Grand Unified Theories. *Phys. Rev. Lett.*, 126(2):021802, 2021. doi:10.1103/PhysRevLett.126.021802.
- [363] Wei-Chih Huang, Manuel Reichert, Francesco Sannino, and Zhi-Wei Wang. Testing the Dark Confined Landscape: From Lattice to Gravitational Waves. 12 2020.
- [364] Edmund J. Copeland, Robert C. Myers, and Joseph Polchinski. Cosmic F and D strings. *JHEP*, 06:013, 2004. doi:10.1088/1126-6708/2004/06/013.
- [365] Gia Dvali and Alexander Vilenkin. Formation and evolution of cosmic D strings. *JCAP*, 0403:010, 2004. doi:10.1088/1475-7516/2004/03/010.
- [366] Joseph Polchinski. Introduction to cosmic F- and D-strings. In *String theory: From gauge interactions to cosmology. Proceedings, NATO Advanced Study Institute, Cargese, France, June 7-19, 2004*, pages 229–253, 2004.
- [367] Mark G. Jackson, Nicholas T. Jones, and Joseph Polchinski. Collisions of cosmic F and D-strings. *JHEP*, 10:013, 2005. doi:10.1088/1126-6708/2005/10/013.

- [368] S. H. Henry Tye, Ira Wasserman, and Mark Wyman. Scaling of multi-tension cosmic superstring networks. *Phys. Rev.*, D71:103508, 2005. doi:10.1103/PhysRevD.71.103508, 10.1103/PhysRevD.71.129906. [Erratum: *Phys. Rev.* D71,129906(2005)].
- [369] T. W. B. Kibble, George Lazarides, and Q. Shafi. Strings in SO(10). *Phys. Lett. B*, 113: 237–239, 1982. doi:10.1016/0370-2693(82)90829-2.
- [370] Mark Hindmarsh. Cosmic strings: Dead again? In *1st International Conference on Particle Physics and the Early Universe*, pages 420–422, 9 1997. doi:10.1142/9789814447263_0057.
- [371] Graham Vincent, Nuno D. Antunes, and Mark Hindmarsh. Numerical simulations of string networks in the Abelian Higgs model. *Phys. Rev. Lett.*, 80:2277–2280, 1998. doi:10.1103/PhysRevLett.80.2277.
- [372] Daiju Matsunami, Levon Pogosian, Ayush Saurabh, and Tanmay Vachaspati. Decay of Cosmic String Loops Due to Particle Radiation. *Phys. Rev. Lett.*, 122(20):201301, 2019. doi:10.1103/PhysRevLett.122.201301.
- [373] Mark Hindmarsh, Joanes Lizarraga, Ander Urrio, and Jon Urrestilla. Loop decay in Abelian-Higgs string networks. *Phys. Rev. D*, 104(4):043519, 2021. doi:10.1103/PhysRevD.104.043519.
- [374] Jose J. Blanco-Pillado, Daniel Jiménez-Aguilar, Joanes Lizarraga, Asier Lopez-Eiguren, Ken D. Olum, Ander Urrio, and Jon Urrestilla. Nambu-Goto dynamics of field theory cosmic string loops. *JCAP*, 05:035, 2023. doi:10.1088/1475-7516/2023/05/035.
- [375] C. J. A. P. Martins and E. P. S. Shellard. Quantitative string evolution. *Phys. Rev. D*, 54: 2535–2556, 1996. doi:10.1103/PhysRevD.54.2535.
- [376] C. J. A. P. Martins and E. P. S. Shellard. Extending the velocity dependent one scale string evolution model. *Phys. Rev. D*, 65:043514, 2002. doi:10.1103/PhysRevD.65.043514.
- [377] Jose J. Blanco-Pillado, Ken D. Olum, and Benjamin Shlaer. The number of cosmic string loops. *Phys. Rev.*, D89(2):023512, 2014. doi:10.1103/PhysRevD.89.023512.
- [378] Jose J. Blanco-Pillado and Ken D. Olum. Stochastic gravitational wave background from smoothed cosmic string loops. *Phys. Rev. D*, 96(10):104046, 2017. doi:10.1103/PhysRevD.96.104046.
- [379] A. Vilenkin. Gravitational radiation from cosmic strings. *Phys. Lett. B*, 107:47–50, 1981. doi:10.1016/0370-2693(81)91144-8.
- [380] Jose J. Blanco-Pillado, Ken D. Olum, and Benjamin Shlaer. Large parallel cosmic string

- simulations: New results on loop production. *Phys. Rev. D*, 83:083514, 2011. doi:10.1103/PhysRevD.83.083514.
- [381] Pierre Auclair et al. Probing the gravitational wave background from cosmic strings with LISA. *JCAP*, 2004:034, 2020. doi:10.1088/1475-7516/2020/04/034.
- [382] L. Sousa and P. P. Avelino. Stochastic Gravitational Wave Background generated by Cosmic String Networks: Velocity-Dependent One-Scale model versus Scale-Invariant Evolution. *Phys. Rev. D*, 88(2):023516, 2013. doi:10.1103/PhysRevD.88.023516.
- [383] Jose J. Blanco-Pillado, Ken D. Olum, and Benjamin Shlaer. Large parallel cosmic string simulations: New results on loop production. *Phys. Rev.*, D83:083514, 2011. doi:10.1103/PhysRevD.83.083514.
- [384] Larissa Lorenz, Christophe Ringeval, and Mairi Sakellariadou. Cosmic string loop distribution on all length scales and at any redshift. *JCAP*, 10:003, 2010. doi:10.1088/1475-7516/2010/10/003.
- [385] Christophe Ringeval, Mairi Sakellariadou, and Francois Bouchet. Cosmological evolution of cosmic string loops. *JCAP*, 0702:023, 2007. doi:10.1088/1475-7516/2007/02/023.
- [386] Chia-Feng Chang and Yanou Cui. Stochastic Gravitational Wave Background from Global Cosmic Strings. *Phys. Dark Univ.*, 29:100604, 2020. doi:10.1016/j.dark.2020.100604.
- [387] Chia-Feng Chang and Yanou Cui. Gravitational waves from global cosmic strings and cosmic archaeology. *JHEP*, 03:114, 2022. doi:10.1007/JHEP03(2022)114.
- [388] Pasquale Di Bari, Stephen F. King, and Moinul Hossain Rahat. Gravitational waves from phase transitions and cosmic strings in neutrino mass models with multiple Majorons. 6 2023.
- [389] Alexander Vilenkin and Tanmay Vachaspati. Radiation of Goldstone Bosons From Cosmic Strings. *Phys. Rev. D*, 35:1138, 1987. doi:10.1103/PhysRevD.35.1138.
- [390] R. A. Battye and E. P. S. Shellard. Recent perspectives on axion cosmology. In *1st International Heidelberg Conference on Dark Matter in Astro and Particle Physics*, pages 554–579, 6 1997.
- [391] Tanmay Vachaspati and Alexander Vilenkin. Gravitational Radiation from Cosmic Strings. *Phys. Rev.*, D31:3052, 1985. doi:10.1103/PhysRevD.31.3052.
- [392] Bruce Allen and E. P. S. Shellard. Gravitational radiation from cosmic strings. *Phys. Rev. D*, 45:1898–1912, 1992. doi:10.1103/PhysRevD.45.1898.

- [393] R. A. Battye and E. P. S. Shellard. Primordial gravitational waves: A Probe of the very early universe. 1996.
- [394] C. J. A. P. Martins, J. N. Moore, and E. P. S. Shellard. A Unified model for vortex string network evolution. *Phys. Rev. Lett.*, 92:251601, 2004. doi:10.1103/PhysRevLett.92.251601.
- [395] C. J. A. P. Martins and M. M. P. V. P. Cabral. Physical and invariant models for defect network evolution. *Phys. Rev. D*, 93(4):043542, 2016. doi:10.1103/PhysRevD.93.043542. [Addendum: Phys.Rev.D 93, 069902 (2016)].
- [396] C. J. A. P. Martins. Scaling properties of cosmological axion strings. *Phys. Lett. B*, 788: 147–151, 2019. doi:10.1016/j.physletb.2018.11.031.
- [397] J. R. C. C. Correia and C. J. A. P. Martins. Extending and Calibrating the Velocity dependent One-Scale model for Cosmic Strings with One Thousand Field Theory Simulations. *Phys. Rev. D*, 100(10):103517, 2019. doi:10.1103/PhysRevD.100.103517.
- [398] Yann Gouttenoire, Géraldine Servant, and Peera Simakachorn. Beyond the Standard Models with Cosmic Strings. *JCAP*, 2007:032, 2020. doi:10.1088/1475-7516/2020/07/032.
- [399] George Lazarides, Rinku Maji, Rishav Roshan, and Qaisar Shafi. Heavier W boson, dark matter, and gravitational waves from strings in an $SO(10)$ axion model. *Phys. Rev. D*, 106(5):055009, 2022. doi:10.1103/PhysRevD.106.055009.
- [400] Debasish Borah, Suruj Jyoti Das, and Rishav Roshan. Probing high scale seesaw and PBH generated dark matter via gravitational waves with multiple tilts. 8 2022.
- [401] George Lazarides, Rinku Maji, Rishav Roshan, and Qaisar Shafi. A predictive $SO(10)$ model. *JCAP*, 12:009, 2022. doi:10.1088/1475-7516/2022/12/009.
- [402] Debasish Borah, Suruj Jyoti Das, Rishav Roshan, and Rome Samanta. Imprint of PBH domination on gravitational waves generated by cosmic strings. *Phys. Rev. D*, 108(2):023531, 2023. doi:10.1103/PhysRevD.108.023531.
- [403] Vitaly Vanchurin, Ken D. Olum, and Alexander Vilenkin. Scaling of cosmic string loops. *Phys. Rev.*, D74:063527, 2006. doi:10.1103/PhysRevD.74.063527.
- [404] C. J. A. P. Martins and E. P. S. Shellard. Fractal properties and small-scale structure of cosmic string networks. *Phys. Rev.*, D73:043515, 2006. doi:10.1103/PhysRevD.73.043515.
- [405] Ken D. Olum and Vitaly Vanchurin. Cosmic string loops in the expanding Universe. *Phys. Rev.*, D75:063521, 2007. doi:10.1103/PhysRevD.75.063521.
- [406] Gerard 't Hooft. Magnetic Monopoles in Unified Gauge Theories. *Nucl. Phys. B*, 79:276–284,

1974. doi:10.1016/0550-3213(74)90486-6.
- [407] Alexander M. Polyakov. Particle Spectrum in the Quantum Field Theory. *JETP Lett.*, 20: 194–195, 1974.
- [408] W. H. Zurek. Cosmological Experiments in Superfluid Helium? *Nature*, 317:505–508, 1985. doi:10.1038/317505a0.
- [409] Jeff A. Dror, Takashi Hiramatsu, Kazunori Kohri, Hitoshi Murayama, and Graham White. Testing the Seesaw Mechanism and Leptogenesis with Gravitational Waves. *Phys. Rev. Lett.*, 124(4):041804, 2020. doi:10.1103/PhysRevLett.124.041804.
- [410] Paul Langacker and So-Young Pi. Magnetic Monopoles in Grand Unified Theories. *Phys. Rev. Lett.*, 45:1, 1980. doi:10.1103/PhysRevLett.45.1.
- [411] George Lazarides, Q. Shafi, and T. F. Walsh. Cosmic Strings and Domains in Unified Theories. *Nucl. Phys. B*, 195:157–172, 1982. doi:10.1016/0550-3213(82)90052-9.
- [412] Alexander Vilenkin. Cosmological evolution of monopoles connected by strings. *Nuclear Physics B*, 196(2):240–258, 1982.
- [413] Wilfried Buchmuller, Valerie Domcke, and Kai Schmitz. Metastable cosmic strings. *JCAP*, 11:020, 2023. doi:10.1088/1475-7516/2023/11/020.
- [414] Xavier Martin and Alexander Vilenkin. Gravitational radiation from monopoles connected by strings. *Phys. Rev. D*, 55:6054–6060, 1997. doi:10.1103/PhysRevD.55.6054.
- [415] Louis Leblond, Benjamin Shlaer, and Xavier Siemens. Gravitational Waves from Broken Cosmic Strings: The Bursts and the Beads. *Phys. Rev. D*, 79:123519, 2009. doi:10.1103/PhysRevD.79.123519.
- [416] Wilfried Buchmuller, Valerie Domcke, and Kai Schmitz. Stochastic gravitational-wave background from metastable cosmic strings. 7 2021.
- [417] Steven Weinberg. *Gravitation and Cosmology: Principles and Applications of the General Theory of Relativity*. John Wiley and Sons, New York, 1972. ISBN 978-0-471-92567-5, 978-0-471-92567-5.
- [418] Alexander Vilenkin and E Paul S Shellard. *Cosmic strings and other topological defects*. Cambridge University Press, 2000.
- [419] T.W.B. Kibble, George Lazarides, and Q. Shafi. Walls Bounded by Strings. *Phys. Rev. D*, 26:435, 1982. doi:10.1103/PhysRevD.26.435.
- [420] John Preskill and Alexander Vilenkin. Decay of metastable topological defects. *Phys. Rev.*

- D*, 47:2324–2342, 1993. doi:10.1103/PhysRevD.47.2324.
- [421] L. Sousa and P. P. Avelino. Stochastic gravitational wave background generated by cosmic string networks: Velocity-dependent one-scale model versus scale-invariant evolution. *Physical Review D*, 88(2), Jul 2013. ISSN 1550-2368. doi:10.1103/physrevd.88.023516. URL <http://dx.doi.org/10.1103/PhysRevD.88.023516>.
- [422] Tanmay Vachaspati and Alexander Vilenkin. Gravitational radiation from cosmic strings. *Phys. Rev. D*, 31:3052–3058, Jun 1985. doi:10.1103/PhysRevD.31.3052. URL <https://link.aps.org/doi/10.1103/PhysRevD.31.3052>.
- [423] Alexander Vilenkin. Cosmic Strings and Domain Walls. *Phys. Rept.*, 121:263–315, 1985. doi:10.1016/0370-1573(85)90033-X.
- [424] R. Holman, T. W. B. Kibble, and Soo-Jong Rey. How efficient is the Langacker-Pi mechanism of monopole annihilation? *Phys. Rev. Lett.*, 69:241–244, 1992. doi:10.1103/PhysRevLett.69.241.
- [425] Xavier Martin and Alexander Vilenkin. Gravitational wave background from hybrid topological defects. *Phys. Rev. Lett.*, 77:2879–2882, 1996. doi:10.1103/PhysRevLett.77.2879.
- [426] John Preskill. Cosmological Production of Superheavy Magnetic Monopoles. *Phys. Rev. Lett.*, 43:1365, 1979. doi:10.1103/PhysRevLett.43.1365.
- [427] T Goldman, Edward W Kolb, and Doug Toussaint. Gravitational clumping and the annihilation of monopoles. *Physical Review D*, 23(4):867, 1981.
- [428] N. Aghanim et al. Planck 2018 results. VI. Cosmological parameters. *Astron. Astrophys.*, 641:A6, 2020. doi:10.1051/0004-6361/201833910.
- [429] Yanou Cui, Marek Lewicki, David E. Morrissey, and James D. Wells. Probing the pre-BBN universe with gravitational waves from cosmic strings. *JHEP*, 01:081, 2019. doi:10.1007/JHEP01(2019)081.
- [430] Yanou Cui, Marek Lewicki, David E. Morrissey, and James D. Wells. Cosmic Archaeology with Gravitational Waves from Cosmic Strings. *Phys. Rev.*, D97(12):123505, 2018. doi:10.1103/PhysRevD.97.123505.
- [431] Simone Blasi, Vedran Brdar, and Kai Schmitz. Fingerprint of low-scale leptogenesis in the primordial gravitational-wave spectrum. *Phys. Rev. Res.*, 2(4):043321, 2020. doi:10.1103/PhysRevResearch.2.043321.
- [432] Yanou Cui, Marek Lewicki, and David E. Morrissey. Gravitational Wave Bursts as Harbingers

- of Cosmic Strings Diluted by Inflation. *Phys. Rev. Lett.*, 125(21):211302, 2020. doi:10.1103/PhysRevLett.125.211302.
- [433] Y. Akrami et al. Planck 2018 results. X. Constraints on inflation. *Astron. Astrophys.*, 641:A10, 2020. doi:10.1051/0004-6361/201833887.
- [434] G. S. F. Guedes, P. P. Avelino, and L. Sousa. Signature of inflation in the stochastic gravitational wave background generated by cosmic string networks. *Phys. Rev.*, D98(12):123505, 2018. doi:10.1103/PhysRevD.98.123505.
- [435] Xavier Siemens, Jolien Creighton, Irit Maor, Saikat Ray Majumder, Kipp Cannon, and Jocelyn Read. Gravitational wave bursts from cosmic (super)strings: Quantitative analysis and constraints. *Phys. Rev.*, D73:105001, 2006. doi:10.1103/PhysRevD.73.105001.
- [436] Christophe Ringeval and Teruaki Suyama. Stochastic gravitational waves from cosmic string loops in scaling. *JCAP*, 1712:027, 2017. doi:10.1088/1475-7516/2017/12/027.
- [437] M. Fukugita and T. Yanagida. Baryogenesis Without Grand Unification. *Phys. Lett. B*, 174:45–47, 1986. doi:10.1016/0370-2693(86)91126-3.
- [438] M. A. Luty. Baryogenesis via leptogenesis. *Phys. Rev. D*, 45:455–465, 1992. doi:10.1103/PhysRevD.45.455.
- [439] Apostolos Pilaftsis. CP violation and baryogenesis due to heavy Majorana neutrinos. *Phys. Rev. D*, 56:5431–5451, 1997. doi:10.1103/PhysRevD.56.5431.
- [440] Peter Minkowski. $\mu \rightarrow e\gamma$ at a Rate of One Out of 10^9 Muon Decays? *Phys. Lett. B*, 67:421–428, 1977. doi:10.1016/0370-2693(77)90435-X.
- [441] Tsutomu Yanagida. Horizontal gauge symmetry and masses of neutrinos. *Conf. Proc. C*, 7902131:95–99, 1979.
- [442] Tsutomu Yanagida. Horizontal Symmetry and Mass of the Top Quark. *Phys. Rev. D*, 20:2986, 1979. doi:10.1103/PhysRevD.20.2986.
- [443] Murray Gell-Mann, Pierre Ramond, and Richard Slansky. Complex Spinors and Unified Theories. *Conf. Proc. C*, 790927:315–321, 1979.
- [444] Rabindra N. Mohapatra and Goran Senjanovic. Neutrino Mass and Spontaneous Parity Nonconservation. *Phys. Rev. Lett.*, 44:912, 1980. doi:10.1103/PhysRevLett.44.912.
- [445] J. Schechter and J. W. F. Valle. Neutrino Masses in $SU(2) \times U(1)$ Theories. *Phys. Rev. D*, 22:2227, 1980. doi:10.1103/PhysRevD.22.2227.
- [446] J. Schechter and J. W. F. Valle. Neutrino Decay and Spontaneous Violation of Lepton

- Number. *Phys. Rev. D*, 25:774, 1982. doi:10.1103/PhysRevD.25.774.
- [447] Arghyajit Datta, Rishav Roshan, and Arunansu Sil. Imprint of the Seesaw Mechanism on Feebly Interacting Dark Matter and the Baryon Asymmetry. *Phys. Rev. Lett.*, 127(23): 231801, 2021. doi:10.1103/PhysRevLett.127.231801.
- [448] Amit Dutta Banik, Rishav Roshan, and Arunansu Sil. Neutrino mass and asymmetric dark matter: study with inert Higgs doublet and high scale validity. *JCAP*, 03:037, 2021. doi: 10.1088/1475-7516/2021/03/037.
- [449] Subhaditya Bhattacharya, Rishav Roshan, Arunansu Sil, and Drona Vatsyayan. Symmetry origin of Baryon Asymmetry, Dark Matter and Neutrino Mass. 5 2021.
- [450] Subhaditya Bhattacharya, Niloy Mondal, Rishav Roshan, and Drona Vatsyayan. Testing the dark and visible sides of the Seesaw. 12 2023.
- [451] V. A. Kuzmin, V. A. Rubakov, and M. E. Shaposhnikov. On the Anomalous Electroweak Baryon Number Nonconservation in the Early Universe. *Phys. Lett. B*, 155:36, 1985. doi: 10.1016/0370-2693(85)91028-7.
- [452] Luis Bento. Sphaleron relaxation temperatures. *JCAP*, 11:002, 2003. doi:10.1088/1475-7516/2003/11/002.
- [453] Michela D’Onofrio, Kari Rummukainen, and Anders Tranberg. Sphaleron Rate in the Minimal Standard Model. *Phys. Rev. Lett.*, 113(14):141602, 2014. doi: 10.1103/PhysRevLett.113.141602.
- [454] Bowen Fu, Anish Ghoshal, and Stephen F. King. Cosmic string gravitational waves from global $U(1)_{B-L}$ symmetry breaking as a probe of the type I seesaw scale. *JHEP*, 11:071, 2023. doi:10.1007/JHEP11(2023)071.
- [455] Stephen F. King, Silvia Pascoli, Jessica Turner, and Ye-Ling Zhou. Confronting $SO(10)$ GUTs with proton decay and gravitational waves. *JHEP*, 10:225, 2021. doi: 10.1007/JHEP10(2021)225.
- [456] Bowen Fu, Stephen F. King, Luca Marsili, Silvia Pascoli, Jessica Turner, and Ye-Ling Zhou. Testing Realistic $SO(10)$ SUSY GUTs with Proton Decay and Gravitational Waves. 8 2023.
- [457] Bowen Fu, Stephen F. King, Luca Marsili, Silvia Pascoli, Jessica Turner, and Ye-Ling Zhou. A predictive and testable unified theory of fermion masses, mixing and leptogenesis. *JHEP*, 11:072, 2022. doi:10.1007/JHEP11(2022)072.
- [458] Tom Banks and Lance J. Dixon. Constraints on String Vacua with Space-Time Supersym-

- metry. *Nucl. Phys. B*, 307:93–108, 1988. doi:10.1016/0550-3213(88)90523-8.
- [459] Tom Banks and Nathan Seiberg. Symmetries and Strings in Field Theory and Gravity. *Phys. Rev. D*, 83:084019, 2011. doi:10.1103/PhysRevD.83.084019.
- [460] Daniel Harlow and Edgar Shaghoulian. Global symmetry, Euclidean gravity, and the black hole information problem. *JHEP*, 04:175, 2021. doi:10.1007/JHEP04(2021)175.
- [461] Gabriella Agazie et al. The NANOGrav 15 yr Data Set: Evidence for a Gravitational-wave Background. *Astrophys. J. Lett.*, 951(1):L8, 2023. doi:10.3847/2041-8213/acdac6.
- [462] Adeela Afzal et al. The NANOGrav 15 yr Data Set: Search for Signals from New Physics. *Astrophys. J. Lett.*, 951(1):L11, 2023. doi:10.3847/2041-8213/acdc91.
- [463] J. Antoniadis et al. The second data release from the European Pulsar Timing Array III. Search for gravitational wave signals. 6 2023.
- [464] J. Antoniadis et al. The second data release from the European Pulsar Timing Array: V. Implications for massive black holes, dark matter and the early Universe. 6 2023.
- [465] Daniel J. Reardon et al. Search for an Isotropic Gravitational-wave Background with the Parkes Pulsar Timing Array. *Astrophys. J. Lett.*, 951(1):L6, 2023. doi:10.3847/2041-8213/acdd02.
- [466] Heng Xu et al. Searching for the Nano-Hertz Stochastic Gravitational Wave Background with the Chinese Pulsar Timing Array Data Release I. *Res. Astron. Astrophys.*, 23(7):075024, 2023. doi:10.1088/1674-4527/acdfa5.
- [467] Kenji Tomita. Non-linear theory of gravitational instability in the expanding universe. *Progress of Theoretical Physics*, 37(5):831–846, 1967.
- [468] Sabino Matarrese, Ornella Pantano, and Diego Saez. General-relativistic approach to the nonlinear evolution of collisionless matter. *Physical Review D*, 47(4):1311, 1993.
- [469] Sabino Matarrese, Ornella Pantano, and Diego Saez. General relativistic dynamics of irrotational dust: Cosmological implications. *Physical review letters*, 72(3):320, 1994.
- [470] Yashar Akrami, Frederico Arroja, M Ashdown, J Aumont, Carlo Baccigalupi, M Ballardini, Anthony J Banday, RB Barreiro, Nicola Bartolo, S Basak, et al. Planck 2018 results-x. constraints on inflation. *Astronomy & Astrophysics*, 641:A10, 2020.
- [471] Guillem Domènech. Scalar Induced Gravitational Waves Review. *Universe*, 7(11):398, 2021. doi:10.3390/universe7110398.
- [472] Assadullahi Hooshyar. Gravitational waves from an early matter era. *Phys. Rev. D*, 79:

- 083511, 2009.
- [473] Laila Alabidi, Kazunori Kohri, Misao Sasaki, and Yuuiti Sendouda. Observable induced gravitational waves from an early matter phase. *Journal of Cosmology and Astroparticle Physics*, 2013(05):033, 2013.
- [474] Keisuke Inomata, Kazunori Kohri, Tomohiro Nakama, and Takahiro Terada. Gravitational waves induced by scalar perturbations during a gradual transition from an early matter era to the radiation era. *Journal of Cosmology and Astroparticle Physics*, 2019(10):071, 2019.
- [475] Keisuke Inomata, Kazunori Kohri, Tomohiro Nakama, and Takahiro Terada. Enhancement of gravitational waves induced by scalar perturbations due to a sudden transition from an early matter era to the radiation era. *Physical Review D*, 100(4):043532, 2019.
- [476] Guido Altarelli and G. Isidori. Lower limit on the Higgs mass in the standard model: An Update. *Phys. Lett. B*, 337:141–144, 1994. doi:10.1016/0370-2693(94)91458-3.
- [477] J. A. Casas, J. R. Espinosa, and M. Quiros. Standard model stability bounds for new physics within LHC reach. *Phys. Lett. B*, 382:374–382, 1996. doi:10.1016/0370-2693(96)00682-X.
- [478] Thomas Hambye and Kurt Riessellmann. Matching conditions and Higgs mass upper bounds revisited. *Phys. Rev. D*, 55:7255–7262, 1997. doi:10.1103/PhysRevD.55.7255.
- [479] Marc Sher. Electroweak Higgs Potentials and Vacuum Stability. *Phys. Rept.*, 179:273–418, 1989. doi:10.1016/0370-1573(89)90061-6.
- [480] Peter Brockway Arnold. Can the Electroweak Vacuum Be Unstable? *Phys. Rev. D*, 40:613, 1989. doi:10.1103/PhysRevD.40.613.
- [481] Gino Isidori, Giovanni Ridolfi, and Alessandro Strumia. On the metastability of the standard model vacuum. *Nucl. Phys. B*, 609:387–409, 2001. doi:10.1016/S0550-3213(01)00302-9.
- [482] J. Ellis, J. R. Espinosa, G. F. Giudice, A. Hoecker, and A. Riotto. The Probable Fate of the Standard Model. *Phys. Lett. B*, 679:369–375, 2009. doi:10.1016/j.physletb.2009.07.054.
- [483] Joan Elias-Miro, Jose R. Espinosa, Gian F. Giudice, Gino Isidori, Antonio Riotto, and Alessandro Strumia. Higgs mass implications on the stability of the electroweak vacuum. *Phys. Lett. B*, 709:222–228, 2012. doi:10.1016/j.physletb.2012.02.013.
- [484] Giuseppe Degrandi, Stefano Di Vita, Joan Elias-Miro, Jose R. Espinosa, Gian F. Giudice, Gino Isidori, and Alessandro Strumia. Higgs mass and vacuum stability in the Standard Model at NNLO. *JHEP*, 08:098, 2012. doi:10.1007/JHEP08(2012)098.
- [485] Fedor Bezrukov, Mikhail Yu. Kalmykov, Bernd A. Kniehl, and Mikhail Shaposhnikov. Higgs

- Boson Mass and New Physics. *JHEP*, 10:140, 2012. doi:10.1007/JHEP10(2012)140.
- [486] A. V. Bednyakov, B. A. Kniehl, A. F. Pikelner, and O. L. Veretin. Stability of the Electroweak Vacuum: Gauge Independence and Advanced Precision. *Phys. Rev. Lett.*, 115(20):201802, 2015. doi:10.1103/PhysRevLett.115.201802.
- [487] Dario Buttazzo, Giuseppe Degrandi, Pier Paolo Giardino, Gian F. Giudice, Filippo Sala, Alberto Salvio, and Alessandro Strumia. Investigating the near-criticality of the Higgs boson. *JHEP*, 12:089, 2013. doi:10.1007/JHEP12(2013)089.
- [488] Jose R. Espinosa, Mathias Garny, Thomas Konstandin, and Antonio Riotto. Gauge-Independent Scales Related to the Standard Model Vacuum Instability. *Phys. Rev. D*, 95(5):056004, 2017. doi:10.1103/PhysRevD.95.056004.
- [489] J. R. Espinosa, D. Racco, and A. Riotto. Cosmological Signature of the Standard Model Higgs Vacuum Instability: Primordial Black Holes as Dark Matter. *Phys. Rev. Lett.*, 120(12):121301, 2018. doi:10.1103/PhysRevLett.120.121301.
- [490] Graham White, Lauren Pearce, Daniel Vagie, and Alexander Kusenko. Detectable Gravitational Wave Signals from Affleck-Dine Baryogenesis. *Phys. Rev. Lett.*, 127(18):181601, 2021. doi:10.1103/PhysRevLett.127.181601.
- [491] Keisuke Inomata, Masahiro Kawasaki, Kyohei Mukaida, Takahiro Terada, and Tsutomu T. Yanagida. Gravitational Wave Production right after a Primordial Black Hole Evaporation. *Phys. Rev. D*, 101(12):123533, 2020. doi:10.1103/PhysRevD.101.123533.
- [492] Juan Garcia-Bellido and Ester Ruiz Morales. Primordial black holes from single field models of inflation. *Phys. Dark Univ.*, 18:47–54, 2017. doi:10.1016/j.dark.2017.09.007.
- [493] Jose Maria Ezquiaga, Juan Garcia-Bellido, and Ester Ruiz Morales. Primordial Black Hole production in Critical Higgs Inflation. *Phys. Lett. B*, 776:345–349, 2018. doi:10.1016/j.physletb.2017.11.039.
- [494] Guillermo Ballesteros and Marco Taoso. Primordial black hole dark matter from single field inflation. *Phys. Rev. D*, 97(2):023501, 2018. doi:10.1103/PhysRevD.97.023501.
- [495] Misao Sasaki. Large Scale Quantum Fluctuations in the Inflationary Universe. *Prog. Theor. Phys.*, 76:1036, 1986. doi:10.1143/PTP.76.1036.
- [496] Viatcheslav F. Mukhanov. Quantum Theory of Gauge Invariant Cosmological Perturbations. *Sov. Phys. JETP*, 67:1297–1302, 1988.
- [497] Bernard J. Carr. The Primordial black hole mass spectrum. *Astrophys. J.*, 201:1–19, 1975.

- doi:10.1086/153853.
- [498] Ryo Saito and Jun'ichi Yokoyama. Gravitational-wave background as a probe of the primordial black-hole abundance. *Physical Review Letters*, 102(16):161101, 2009.
- [499] Ryo Saito and Jun'ichi Yokoyama. Gravitational-wave constraints on the abundance of primordial black holes. *Progress of theoretical physics*, 123(5):867–886, 2010.
- [500] Juan Garcia-Bellido, Marco Peloso, and Caner Unal. Gravitational waves at interferometer scales and primordial black holes in axion inflation. *JCAP*, 12:031, 2016. doi:10.1088/1475-7516/2016/12/031.
- [501] Keisuke Inomata, Masahiro Kawasaki, Kyohei Mukaida, Yuichiro Tada, and Tsutomu T. Yanagida. Inflationary primordial black holes for the LIGO gravitational wave events and pulsar timing array experiments. *Phys. Rev. D*, 95(12):123510, 2017. doi:10.1103/PhysRevD.95.123510.
- [502] Sai Wang, Takahiro Terada, and Kazunori Kohri. Prospective constraints on the primordial black hole abundance from the stochastic gravitational-wave backgrounds produced by coalescing events and curvature perturbations. *Phys. Rev. D*, 99(10):103531, 2019. doi:10.1103/PhysRevD.99.103531. [Erratum: Phys.Rev.D 101, 069901 (2020)].
- [503] Albert Escrivà, Florian Kuhnel, and Yuichiro Tada. Primordial Black Holes. 11 2022.
- [504] Jason Kristiano and Jun'ichi Yokoyama. Ruling Out Primordial Black Hole Formation From Single-Field Inflation. 11 2022.
- [505] Jason Kristiano and Jun'ichi Yokoyama. Response to criticism on "Ruling Out Primordial Black Hole Formation From Single-Field Inflation": A note on bispectrum and one-loop correction in single-field inflation with primordial black hole formation. 3 2023.
- [506] A. Riotto. The Primordial Black Hole Formation from Single-Field Inflation is Still Not Ruled Out. 3 2023.
- [507] Sayantan Choudhury, Mayukh R. Gangopadhyay, and M. Sami. No-go for the formation of heavy mass Primordial Black Holes in Single Field Inflation. 1 2023.
- [508] Hassan Firouzjahi and Antonio Riotto. Primordial Black Holes and Loops in Single-Field Inflation. 4 2023.
- [509] Yi-Fu Cai, Chao Chen, Xi Tong, Dong-Gang Wang, and Sheng-Feng Yan. When primordial black holes from sound speed resonance meet a stochastic background of gravitational waves. *Physical Review D*, 100(4):043518, 2019.

- [510] M Kawasaki, Naoshi Sugiyama, and T Yanagida. Primordial black hole formation in a double inflation model in supergravity. *Physical Review D*, 57(10):6050, 1998.
- [511] Paul H Frampton, Masahiro Kawasaki, Fuminobu Takahashi, and Tsutomu T Yanagida. Primordial black holes as all dark matter. *Journal of Cosmology and Astroparticle Physics*, 2010(04):023, 2010.
- [512] Masahiro Kawasaki, Naoya Kitajima, and Tsutomu T Yanagida. Primordial black hole formation from an axionlike curvaton model. *Physical Review D*, 87(6):063519, 2013.
- [513] Keisuke Inomata, Masahiro Kawasaki, Kyohei Mukaida, Yuichiro Tada, and Tsutomu T Yanagida. Inflationary primordial black holes as all dark matter. *Physical Review D*, 96(4):043504, 2017.
- [514] Shi Pi, Ying-li Zhang, Qing-Guo Huang, and Misao Sasaki. Scalaron from r2-gravity as a heavy field. *Journal of Cosmology and Astroparticle Physics*, 2018(05):042, 2018.
- [515] Yi-Fu Cai, Xi Tong, Dong-Gang Wang, and Sheng-Feng Yan. Primordial black holes from sound speed resonance during inflation. *Physical Review Letters*, 121(8):081306, 2018.
- [516] Chao Chen and Yi-Fu Cai. Primordial black holes from sound speed resonance in the inflaton-curvaton mixed scenario. *Journal of Cosmology and Astroparticle Physics*, 2019(10):068, 2019.
- [517] Chao Chen, Xiao-Han Ma, and Yi-Fu Cai. Dirac-born-infeld realization of sound speed resonance mechanism for primordial black holes. *Physical Review D*, 102(6):063526, 2020.
- [518] Christian T Byrnes, Philippa S Cole, and Subodh P Patil. Steepest growth of the power spectrum and primordial black holes. *Journal of Cosmology and Astroparticle Physics*, 2019(06):028, 2019.
- [519] Ogan Özsoy and Gianmassimo Tasinato. On the slope of the curvature power spectrum in non-attractor inflation. *Journal of Cosmology and Astroparticle Physics*, 2020(04):048, 2020.
- [520] Gonzalo A Palma, Spyros Sypsas, and Cristobal Zenteno. Seeding primordial black holes in multifield inflation. *Physical Review Letters*, 125(12):121301, 2020.
- [521] Amjad Ashoorioon, Abasalt Rostami, and Javad T Firouzjaee. Eft compatible pbhs: effective spawning of the seeds for primordial black holes during inflation. *Journal of High Energy Physics*, 2021(7):1–23, 2021.
- [522] José Ramón Espinosa, Davide Racco, and Antonio Riotto. A cosmological signature of the sm higgs instability: gravitational waves. *Journal of Cosmology and Astroparticle Physics*,

- 2018(09):012, 2018.
- [523] Kazunori Kohri and Takahiro Terada. Semianalytic calculation of gravitational wave spectrum nonlinearly induced from primordial curvature perturbations. *Physical Review D*, 97(12):123532, 2018.
- [524] Kenta Ando, Masahiro Kawasaki, and Hiromasa Nakatsuka. Formation of primordial black holes in an axionlike curvaton model. *Physical Review D*, 98(8):083508, 2018.
- [525] Kenta Ando, Keisuke Inomata, Masahiro Kawasaki, Kyohei Mukaida, and Tsutomu T Yanagida. Primordial black holes for the ligo events in the axionlike curvaton model. *Physical Review D*, 97(12):123512, 2018.
- [526] Juan Garcia-Bellido, Andrei Linde, and David Wands. Density perturbations and black hole formation in hybrid inflation. *Physical Review D*, 54(10):6040, 1996.
- [527] Jun'ichi Yokoyama. Chaotic new inflation and formation of primordial black holes. *Physical Review D*, 58(8):083510, 1998.
- [528] Vicente Atal and Cristiano Germani. The role of non-gaussianities in primordial black hole formation. *Physics of the Dark Universe*, 24:100275, 2019.
- [529] Jing Liu, Zong-Kuan Guo, and Rong-Gen Cai. Analytical approximation of the scalar spectrum in the ultraslow-roll inflationary models. *Physical Review D*, 101(8):083535, 2020.
- [530] Vicente Atal and Guillem Domènech. Probing non-gaussianities with the high frequency tail of induced gravitational waves. *Journal of Cosmology and Astroparticle Physics*, 2021(06):001, 2021.
- [531] Wu-Tao Xu, Jing Liu, Tie-Jun Gao, and Zong-Kuan Guo. Gravitational waves from double-inflection-point inflation. *Physical Review D*, 101(2):023505, 2020.
- [532] Ryan M Shannon, Vikram Ravi, LT Lentati, Paul Daniel Lasky, G Hobbs, Matthew Kerr, Richard Norman Manchester, William A Coles, Yuri Levin, Matthew Bailes, et al. Gravitational waves from binary supermassive black holes missing in pulsar observations. *Science*, 349(6255):1522–1525, 2015.
- [533] Flavio Ricciardi, Marco Taoso, and Alfredo Urbano. Solving peak theory in the presence of local non-gaussianities. *Journal of Cosmology and Astroparticle Physics*, 2021(08):060, 2021.
- [534] Keisuke Harigaya, Keisuke Inomata, and Takahiro Terada. Gravitational wave production from axion rotations right after a transition to kination. *Phys. Rev. D*, 108(8):L081303, 2023. doi:10.1103/PhysRevD.108.L081303.

- [535] Masahiro Kawasaki and Kai Murai. Enhancement of gravitational waves at Q-ball decay including non-linear density perturbations. 8 2023.
- [536] Matthew Pearce, Lauren Pearce, Graham White, and Csaba Balázs. Gravitational Wave Signals From Early Matter Domination: Interpolating Between Fast and Slow Transitions. 11 2023.
- [537] Jai-Chan Hwang, Donghui Jeong, and Hyerim Noh. Gauge dependence of gravitational waves generated from scalar perturbations. *Astrophys. J.*, 842(1):46, 2017. doi:10.3847/1538-4357/aa74be.
- [538] V. De Luca, G. Franciolini, A. Kehagias, and A. Riotto. On the Gauge Invariance of Cosmological Gravitational Waves. *JCAP*, 03:014, 2020. doi:10.1088/1475-7516/2020/03/014.
- [539] Keisuke Inomata and Takahiro Terada. Gauge Independence of Induced Gravitational Waves. *Phys. Rev. D*, 101(2):023523, 2020. doi:10.1103/PhysRevD.101.023523.
- [540] Chen Yuan, Zu-Cheng Chen, and Qing-Guo Huang. Scalar induced gravitational waves in different gauges. *Phys. Rev. D*, 101(6):063018, 2020. doi:10.1103/PhysRevD.101.063018.
- [541] Yizhou Lu, Arshad Ali, Yungui Gong, Jiong Lin, and Fengge Zhang. Gauge transformation of scalar induced gravitational waves. *Phys. Rev. D*, 102(8):083503, 2020. doi:10.1103/PhysRevD.102.083503(2020).
- [542] Zhe Chang, Sai Wang, and Qing-Hua Zhu. Note on gauge invariance of second order cosmological perturbations. *Chin. Phys. C*, 45(9):095101, 2021. doi:10.1088/1674-1137/ac0c74.
- [543] Guillem Domènech and Misao Sasaki. Approximate gauge independence of the induced gravitational wave spectrum. *Phys. Rev. D*, 103(6):063531, 2021. doi:10.1103/PhysRevD.103.063531.
- [544] José Ramón Espinosa, Davide Racco, and Antonio Riotto. A Cosmological Signature of the SM Higgs Instability: Gravitational Waves. *JCAP*, 09:012, 2018. doi:10.1088/1475-7516/2018/09/012.
- [545] Guillem Domènech, Chunshan Lin, and Misao Sasaki. Gravitational wave constraints on the primordial black hole dominated early universe. *JCAP*, 04:062, 2021. doi:10.1088/1475-7516/2021/11/E01. [Erratum: *JCAP* 11, E01 (2021)].
- [546] Nilanjandev Bhaumik and Rajeev Kumar Jain. Small scale induced gravitational waves from primordial black holes, a stringent lower mass bound, and the imprints of an early matter to radiation transition. *Phys. Rev. D*, 104(2):023531, 2021. doi:

- 10.1103/PhysRevD.104.023531.
- [547] Ioannis Dalianis and Chris Kouvaris. Gravitational waves from density perturbations in an early matter domination era. *JCAP*, 07:046, 2021. doi:10.1088/1475-7516/2021/07/046.
- [548] Jonathan Kozaczuk, Tongyan Lin, and Ethan Villarama. Signals of primordial black holes at gravitational wave interferometers. *Phys. Rev. D*, 105(12):123023, 2022. doi:10.1103/PhysRevD.105.123023.
- [549] Md Riajul Haque, Debaprasad Maity, Tanmoy Paul, and L. Sriramkumar. Decoding the phases of early and late time reheating through imprints on primordial gravitational waves. *Phys. Rev. D*, 104(6):063513, 2021. doi:10.1103/PhysRevD.104.063513.
- [550] Guillem Domènech, Volodymyr Takhistov, and Misao Sasaki. Exploring evaporating primordial black holes with gravitational waves. *Phys. Lett. B*, 823:136722, 2021. doi:10.1016/j.physletb.2021.136722.
- [551] Nilanjandev Bhaumik, Anish Ghoshal, and Marek Lewicki. Doubly peaked induced stochastic gravitational wave background: testing baryogenesis from primordial black holes. *JHEP*, 07:130, 2022. doi:10.1007/JHEP07(2022)130.
- [552] Nilanjandev Bhaumik, Anish Ghoshal, Rajeev Kumar Jain, and Marek Lewicki. Distinct signatures of spinning PBH domination and evaporation: doubly peaked gravitational waves, dark relics and CMB complementarity. *JHEP*, 05:169, 2023. doi:10.1007/JHEP05(2023)169.
- [553] Dan Hooper, Gordan Krnjaic, and Samuel D. McDermott. Dark Radiation and Superheavy Dark Matter from Black Hole Domination. *JHEP*, 08:001, 2019. doi:10.1007/JHEP08(2019)001.
- [554] Savvas Nesseris, Domenico Sapone, and Spyros Sypsas. Evaporating primordial black holes as varying dark energy. *Phys. Dark Univ.*, 27:100413, 2020. doi:10.1016/j.dark.2019.100413.
- [555] Cecilia Lunardini and Yuber F. Perez-Gonzalez. Dirac and Majorana neutrino signatures of primordial black holes. *JCAP*, 08:014, 2020. doi:10.1088/1475-7516/2020/08/014.
- [556] D. Toussaint, S. B. Treiman, Frank Wilczek, and A. Zee. Matter - Antimatter Accounting, Thermodynamics, and Black Hole Radiation. *Phys. Rev. D*, 19:1036–1045, 1979. doi:10.1103/PhysRevD.19.1036.
- [557] Michael S. Turner and David N. Schramm. The Origin of Baryons in the Universe and the Astrophysical Implications. *Nature*, 279:303–305, 1979. doi:10.1038/279303a0.
- [558] Michael S. Turner. BARYON PRODUCTION BY PRIMORDIAL BLACK HOLES. *Phys.*

- Lett. B*, 89:155–159, 1979. doi:10.1016/0370-2693(79)90095-9.
- [559] John D. Barrow, Edmund J. Copeland, Edward W. Kolb, and Andrew R. Liddle. Baryogenesis in extended inflation. 2. Baryogenesis via primordial black holes. *Phys. Rev. D*, 43:984–994, 1991. doi:10.1103/PhysRevD.43.984.
- [560] A. S. Majumdar, P. Das Gupta, and R. P. Saxena. Baryogenesis from black hole evaporation. *Int. J. Mod. Phys. D*, 4:517–529, 1995. doi:10.1142/S0218271895000363.
- [561] Niraj Upadhyay, Patrick Das Gupta, and R. P. Saxena. Baryogenesis from primordial black holes after electroweak phase transition. *Phys. Rev. D*, 60:063513, 1999. doi:10.1103/PhysRevD.60.063513.
- [562] A. D. Dolgov, P. D. Naselsky, and I. D. Novikov. Gravitational waves, baryogenesis, and dark matter from primordial black holes. 9 2000.
- [563] E. V. Bugaev, M. G. Elbakidze, and K. V. Konishchev. Baryon asymmetry of the universe from evaporation of primordial black holes. *Phys. Atom. Nucl.*, 66:476–480, 2003. doi:10.1134/1.1563709.
- [564] Daniel Baumann, Paul J. Steinhardt, and Neil Turok. Primordial Black Hole Baryogenesis. 3 2007.
- [565] Tomohiro Fujita, Masahiro Kawasaki, Keisuke Harigaya, and Ryo Matsuda. Baryon asymmetry, dark matter, and density perturbation from primordial black holes. *Phys. Rev. D*, 89(10):103501, 2014. doi:10.1103/PhysRevD.89.103501.
- [566] Yuta Hamada and Satoshi Iso. Baryon asymmetry from primordial black holes. *PTEP*, 2017(3):033B02, 2017. doi:10.1093/ptep/ptx011.
- [567] Olivier Lennon, John March-Russell, Rudin Petrossian-Byrne, and Hannah Tillim. Black Hole Genesis of Dark Matter. *JCAP*, 04:009, 2018. doi:10.1088/1475-7516/2018/04/009.
- [568] Logan Morrison, Stefano Profumo, and Yan Yu. Melanopogenesis: Dark Matter of (almost) any Mass and Baryonic Matter from the Evaporation of Primordial Black Holes weighing a Ton (or less). *JCAP*, 05:005, 2019. doi:10.1088/1475-7516/2019/05/005.
- [569] Thomas C. Gehrman, Barmak Shams Es Haghi, Kuver Sinha, and Tao Xu. The primordial black holes that disappeared: connections to dark matter and MHz-GHz gravitational Waves. *JCAP*, 10:001, 2023. doi:10.1088/1475-7516/2023/10/001.
- [570] Guillem Domènech and Misao Sasaki. Gravitational wave hints black hole remnants as dark matter. *Class. Quant. Grav.*, 40(17):177001, 2023. doi:10.1088/1361-6382/ace493.

- [571] Marcos M. Flores, Alexander Kusenko, Lauren Pearce, Yuber F. Perez-Gonzalez, and Graham White. Testing high scale supersymmetry via second order gravitational waves. 8 2023.
- [572] Shinta Kasuya, Masahiro Kawasaki, and Kai Murai. Enhancement of second-order gravitational waves at Q-ball decay. *JCAP*, 05:053, 2023. doi:10.1088/1475-7516/2023/05/053.
- [573] Marcelo Gleiser. Pseudostable bubbles. *Physical Review D*, 49(6):2978, 1994.
- [574] Mustafa A Amin and David Shirokoff. Flat-top oscillons in an expanding universe. *Physical Review D*, 81(8):085045, 2010.
- [575] Mustafa A Amin, Richard Easther, and Hal Finkel. Inflaton fragmentation and oscillon formation in three dimensions. *Journal of Cosmology and Astroparticle Physics*, 2010(12):001, 2010.
- [576] Mustafa A Amin, Richard Easther, Hal Finkel, Raphael Flauger, and Mark P Hertzberg. Oscillons after inflation. *Physical review letters*, 108(24):241302, 2012.
- [577] Shuang-Yong Zhou, Edmund J Copeland, Richard Easther, Hal Finkel, Zong-Gang Mou, and Paul M Saffin. Gravitational waves from oscillon preheating. *Journal of High Energy Physics*, 2013(10):1–19, 2013.
- [578] Mustafa A Amin. K-oscillons: Oscillons with noncanonical kinetic terms. *Physical Review D*, 87(12):123505, 2013.
- [579] Kaloian D Lozanov and Mustafa A Amin. End of inflation, oscillons, and matter-antimatter asymmetry. *Physical Review D*, 90(8):083528, 2014.
- [580] Stefan Antusch, Francesco Cefala, David Nolde, and Stefano Orani. Parametric resonance after hilltop inflation caused by an inhomogeneous inflaton field. *Journal of Cosmology and Astroparticle Physics*, 2016(02):044, 2016.
- [581] Stefan Antusch and Stefano Orani. Impact of other scalar fields on oscillons after hilltop inflation. *Journal of Cosmology and Astroparticle Physics*, 2016(03):026, 2016.
- [582] Stefan Antusch, Francesco Cefala, and Stefano Orani. Gravitational waves from oscillons after inflation. *Physical Review Letters*, 118(1):011303, 2017.
- [583] Stefan Antusch, Francesco Cefala, Sven Krippendorff, Francesco Muia, Stefano Orani, and Fernando Quevedo. Oscillons from string moduli. *Journal of High Energy Physics*, 2018(1):1–42, 2018.
- [584] Stefan Antusch, Francesco Cefala, and Stefano Orani. What can we learn from the stochastic gravitational wave background produced by oscillons? *Journal of Cosmology and Astropar-*

- ticle Physics*, 2018(03):032, 2018.
- [585] Kaloian D Lozanov and Mustafa A Amin. Self-resonance after inflation: Oscillons, transients, and radiation domination. *Physical Review D*, 97(2):023533, 2018.
- [586] Stefan Antusch, Francesco Cefala, and Francisco Torrenti. Properties of oscillons in hilltop potentials: energies, shapes, and lifetimes. *Journal of Cosmology and Astroparticle Physics*, 2019(10):002, 2019.
- [587] Yu Sang and Qing-Guo Huang. Stochastic gravitational-wave background from axion-monodromy oscillons in string theory during preheating. *Physical Review D*, 100(6):063516, 2019.
- [588] Kaloian D Lozanov and Mustafa A Amin. Gravitational perturbations from oscillons and transients after inflation. *Physical Review D*, 99(12):123504, 2019.
- [589] Takashi Hiramatsu, Evangelos I Sfakianakis, and Masahide Yamaguchi. Gravitational wave spectra from oscillon formation after inflation. *Journal of High Energy Physics*, 2021(3): 1–35, 2021.
- [590] VA Rubakov and ME Shaposhnikov. Do we live inside a domain wall? *Physics Letters B*, 125(2-3):136–138, 1983.
- [591] Lisa Randall and Raman Sundrum. Out of this world supersymmetry breaking. *Nuclear Physics B*, 557(1-2):79–118, 1999.
- [592] Sanjeev S Seahra, Chris Clarkson, and Roy Maartens. Detecting extra dimensions with gravity-wave spectroscopy: the black-string brane world. *Physical review letters*, 94(12): 121302, 2005.
- [593] Chris Clarkson and Sanjeev S Seahra. A gravitational wave window on extra dimensions. *Classical and Quantum Gravity*, 24(9):F33, 2007.
- [594] Maurizio Gasperini and Gabriele Veneziano. The pre-big bang scenario in string cosmology. *Physics Reports*, 373(1-2):1–212, 2003.
- [595] M Gasperini and G Veneziano. String theory and pre-big bang cosmology. *arXiv preprint hep-th/0703055*, 2007.
- [596] R Brustein, M Gasperini, Massimo Giovannini, and G Veneziano. Gravitational radiation from string cosmology. *arXiv preprint hep-th/9510081*, 1995.
- [597] L. P. Grishchuk. Amplification of gravitational waves in an isotropic universe. *Sov. Phys. JETP*, 40:409–415, 1975. [Zh. Eksp. Teor. Fiz.67,825(1974)].

- [598] Alexei A Starobinsky. Relict gravitation radiation spectrum and initial state of the universe. *JETP lett*, 30(682-685):131–132, 1979.
- [599] VA Rubakov, M Verjaskin Sazhin, and AV Veryaskin. Graviton creation in the inflationary universe and the grand unification scale. *Physics Letters B*, 115(3):189–192, 1982.
- [600] R. Fabbri and M. d. Pollock. The Effect of Primordially Produced Gravitons upon the Anisotropy of the Cosmological Microwave Background Radiation. *Phys. Lett. B*, 125:445–448, 1983. doi:10.1016/0370-2693(83)91322-9.
- [601] L. F. Abbott and Mark B. Wise. Constraints on Generalized Inflationary Cosmologies. *Nucl. Phys. B*, 244:541–548, 1984. doi:10.1016/0550-3213(84)90329-8.
- [602] Sachiko Kuroyanagi, Tomo Takahashi, and Shuichiro Yokoyama. Blue-tilted tensor spectrum and thermal history of the universe. *Journal of Cosmology and Astroparticle Physics*, 2015 (02):003, 2015.
- [603] Andrew R Liddle and David H Lyth. *Cosmological inflation and large-scale structure*. Cambridge university press, 2000.
- [604] Jessica L. Cook and Lorenzo Sorbo. Particle production during inflation and gravitational waves detectable by ground-based interferometers. *Phys. Rev. D*, 85:023534, 2012. doi:10.1103/PhysRevD.85.023534. [Erratum: Phys.Rev.D 86, 069901 (2012)].
- [605] Mohamed M. Anber and Lorenzo Sorbo. Non-Gaussianities and chiral gravitational waves in natural steep inflation. *Phys. Rev. D*, 85:123537, 2012. doi:10.1103/PhysRevD.85.123537.
- [606] Ryo Namba, Marco Peloso, Maresuke Shiraishi, Lorenzo Sorbo, and Caner Unal. Scale-dependent gravitational waves from a rolling axion. *JCAP*, 01:041, 2016. doi:10.1088/1475-7516/2016/01/041.
- [607] Emanuela Dimastrogiovanni, Matteo Fasiello, and Tomohiro Fujita. Primordial Gravitational Waves from Axion-Gauge Fields Dynamics. *JCAP*, 01:019, 2017. doi:10.1088/1475-7516/2017/01/019.
- [608] R. R. Caldwell and C. Devulder. Axion Gauge Field Inflation and Gravitational Leptogenesis: A Lower Bound on B Modes from the Matter-Antimatter Asymmetry of the Universe. *Phys. Rev. D*, 97(2):023532, 2018. doi:10.1103/PhysRevD.97.023532.
- [609] Tomohiro Fujita, Sachiko Kuroyanagi, Shuntaro Mizuno, and Shinji Mukohyama. Blue-tilted Primordial Gravitational Waves from Massive Gravity. *Phys. Lett. B*, 789:215–219, 2019. doi:10.1016/j.physletb.2018.12.025.

- [610] Yun-Song Piao and Yuan-Zhong Zhang. Phantom inflation and primordial perturbation spectrum. *Phys. Rev. D*, 70:063513, 2004. doi:10.1103/PhysRevD.70.063513.
- [611] Masaki Satoh and Jiro Soda. Higher Curvature Corrections to Primordial Fluctuations in Slow-roll Inflation. *JCAP*, 09:019, 2008. doi:10.1088/1475-7516/2008/09/019.
- [612] Tsutomu Kobayashi, Masahide Yamaguchi, and Jun'ichi Yokoyama. G-inflation: Inflation driven by the Galileon field. *Phys. Rev. Lett.*, 105:231302, 2010. doi:10.1103/PhysRevLett.105.231302.
- [613] Solomon Endlich, Alberto Nicolis, and Junpu Wang. Solid Inflation. *JCAP*, 10:011, 2013. doi:10.1088/1475-7516/2013/10/011.
- [614] S. Yu. Khlebnikov and I. I. Tkachev. Classical decay of inflaton. *Phys. Rev. Lett.*, 77:219–222, 1996. doi:10.1103/PhysRevLett.77.219.
- [615] Jeffrey M. Hyde. Sensitivity of gravitational waves from preheating to a scalar field's interactions. *Phys. Rev. D*, 92(4):044026, 2015. doi:10.1103/PhysRevD.92.044026.
- [616] Andrei D. Linde. A New Inflationary Universe Scenario: A Possible Solution of the Horizon, Flatness, Homogeneity, Isotropy and Primordial Monopole Problems. *Phys. Lett. B*, 108:389–393, 1982. doi:10.1016/0370-2693(82)91219-9.
- [617] Andreas Albrecht and Paul J. Steinhardt. Cosmology for Grand Unified Theories with Radiatively Induced Symmetry Breaking. *Phys. Rev. Lett.*, 48:1220–1223, 1982. doi:10.1103/PhysRevLett.48.1220.
- [618] Andrei D. Linde. Chaotic Inflation. *Phys. Lett. B*, 129:177–181, 1983. doi:10.1016/0370-2693(83)90837-7.
- [619] Jennie H. Traschen and Robert H. Brandenberger. Particle Production During Out-of-equilibrium Phase Transitions. *Phys. Rev. D*, 42:2491–2504, 1990. doi:10.1103/PhysRevD.42.2491.
- [620] Lev Kofman, Andrei D. Linde, and Alexei A. Starobinsky. Reheating after inflation. *Phys. Rev. Lett.*, 73:3195–3198, 1994. doi:10.1103/PhysRevLett.73.3195.
- [621] Lev Kofman, Andrei D. Linde, and Alexei A. Starobinsky. Towards the theory of reheating after inflation. *Phys. Rev. D*, 56:3258–3295, 1997. doi:10.1103/PhysRevD.56.3258.
- [622] Andrei D. Linde. Hybrid inflation. *Phys. Rev. D*, 49:748–754, 1994. doi:10.1103/PhysRevD.49.748.
- [623] Gary N. Felder, Juan Garcia-Bellido, Patrick B. Greene, Lev Kofman, Andrei D. Linde, and

- Igor Tkachev. Dynamics of symmetry breaking and tachyonic preheating. *Phys. Rev. Lett.*, 87:011601, 2001. doi:10.1103/PhysRevLett.87.011601.
- [624] C. Guzzetti, M., N. Bartolo, M. Liguori, and S. Matarrese. Gravitational waves from inflation. *Riv. Nuovo Cim.*, 39(9):399–495, 2016. doi:10.1393/ncr/i2016-10127-1.
- [625] Jean Francois Dufaux, Amanda Bergman, Gary N. Felder, Lev Kofman, and Jean-Philippe Uzan. Theory and Numerics of Gravitational Waves from Preheating after Inflation. *Phys. Rev. D*, 76:123517, 2007. doi:10.1103/PhysRevD.76.123517.
- [626] Jean-Francois Dufaux, Gary Felder, Lev Kofman, and Olga Navros. Gravity Waves from Tachyonic Preheating after Hybrid Inflation. *JCAP*, 03:001, 2009. doi:10.1088/1475-7516/2009/03/001.
- [627] Daniel G. Figueroa, Adrien Florio, Nicolas Loayza, and Mauro Pieroni. Spectroscopy of particle couplings with gravitational waves. *Phys. Rev. D*, 106(6):063522, 2022. doi:10.1103/PhysRevD.106.063522.
- [628] Anish Ghoshal and Pankaj Saha. Detectable Gravitational Waves from (P)-reheating probes non-thermal Dark Matter. 3 2022.
- [629] M. Kawasaki, Kazunori Kohri, and Naoshi Sugiyama. Cosmological constraints on late time entropy production. *Phys. Rev. Lett.*, 82:4168, 1999. doi:10.1103/PhysRevLett.82.4168.
- [630] M. Kawasaki, Kazunori Kohri, and Naoshi Sugiyama. MeV scale reheating temperature and thermalization of neutrino background. *Phys. Rev.*, D62:023506, 2000. doi:10.1103/PhysRevD.62.023506.
- [631] Gian Francesco Giudice, Edward W. Kolb, and Antonio Riotto. Largest temperature of the radiation era and its cosmological implications. *Phys. Rev. D*, 64:023508, 2001. doi:10.1103/PhysRevD.64.023508.
- [632] Takuya Hasegawa, Nagisa Hiroshima, Kazunori Kohri, Rasmus S. L. Hansen, Thomas Tram, and Steen Hannestad. MeV-scale reheating temperature and thermalization of oscillating neutrinos by radiative and hadronic decays of massive particles. *JCAP*, 12:012, 2019. doi:10.1088/1475-7516/2019/12/012.
- [633] Andrei Sakharov. Maximum temperature of thermal radiation. *Pisma Zh. Eksp. Teor. Fiz.*, 3:012, 439-441.
- [634] Ken'ichi Saikawa and Satoshi Shirai. Primordial gravitational waves, precisely: The role of thermodynamics in the Standard Model. *JCAP*, 1805(05):035, 2018. doi:10.1088/1475-

7516/2018/05/035.